U.S.N.A. --- Trident Scholar project report; no. 371 (2008)

A MATHEMATICAL MODEL FOR THE ACOUSTIC AND SEISMIC PROPERTIES OF THE LANDMINE DETECTION PROBLEM

by

Midshipman 1/c Michelle B. Mattingly
United States Naval Academy
Annapolis, Maryland

_____
(signature)

Certification of Adviser(s) Approval

Professor James Buchanan
Mathematics Department

_____
(signature)

_____
(date)

Professor Murray Korman
Physics Department

_____
(signature)

_____
(date)

Professor Reza Malek-Madani
Mathematics Department

_____
(signature)

_____
(date)

Acceptance for the Trident Scholar Committee

Professor Joyce E. Shade
Deputy Director of Research & Scholarship

_____
(signature)

_____
(date)

USNA-1531-2

REPORT DOCUMENTATION PAGE

Form Approved
OMB No. 074-0188

1. AGENCY USE ONLY (Leave blank)	2. REPORT DATE	3. REPORT TYPE AND DATE COVERED
	6 May 2008	

4. TITLE AND SUBTITLE
A Mathematical Model for the Acoustic and Seismic Properties of the Landmine Detection Problem

5. FUNDING NUMBERS

6. AUTHOR(S)

Mattingly, Michelle B.

7. PERFORMING ORGANIZATION NAME(S) AND ADDRESS(ES)		8. PERFORMING ORGANIZATION REPORT NUMBER

9. SPONSORING/MONITORING AGENCY NAME(S) AND ADDRESS(ES)		10. SPONSORING/MONITORING AGENCY REPORT NUMBER
US Naval Academy Annapolis, MD 21402		Trident Scholar project report no. 371 (2008)

11. SUPPLEMENTARY NOTES

12a. DISTRIBUTION/AVAILABILITY STATEMENT	12b. DISTRIBUTION CODE
This document has been approved for public release; its distribution is UNLIMITED.	

13. ABSTRACT (cont from p. 1) of pressure and particle velocity vs. frequency and spatial variables. In the presence of the buried circular target, membrane resonances were predicted by similar modeling techniques. The top plate of the buried landmine was modeled as a circular elastic membrane stretched flush over a cylindrical cavity in a rigid substrate beneath the porous layer. The Helmholtz equation was again solved in the atmospheric layer using cylindrical coordinates and a point source. The homogeneous Helmholtz equation was again used in the porous layer, with a Green's function representation of the membrane response. In the soil resonance predictions, pressure was plotted as a function of frequency, and the resonances appear as local minimums and maximums. A MATLABTM user interface was created to allow researchers to access the soil resonance information particular to their experiment. The resonances of the membrane-soil model were determined using MATLABTM; describing the effects of frequency, depth, density, and sound, to include radius and elastic parameters of the membrane. Comparison of the results (involving the fluid surface particle velocity profiles across the target) has been made with experiments reported in the literature to evaluate the model's usefulness.

14. SUBJECT TERMS	15. NUMBER OF PAGES
landmine, waveguide, Sabatier, scattering	**113**
	16. PRICE CODE

17. SECURITY CLASSIFICATION OF REPORT	18. SECURITY CLASSIFICATION OF THIS PAGE	19. SECURITY CLASSIFICATION OF ABSTRACT	20. LIMITATION OF ABSTRACT

Contents

[1] [27]
[2] [27]
[3] [2], pg. 362.

Abstract

Acoustic landmine detection is accomplished by using a loud speaker to generate airborne source low-frequency waves that are transmitted to the soil above a buried landmine target. At a specific frequency, the landmine will "vibrate" at resonance, imparting an enhanced velocity on the soil particles above it at the surface that is detected by a scanning Laser Doppler Vibrometer system. If the soil surface velocity profiles measured from these experiments could be predicted mathematically under a variety of conditions, the physical system would be able to accurately detect landmines in more challenging environments.

The mathematical modeling of the buried landmine detection problem involved wave propagation in a layered waveguide in the presence and absence of a buried circular target. In this study, emphasis was placed on acoustic to seismic coupling of an airborne continuous wave point source into the soil. Soil resonances were calculated with a model that represents the soil as a finite, fluid-filled rigid porous layer below a finite atmospheric layer. This two-layer waveguide incorporated density and sound speed in both the soil and atmosphere, which was adjusted based on soil type, compactness, and moisture content in both the air and soil. An analytic solution of the two-layer waveguide problem involved solving the Helmholtz equation in cylindrical coordinates in both layers along with using a delta function point source to simulate a compact loudspeaker in the upper layer. Boundary conditions along with conditions of orthogonality were used to obtain complicated analytical expressions for the eigenvalues and eigenfunctions of the problem. A MATLAB^{TM} program was used to numerically solve for the eigenvalues and plot solutions of pressure and particle velocity vs. frequency and spatial variables.

In the presence of the buried circular target, membrane resonances were predicted by similar modeling techniques. The top plate of the buried landmine was modeled as a circular elastic membrane stretched flush over a cylindrical cavity in a rigid substrate beneath the porous layer. The Helmholtz equation was again solved in the atmospheric layer using cylindrical coordinates and a point source. The homogeneous Helmholtz equation was again used in the porous layer, with a Green's function representation of the membrane response.

In the soil resonance predictions, pressure was plotted as a function of frequency, and the resonances appear as local minimums and maximums. A MATLAB^{TM} user interface was created to allow researchers to access the soil resonance information particular to their experiment. The resonances of the membrane-soil model were determined using MATLAB^{TM}; describing the effects of frequency, depth, density, and sound, to include radius and elastic parameters of the membrane. Comparison of the results (involving the fluid surface particle velocity profiles across the target) has been made with experiments reported in the literature to evaluate the model's usefulness.

Keywords: landmine, waveguide, Sabatier, scattering

Chapter 1

Acknowledgements

I would like to thank Prof. James Buchanan, Prof. Murray Korman, and Prof. Reza Malek-Madani for the long hours spent working on this problem and this project,

Prof. Kevin McIlhany, for the long hours spent working with COMSOL®,

Dr. David Burnett, of the Naval Surface Warfare Center, for his assistance with COMSOL®,

Dr. James Sabatier, of the National Center for Physical Acoustics, for his information and support,

Dr. Harley Cudney and Dr. Keith Wilson, of the U.S. Army Corps of Engineers, for their assistance and data in the user interface, and the

United States Naval Academy Mathematics Department and Physics Department, for their support and assistance with administrative portions of this project.

adgoansdgkmlasdfion

adgfonisadgnfsdomafsd

asgdonsdfmacong

sgosomgaognsdfmadcongbasd

Chapter 2

Introduction

Landmines first appeared in warfare in the third century BC, however, the first use of non-metallic landmines was in World War I. Due to metal shortages at the end of the war, Germany began implementing primitive wooden antitank mines against Allied forces. However, the Germans reverted to metallic mines by the start of the Second World War. By 1942, Allied landmine detection technology had advanced significantly: from a long stick with a metal point used to prod the ground, to the conventional metal detectors common today. The natural solution was to begin making landmines from other materials, notably wood, Bakelite (a simple plastic), and glass. For example, the German Topfmine was an antitank mine made of plastic, wood, glass, and cardboard; it required over 300 pounds of pressure to be applied to its top to discharge the mine. Approximately 800,000 of these mines were constructed during the last year of the war.[1] Similar to the Topfmine, the Glasmine-43 was the non-metallic antipersonnel landmine developed by the Germans. Each mine was laid precisely and strategically, and the Germans kept meticulous records of their minefields throughout the war. Non-metallic landmines were also used in both the Korean and Vietnam Wars. Frequently, the landmines that were laid in both of these countries and around the world during the Cold War era were not documented, and the rare instances of documentation are no longer accurate due to soil shifting over time.

Today, Afghanistan is one of the most heavily mined nations in the world.[2] The first widespread, massive deployment of landmines in Afganistan was on the Pakistan and Iran borders by the Soviet Army to enforce a policy of area-denial around 1979. U.S. soldiers continue to lose their lives to landmines in Operation Enduring Freedom.[3] Landmines also affect the civilian population. Red Cross estimates indicate 17 in 1,000 children in Afghanistan have been injured or killed by a landmine.[4] The area that could not be controlled by the Soviets in 1979 is still unavailable to the people of Afghanistan, who are mostly farmers in need of more crop land. A cost effective method for landmine detection and removal is essential for political and economic reasons in this nation.

Landmines are used in a wide variety of political and economic situations, including wars, bor-

[1] [28] pg. 113.
[2] [7], pg. 131.
[3] [1], pg. 1.
[4] [14], pg. 1.

der disputes, conflicts, and coup d'etats.[5] The broad usage of landmines is partially made possible by a variety of methods of detonation, including a change in pressure from personnel or tanks transiting over them, trip wires, or remote firing from a predetermined location.[6] Additionally, the low cost (between $3-5 U.S.) [7] and effectiveness of killing or maiming humans and destroying machinery has made the landmine a tactical military asset. For factions seeking to overthrow a government, the laying of landmines instills both chaos and panic within the civilian population that the government is seemingly powerless to stop. Landmines are present in approximately one-third of developing nations and continue to kill and affect lives long after wars and conflicts have ended. According to the United Nations in 1995, over 100 million landmines were in use in conflicts throughout the world.[8] Estimates of the cost to remove landmines range from $200 (U.S.) to over $1000 (U.S.) per mine,[9] making removal by many third world governments economically impossible.

The acoustic landmine detection problem has gained much interest in the scientific research community in landmine detection and removal over the last ten years. Some landmine detection equipment has not been updated significantly since World War II, and the current techniques using ground penetrating radar still need to be perfected for finding non-metallic landmines due to the high rate of false alarms. Radar also generates large numbers of false alarms due to soil inhomogenities, that is, it cannot discriminate between the frequency response of the soil inhomogenities and landmine resonances. To further complicate matters, the technology for detecting non-metallic landmines is very limited; the only effective known methods are seismic acoustic wave penetration and vapor detection. Vapor detection, a chemical method for detection which analyzes gas emissions from the mine, is slow, expensive, and dangerous. Additionally, this method only indicates that a mine was present at some time in the soil, and cannot predict its exact location, making it particularly dangerous. Tests require new chemicals that are not reusable, which increase the cost of landmine detection.

Sabatier and Waxler's work at the National Center for Physical Acoustics (NCPA), supported by the U.S. Army, Navy, and Marine Corps de-mining programs, suggests that acoustic and seismic technology may be the most cost effective and accurate way to detect landmines.[10] NCPA's work on acoustic to seismic landmine detection is one of the most promising methods for detecting non-metallic landmines at shallow burial depths with low false-alarm rates. A loud speaker acts as an airborne source, generating low-frequency waves which enter the soil over a buried target. At a specific frequency known as the resonant frequency, the mine will "vibrate" with a relatively large amplitude, imparting a certain velocity on the soil particles above it that is detected at the surface by a scanning Laser Doppler Vibrometer system. In field tests with the Valmara VS 1.6 plastic-cased, anti-tank landmine, the system has worked very well, with a probability of detection exceeding 95% in desert environments.[11] There was only one false alarm during the experiment,

[5] [7], pg. 126.
[6] [21], pg. 18.
[7] [14], pg. 1.
[8] [14], pg. 1.
[9] [14], pg. 1.
[10] [19], pg. 149.
[11] [19], pg. 28.

despite rocky soil in an Arizona desert test site. If the soil surface velocity plots could be predicted mathematically under a variety of conditions, the physical system would be able to better discriminate between the frequency response of the false alarms and the landmine in more challenging environments.

Sabatier suggests that the success of airborne acoustics in landmine detection depends on three assumptions. The first assumption is that landmines are significantly more acoustically compliant than soil and other natural materials (rocks, roots, etc.). Second, the acoustic properties of a landmine case are assumed to further differentiate the mine through contrast with the porous soil. Last, the interface between the soil and mine is thought to be non-linear, which implies that the interface relation is complicated, further contrasting the mine from the soil (although it is assumed linear in this paper for simplicity). The nonlinearity of soil vibration and soil interacting with the top plate of the mine case is a future problem that could be developed from this Trident Research Project down the road. The use of algorithms implemented in the experimental testing has resulted in "almost perfect detection and zero false alarm rates."[12]

Sabatier also indicates that acoustic to seismic mine detection works best in a dry, sandy soil environment.[13] However, he also states that landmine detection is immune to atmospheric moisture, weather, other acoustic (noise) sources, and natural materials, according to his experiments.[14] Any man-made objects (soda cans, etc.) scattered in the soil may be detected as false positives. Large amounts of vegetation or grass, as well as frozen soil, appear to compromise detection, since the majority of acoustic energy is absorbed or deflected. Despite these limitations, Sabatier is highly encouraged by the results that he has been able to obtain in such a short time, and reports that the system should be ready for implementation in 4-5 years.[15]

The goal of this project is to theoretically predict the acoustic to seismic soil vibration velocity profiles that are related to the experiments reported by Sabatier and others. The landmine scattering problem has not been solved analytically because of its complexity, but has been solved computationally for one special case.[16] The two mathematical scattering geometries include (1) an atmospheric layer over a single layer of soil bounded by a rigid substrate, and (2) the simplified geometry demonstrating propagation through a homogeneous soil onto a rigid surface with a circular clamped vibrating membrane over a cavity in the rigid surface. Secondly, the models include soil variations, angle of incidence, effects of acoustic wave scattering, size and other characteristics of the target, and depth of the target from the surface through the programs devised for each geometry (with the exception of soil variation, which is incorporated individually into the program).

The mathematical modeling of the wave equation includes implementation of various computational tools, including MATLAB™ and COMSOL™. COMSOL™ is a finite element partial differential equation solver, which includes a specialized acoustics interface. COMSOL™ was used as a method of comparison to evaluate the effectiveness of the model. Both methods are

[12][19], pg. 151.
[13][27], pg. 1-2.
[14][27], pg. 1-2.
[15][19], pg. 151.
[16][27].

compared to verify accuracy. Finally, a user friendly interface program allows researchers in the acoustic field to use the mathematical profile predictions in this project. The user interface will hopefully contribute to future research in the acoustics detection of the buried landmine problem.

Chapter 3

Background and Prerequisites

3.1 Derivation of the Wave Equation

3.1.1 Overview

The derivation of the wave equation presented in this paper follows the argument in Morse and Ingard,[1] and Zwikker and Kosten[2]. Suppose a fluid infiltrates a rigid porous solid that resists the fluid's flow and allows for changes the properties of the fluid. The pores of the solid material are randomly interconnected, and it is assumed that fluid flow in each direction has identical acoustic impedance. Let $\mathcal{H}$ denote the porosity, the ratio of the fluid volume to the total volume. Let w be the mean flow velocity for the porous solid. The fluid has uniform density (ρ), pressure (P), entropy (S), and temperature (T) in the absence of sound. When an incident sound wave impacts the fluid, the pressure changes to $\overline{P} = P + p\,(x,t)$, assuming the wave is one dimensional and propagating in the x direction. The density, entropy, and temperature also change to $\overline{\rho} = \rho + \delta\,(x,t)$, $\overline{S} = S + s\,(x,t)$, and $\overline{T} = T + \tau\,(x,t)$, respectively. Assume that p, δ, s, and τ are small when compared with P, ρ, S, and T, respectively. The only energy resulting from the acoustic motion is mechanical, since other forms of energy are eliminated by assuming the medium is nonviscous and non-conducting.

3.1.2 Adiabatic Compressibility

Due to the acoustic motion being completely mechanical, the forces in the problem are limited to compressive elasticity. Morse and Ingard conclude that at frequencies lower than 1 GHz, compression is adiabatic.[3] The compression is referred to as adiabatic because no heat is transferred to or from the fluid during the compression. Thus, for an ideal gas, $\overline{\rho} = \overline{\rho}\left(\overline{P}, \overline{S}\right)$, and therefore,

$$\overline{\rho}\left(\overline{P}, \overline{S}\right) = \rho\,(P,S) + \frac{\partial}{\partial P}\rho\,(P,S)\,p + \frac{\partial}{\partial S}\rho\,(P,S)\,s$$

[1] [22], pg. 253.
[2] [29], pg. 18.
[3] [22], pg. 230.

to the first order. Since adiabatic compressibility implies $s = 0$,

$$\overline{\rho}\left(\overline{P},\overline{S}\right) = \rho\left(P,S\right) + \frac{\partial}{\partial P}\rho\left(P,S\right)p = \rho + \rho\kappa_s p \tag{3.1}$$

where the adiabatic compressibility is

$$\kappa_s = \frac{1}{\rho}\frac{\partial\rho}{\partial P}.$$

Since $P = f\left(S\right)\rho^\gamma$ for an ideal gas (where $f\left(S\right)$ is a function of entropy and γ is the ratio of the specific heat at constant pressure of the gas to the specific heat at constant volume, ie, $\gamma = \frac{C_p}{C_v}$),

$$1 = f\left(S\right)\gamma\rho^{\gamma-1}\frac{\partial\rho}{\partial P}$$

$$\frac{\partial\rho}{\partial P} = \frac{1}{f\left(S\right)\gamma\rho^{\gamma-1}} = \frac{1}{\frac{P}{\rho^\gamma}\gamma\rho^{\gamma-1}} = \frac{\rho}{\gamma P},$$

and therefore,

$$\kappa_s = \frac{1}{\gamma P}.$$

From equation (3.1),

$$\delta = \rho\kappa_s p. \tag{3.2}$$

3.1.3 Conservation of Momentum

Consider a small volume $\Delta V = \Delta x\Delta y\Delta z$ moving in a vector velocity field w. The pressure exerted on the x-faces of the cube is

$$\begin{aligned} p\left(x,y,z,t\right)\Delta y\Delta z - p\left(x+\Delta x,y,z,t\right)\Delta y\Delta z &= \frac{p\left(x,y,z,t\right) - p\left(x+\Delta x,y,z,t\right)}{\Delta x}\Delta V \\ &\approx -\frac{\partial}{\partial x}p\left(x,y,z,t\right)\Delta V. \end{aligned}$$

The total pressure exerted on the entire cube is then $-\nabla p\Delta V$. Newton's second law gives

$$\rho\Delta V\frac{\partial\mathbf{w}}{\partial t} = -\nabla p\Delta V, \tag{3.3}$$

where ∇ is the vector differential operator. Gravitational force is not included in this derivation. (See the discussion in Appendix) The volume element follows a trajectory $\langle x(t), y(t), z(t)\rangle$. The velocity vector is tangent to the curve: $\mathbf{w} = \langle w_x, w_y, w_z\rangle = \langle x'(t), y'(t), z'(t)\rangle$. From the chain rule,

$$\begin{aligned} \frac{d}{dt}\mathbf{w}\left(x(t),y(t),z(t),t\right) &= \left(\frac{\partial}{\partial x}\mathbf{w}\right)x'(t) + \left(\frac{\partial}{\partial y}\mathbf{w}\right)y'(t) + \left(\frac{\partial}{\partial z}\mathbf{w}\right)z'(t) + \frac{\partial}{\partial t}\mathbf{w} \\ &= w_x\frac{\partial}{\partial x}\mathbf{w} + w_y\frac{\partial}{\partial y}\mathbf{w} + w_z\frac{\partial}{\partial z}\mathbf{w} + \frac{\partial}{\partial t}\mathbf{w} \\ &= \left(\mathbf{w}\cdot\nabla\right)\mathbf{w} + \frac{\partial}{\partial t}\mathbf{w} \end{aligned}$$

From equation (3.3)

$$\rho\left(\left(\mathbf{w}\cdot\nabla\right)\mathbf{w}+\frac{\partial}{\partial t}\mathbf{w}\right)=-\nabla p.$$

Assuming the components of $\mathbf{w}$ are small, the linearized equation for continuity of momentum is

$$\rho\frac{\partial\mathbf{w}}{\partial t}=-\nabla p \tag{3.4}$$

3.1.4 Equation of Continuity (or Conservation of Mass)

The mass in a small volume element is

$$m=\iiint_R\overline{\rho}dV,$$

where m is mass and R is a small volume element. Therefore,

$$\frac{dm}{dt}=\iiint_R\frac{\partial\overline{\rho}}{\partial t}dV$$

$\frac{dm}{dt}$ represents the mass flowing into or out of R. Assuming conservation of mass,

$$\frac{dm}{dt}=-\iint_{\partial R}\overline{\rho}\mathbf{w}\cdot\overrightarrow{n}\,dS$$

where $\overrightarrow{n}$ is the outward normal vector to ∂R. According to the divergence theorem,

$$\frac{dm}{dt}=-\iiint_R\nabla\cdot\left(\overline{\rho}\mathbf{w}\right)dV.$$

Therefore,

$$\iiint_R\frac{\partial\overline{\rho}}{\partial t}dV=-\iiint_R\nabla\cdot\left(\overline{\rho}\mathbf{w}\right)dV$$

and

$$\iiint_R\left(\frac{\partial\overline{\rho}}{\partial t}+\nabla\cdot\left(\overline{\rho}\mathbf{w}\right)\right)dV=0.$$

Letting R shrink down to a point, (x,y,z), yields

$$\frac{\partial\overline{\rho}}{\partial t}+\nabla\cdot\left(\overline{\rho}\mathbf{w}\right)=0.$$

Assuming $\mathbf{w}$ is small (and since δ was already assumed small), $\left(\rho+\delta\right)\mathbf{w}\approx\rho\mathbf{w}$. Thus, the linearized equation for conservation of mass is

$$\frac{\partial\delta}{\partial t}+\nabla\cdot\left(\rho\mathbf{w}\right)=0$$

and from equation (3.2)

$$\kappa_s\frac{\partial p}{\partial t}=-\nabla\cdot\left(\rho\mathbf{w}\right). \tag{3.5}$$

3.1.5 The One Dimensional Wave Equation

From conservation of momentum, (eqn. (3.4)).

$$\rho \frac{\partial w_x}{\partial t} = -\frac{\partial p}{\partial x} \tag{3.6}$$

where w is velocity. The equation for continuity for the density is

$$\frac{\partial \delta}{\partial t} = -\frac{\partial (\rho w_x)}{\partial x}.$$

If we assume that the change in pressure is related to the change in density by $\delta(x,t) \simeq \rho \kappa_s p(x,t)$ (eqn. 3.2), then

$$\rho \kappa_s \frac{\partial p}{\partial t} = -\rho (1 + \kappa_s p) \frac{\partial w_x}{\partial x} - \rho \kappa_s w_x \frac{\partial p}{\partial x} \tag{3.7}$$

Since p, δ, and τ are small in comparison to P, ρ, and T, the second and third order terms containing p, δ, and τ in both equation (3.6) and equation (3.7) are neglected. Therefore, eqns. (3.6) and (3.7) are now

$$\frac{\partial p}{\partial x} = -\rho \frac{\partial w_x}{\partial t}$$
$$\kappa_s \frac{\partial p}{\partial t} = -\frac{\partial w_x}{\partial x}$$

According to Morse and Ingard,[4]

> The first of these states that a pressure gradient [along the x-direction] produces an acceleration of the fluid; the second states that a velocity gradient [along the x-direction] produces a compression of the fluid.

By differentiating the first equation by x and the second equation by t eliminates w_x, thereby yielding the acoustic motion equation

$$\frac{\partial^2 p}{\partial x^2} = \frac{1}{c^2} \frac{\partial^2 p}{\partial t^2}, \text{ where } c^2 = \frac{1}{\kappa_s \rho}.$$

The one-dimensional wave equation above can be easily extended to the three-dimensional case. Equation (3.6), relating pressure gradient to fluid acceleration, becomes

$$(\rho + \delta) \frac{\partial \mathbf{w}}{\partial t} = -\nabla p$$

where $\mathbf{w}$, velocity, is a vector. Equation (3.7), relating velocity and compression of the fluid, is now

$$\frac{\partial \delta}{\partial t} = -\rho (1 + \kappa_s p) \nabla \cdot \mathbf{w} - \kappa_s \rho \mathbf{w} \cdot (\nabla p)$$

[4] [22], pg. 242.

If the same assumptions from the one-dimensional case regarding the significance of small quantities are applied, the equations are now

$$-\nabla p = \rho \frac{\partial \mathbf{w}}{\partial t}$$

$$\kappa_s \frac{\partial \delta}{\partial t} = -\nabla \cdot \mathbf{w}$$

By taking the divergence of the first equation, and solving the second to eliminate $\mathbf{w}$ gives

$$\nabla \cdot \nabla p = \nabla^2 p = \kappa_s \rho \frac{\partial^2 p}{\partial t^2} = \frac{1}{c^2} \frac{\partial^2 p}{\partial t^2}$$

commonly known as the three-dimensional wave equation.

3.2 Application to the Two Layer Waveguide Problem

The approach to the two layer waveguide problem begins with the partial differential equation governing the propagation of waves through a medium, also known as "the wave equation" in homogeneous form

$$\nabla^2 p - \frac{1}{c^2} \frac{\partial^2 p}{\partial t^2} = 0. \tag{3.8}$$

Time-harmonic motion refers to the repetition of function behavior within a specified period. Let $T(t) = Ae^{-i\omega t}$, where $i = \sqrt{-1}$, so that T is time-harmonic. Solutions to the wave equation are of the form $p = P(r, \theta, z)\, T(t)$. Then

$$\nabla^2 (PT) - \frac{1}{c^2} \frac{\partial^2 (PT)}{\partial t^2} = 0.$$

Recognizing that ∇ does not contain a t component and the time derivative does not concern P,

$$T \nabla^2 P - \frac{1}{c^2} P \frac{\partial^2 T}{\partial t^2} = 0.$$

Assuming time-harmonic motion,

$$\nabla^2 P - \frac{1}{c^2} \left(-\omega^2\right) P = 0.$$

Simplification gives

$$\nabla^2 P + \frac{\omega^2}{c^2} P = 0$$

and the substitution of the wave number notation, $k = \frac{\omega}{c}$, results in

$$\nabla^2 P + k^2 P = 0. \tag{3.9}$$

Equation (3.9) is known as the Helmholtz Equation, and describes acoustic sound waves in terms of their pressure, P. For the remainder of this paper, no distinction will be made between lower case p and upper case P, that is $P = p$, referred to as "pressure".

3.3 Fluid Flow Through a Porous Media

According to Morse and Ingard,[5] the equation of continuity (equation (3.5)) becomes

$$-\nabla \cdot \mathbf{w} = \kappa_p \mathcal{H} \frac{\partial p}{\partial t}$$

for fluid flow through a rigid, porous solid. κ_p replaces κ_s, and is the effective compressibility of the fluid in the pores. According to Morse and Ingard, $\kappa_p = \kappa_s$ at high frequencies, since the behavior of the fluid in the pores is best modeled adiabatically. At low frequencies, the presence of the solid material tends to hold the temperature constant, thus, $\kappa_p = \kappa_T$, the isothermal compressibility of the fluid.[6] Conservation of momentum is also changed within the porous medium, and becomes

$$i\omega\rho_p \left[1 + i\frac{\sigma}{\omega\rho_p}\right] \mathbf{w} = \nabla p,$$

where σ is the flow resistivity, and ρ_p is the effective density of the fluid in the pores. ρ_p is expected to be 1.5 to 5 times greater than ρ, the original fluid density, because of the tortuosity of the medium. The tortuosity parameter measures the deviation of the pore orientation of the medium from uniform.[7] A commonly used mathematical definition of tortuosity is $\left(\frac{m_d}{E_l}\right)^2$, where m_d is the length of the mean flow path between two points and E_l is the linear distance between the two points. Let $\mathbf{w} = -\nabla\Psi$. Then $p = \rho_p\left(\partial\Psi/\partial t\right) + \sigma\Psi$, and

$$\nabla^2\Psi = \kappa_p\rho_p\mathcal{H}\frac{\partial^2\Psi}{\partial t^2} + \kappa_p\sigma\mathcal{H}\frac{\partial\Psi}{\partial t}.$$

With the exception of the last term, this is the wave equation derived in equation (3.9), with a wave velocity of $c_p = \sqrt{1/\kappa_p\rho_p\mathcal{H}}$. Assuming time-harmonic motion, as in the derivation above, gives

$$\nabla^2\Psi + \left(\frac{\omega}{c_e}\right)^2\Psi = 0, \tag{3.10}$$

where

$$c_e = c_p\frac{1}{\sqrt{1 + \frac{i\sigma}{\rho_p\omega}}}.$$

Note that since $p = (-i\omega\rho_p + \sigma)\Psi$ in the time-harmonic case, p also satisfies equation (3.10).

[5] [22], pg. 253.
[6] [22], pg. 253.
[7] [22], pg. 253.

Chapter 4

The Two Layer Waveguide

The two layer waveguide problem is the simplest model of the soil-air interface (Figure 4.1). A layer of soil of height z_s is bounded by a rigid surface on the bottom, and by the atmosphere on the top. The partial differential equation governing wave propagation in the soil and air is the Helmholtz Equation, eqn (3.9), which will be solved in cylindrical coordinates.

4.1 Analytical Approach and Separation of Variables

First consider the homogeneous problem. Wave propagation through the air and soil, respectively, is described through the following two equations

$$\nabla^2 p_a + k_a^2 p_a = 0$$

$$\nabla^2 p_s + k_s^2 p_s = 0,$$

where $k_a = \frac{\omega}{c_a}$ and $k_s = \sqrt{\frac{\omega^2 + \frac{i\omega\sigma}{\rho_p}}{c_s^2}}$, from substitutions into equations (3.8) and (3.10). Since the partial differential equations are identical with the exception of the subscripts that determine the appropriate boundary conditions, a "generalized form" of the Helmholtz Equation is used until boundary conditions with respect to depth are applied. The generalized form of the Helmholtz Equation neglects the difference in acoustic properties between the atmospheric and soil layers, which do not effect the general separation of variables solution with regard to the radial or angular conditions.

$$\nabla^2 p + k^2 p = 0$$

Cylindrical coordinates were selected due to the cylindrical features of the membrane problem.[1] The Helmholtz Equation, rewritten in cylindrical coordinates, is

$$\frac{1}{r}\frac{\partial}{\partial r}\left(r\frac{\partial p}{\partial r}\right) + \frac{1}{r^2}\frac{\partial^2 p}{\partial \theta^2} + \frac{\partial^2 p}{\partial z^2} + k^2 p = 0$$

[1] [16], pg. 2051.

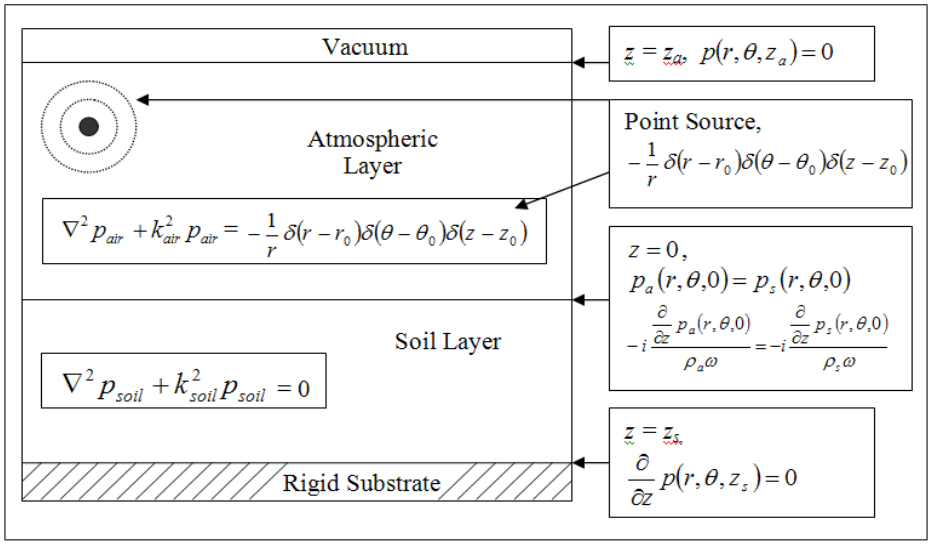

Figure 4.1: A mathematical schematic of the two layer waveguide in cylindrical coordinates displaying this paper's notation. ρ_a and ρ_s are the density of air and soil, respectively, and ω is the angular frequency imparted from the point source.

Separation of variables, assuming $p(r,\theta,z) = F(r)\,G(\theta)\,Z(z)$, yields

$$\frac{1}{r}\frac{\frac{\partial}{\partial r}(rF'(r))}{F(r)} + \frac{1}{r^2}\frac{G''(\theta)}{G(\theta)} = -k^2 - \frac{Z''(z)}{Z(z)}. \tag{4.1}$$

Equation (4.1) indicates that the two arguments on either side of the equation must equal the same constant. This assumption is valid because differentiation of both sides with respect to z implies the derivative of $\frac{Z''(z)}{Z(z)}$ is 0. Therefore, $\frac{Z''(z)}{Z(z)}$ is a constant. This argument works for each variable in equation (4.1). Since sound waves propagate in a way that resembles sinusoidal functions (and not exponentials), choose $-\mu$ be an arbitrary constant. Then

$$-\frac{Z''(z)}{Z(z)} - k^2 = -\mu \tag{4.2}$$

and

$$\frac{1}{r}\frac{\frac{\partial}{\partial r}(rF'(r))}{F(r)} + \frac{1}{r^2}\frac{G''(\theta)}{G(\theta)} = -\mu. \tag{4.3}$$

Continuing with separation of variables, consider equation (4.3). Multiplication by r^2 and rearranging yields

$$r\frac{\frac{\partial}{\partial r}(rF'(r))}{F(r)} + r^2\mu = -\frac{G''(\theta)}{G(\theta)}. \tag{4.4}$$

4.1.1 Theta Equation

Equation (4.4) indicates that the two arguments must equal constants, from the same argument given for equation (4.1). Choose λ to create sinusoidal functions that will satisfy the periodicity conditions in equation (4.8).

$$-\frac{G''(\theta)}{G(\theta)} = \lambda \tag{4.5}$$

$$r\frac{\frac{\partial}{\partial r}\left(rF'(r)\right)}{F(r)} + \mu r^2 = \lambda \tag{4.6}$$

Equation (4.5) is equal to

$$G''(\theta) + \lambda G(\theta) = 0 \tag{4.7}$$

Assume $\lambda > 0$. ($\lambda \leq 0$ result in trivial solutions) This assumption is made based on the periodicity condition implied by the problem configuration.[2] Therefore, solutions are of the form

$$G(\theta) = A\cos\left(\sqrt{\lambda}\theta\right) + B\sin\left(\sqrt{\lambda}\theta\right)$$

Boundary conditions are now imposed, as described by the periodicity condition below. The solution G must therefore satisfy the periodicity conditions

$$G(-\pi) = G(\pi) \tag{4.8}$$

$$G'(-\pi) = G'(\pi)$$

for continuity at π. After imposing the boundary conditions, the solution becomes

$$G(\theta) = A\cos(m\theta), \tag{4.9}$$

with $\lambda = m^2$ where $m = 0, 1, 2, ..$

Orthogonality of the Theta Eigenfunctions

Orthogonality is a particularly useful tool in solving partial differential equations. Because orthogonality will be used in later portions of the mathematical analysis of this problem, it is necessary to prove the orthogonality of the theta-dependent function, G. By definition, a set of functions, $\{\phi_n\}_{n=1}^{\infty}$ is orthogonal on $[0, L]$ if $\int_0^L \phi_n(x)\,\phi_m(x)\,dx = 0$, when $n \neq m$. Using the trigonometric identity $\cos(a)\cos(b) = \frac{1}{2}\left[\cos(a+b) + \cos(a-b)\right]$, we obtain that

$$\begin{aligned} & \int_{-\pi}^{\pi} A_n\cos(n\theta)\,A_m\cos(m\theta)\,d\theta \\ = \; & \frac{A_nA_m}{2}\int_{-\pi}^{\pi}\left[\cos\left((n+m)\theta\right) + \cos\left((n-m)\theta\right)\right]d\theta \end{aligned}$$

[2] [11], pg. 307.

Performing the integral results in

$$\delta_{nm} = \left\{ \begin{array}{ll} 1 & m = n \\ 0 & m \neq n \end{array} \right\}$$

The Kronecker delta function results from $A_n = \sqrt{\frac{1}{\pi}}$ in the case where $m = n$. This selection of A_n forms an orthogonal, normalized basis.

4.1.2 Radial Condition

The radial condition on pressure is established through solving for $F(r)$ (eqn.(4.6))

$$r\frac{\partial}{\partial r}\left(rF'(r)\right) = -\mu r^2 F(r) + m^2 F(r).$$

Rearrangement and multiplication by r^2 results in

$$r^2 F''(r) + rF'(r) + \left(\mu r^2 - m^2\right) F(r) = 0. \tag{4.10}$$

Let $\zeta^2 = \mu r^2$. Then equation (4.10) becomes a Bessel Differential Equation[3]

$$\zeta^2 \widetilde{F}''(\zeta) + \zeta \widetilde{F}'(\zeta) + \left(\zeta^2 - m^2\right) \widetilde{F}(\zeta) = 0.$$

Solutions to the Bessel Differential Equation are known as Bessel Functions of the first and second kind. Mathematically, these are represented by $J_m(\zeta)$and $Y_m(\zeta)$. By the principle of superposition, any linear combination of Bessel functions is also a solution to the Bessel Differential Equation. One of these combinations is known as a Hankel Function (represented by $H_m^{(1)}(\zeta)$), which is linear combinations of Bessel Functions of the first and second kind

$$\widetilde{F}_\lambda(\zeta) = H_m^{(1)}(\zeta) = J_m(\zeta) + iY_m(\zeta) \tag{4.11}$$

$$\widetilde{F}_\lambda(\zeta) = H_m^{(2)}(\zeta) = J_m(\zeta) - iY_m(\zeta). \tag{4.12}$$

4.1.3 Depth Equation

We now consider the z equation, equation (4.2), written in terms of the value of z.

$$\left\{ \begin{array}{ll} -\frac{Z_a''(z)}{Z_a(z)} - k_a^2 = -\mu & 0 \leq z \leq z_a \\ -\frac{Z_s''(z)}{Z_s(z)} - k_s^2 = -\mu & z_s \leq z < 0 \end{array} \right. .$$

Rearrangement, multiplication by $-Z(z)$, and subtraction of $(k^2 - \mu)$ results in

$$\left\{ \begin{array}{ll} Z_a''(z) + \left(k_a^2 - \mu\right) Z_a(z) = 0 & 0 \leq z \leq z_a \\ Z_s''(z) + \left(k_s^2 - \mu\right) Z_s(z) = 0 & z_s \leq z < 0 \end{array} \right. . \tag{4.13}$$

[3] [11], pg. 306.

Suppose $k_a^2 > \mu$. Solutions are then of the form

$$Z(z) = \begin{cases} A\cos\left(\sqrt{k_a^2-\mu}z\right) + B\sin\left(\sqrt{k_a^2-\mu}z\right) & 0 \le z \le z_a \\ C\cos\left(\sqrt{k_s^2-\mu}z\right) + D\sin\left(\sqrt{k_s^2-\mu}z\right) & z_s \le z < 0 \end{cases}.$$

As shown in Figure (4.1), there are several boundary conditions that define the solution in the z direction. First, it is necessary to define an upper limit, z_a, for the atmosphere when using a point source. At and above this limit, the atmosphere is assumed to be a vacuum, that is, the pressure is 0. Mathematically, this is written as

$$p(z_a) = 0. \tag{4.14}$$

At the soil-rigid substrate interface, it is expected that some of the energy is reflected, while some energy is also absorbed by the rigid substrate. However, the pressure at the interface should be constant. Therefore,

$$\frac{\partial}{\partial z}p(z_s) = 0 \tag{4.15}$$

At the interface between the atmosphere and soil, ($z = 0$), the atmospheric pressure should be equal to the acoustic pressure in the soil (Continuity of Pressure).

$$p_a(0) = p_s(0) \tag{4.16}$$

Similarly, at the interface between the atmosphere and soil, the velocity of the acoustic wave should be equal in both the atmosphere and soil. Acoustic impedance relates the fluid velocity to the acoustic pressure.[4] Mathematically, acoustic impedance[5] is the ratio between acoustic pressure, p, and fluid velocity, represented by the following equation in this problem

$$-i\frac{\frac{\partial}{\partial z}p_a(0)}{\rho_a\omega} = -i\frac{\frac{\partial}{\partial z}p_s(0)}{\rho_s\omega}. \tag{4.17}$$

Note that this is also continuity of velocity across the air-soil boundary. Equation (4.17) is derived by assuming time-harmonic oscillations in equation (3.4). Applying the boundary conditions (eqns. (4.14), (4.15), (4.16), and (4.17)) results in

$$Z(z) = \begin{cases} B_1\left[\cos\left(\sqrt{k_s^2-\mu}z_s\right)\sin\left(\sqrt{k_a^2-\mu}(z_a-z)\right)\right] & 0 \le z \le z_a \\ B_1\left[\sin\left(\sqrt{k_a^2-\mu}z_a\right)\cos\left(\sqrt{k_s^2-\mu}(z-z_s)\right)\right] & z_s \le z < 0 \end{cases},$$

where B_1 is an arbitrary constant. From the boundary conditions,

$$\begin{bmatrix} \sin\left(\sqrt{k_a^2-\mu}z_a\right) & \cos\left(\sqrt{k_s^2-\mu}z_s\right) \\ i\frac{\left(\cos z_a\sqrt{k_a^2-\mu}\right)\sqrt{k_a^2-\mu}}{\rho_a\omega} & -i\frac{\left(\sin z_s\sqrt{k_s^2-\mu}\right)\sqrt{k_s^2-\mu}}{\rho_s\omega} \end{bmatrix}\begin{bmatrix} B \\ D \end{bmatrix} = \begin{bmatrix} 0 \\ 0 \end{bmatrix}.$$

[4] [22], pg. 376, 423.
[5] [22], pg. 259.

To ensure that B and D are non-zero, the eigenvalues, μ, must force the determinant of the coefficient matrix equal to zero. The determinant of the matrix, set equal to zero, is

$$\begin{aligned} & \rho_s \sqrt{k_a^2 - \mu} \cos z_a \sqrt{k_a^2 - \mu} \cos z_s \sqrt{k_s^2 - \mu} \\ & + \rho_a \sqrt{k_s^2 - \mu} \sin z_a \sqrt{k_a^2 - \mu} \sin z_s \sqrt{k_s^2 - \mu} \\ = \; & 0. \end{aligned} \tag{4.18}$$

The solutions to equation (4.18) must be found numerically. A MATLAB™ program was written to solve for the eigenvalues. In order to program this specific function into MATLAB™, it was necessary to perform a change of variables. This was done so that the eigenvalues would be evenly spaced, and thus, could be found numerically over a long range of values. Therefore, let $\kappa = z_a \sqrt{k_a^2 - \mu}$. So

$$\mu = k_a^2 - \left(\frac{\kappa}{z_a} \right)^2$$

and

$$\begin{aligned} & \rho_s \left(\cos(\kappa) \cos z_s \sqrt{k_s^2 - k_a^2 + \left(\frac{\kappa}{z_a} \right)^2} \right) \frac{\kappa}{z_a} \\ & + \rho_a \left(\sin(\kappa) \sin z_s \sqrt{k_s^2 - k_a^2 + \left(\frac{\kappa}{z_a} \right)^2} \right) \sqrt{k_s^2 - k_a^2 + \left(\frac{\kappa}{z_a} \right)^2} = 0. \end{aligned} \tag{4.19}$$

Using MATLAB™ and a program for the secant method[6], eigenvalues for the depth condition were determined.

Air and Soil Eigenvalues

Note that in equation (4.18), $\rho_a \ll \rho_s$. Therefore, eigenvalues occur when

$$\cos z_a \sqrt{k_a^2 - \mu} \cos z_s \sqrt{k_s^2 - \mu} \approx 0.$$

If κ is taken to be $z_a \sqrt{k_a^2 - \mu}$, then two sequences of eigenvalues exist; one sequence exists for the air eigenvalues and another for the soil eigenvalues. The air eigenvalues $(\kappa_{a,n})$ are given by

$$\kappa_{a,n} \approx (2n - 1) \frac{\pi}{2},$$

while the soil eigenvalues $(\kappa_{s,n})$ are given by

$$z_s \sqrt{k_s^2 - \mu_n} = z_s \sqrt{k_s^2 - k_a^2 + \left(\frac{\kappa_{s,n}}{z_a} \right)^2} \approx (2n - 1) \frac{\pi}{2},$$

[6] [17], pg. 70.

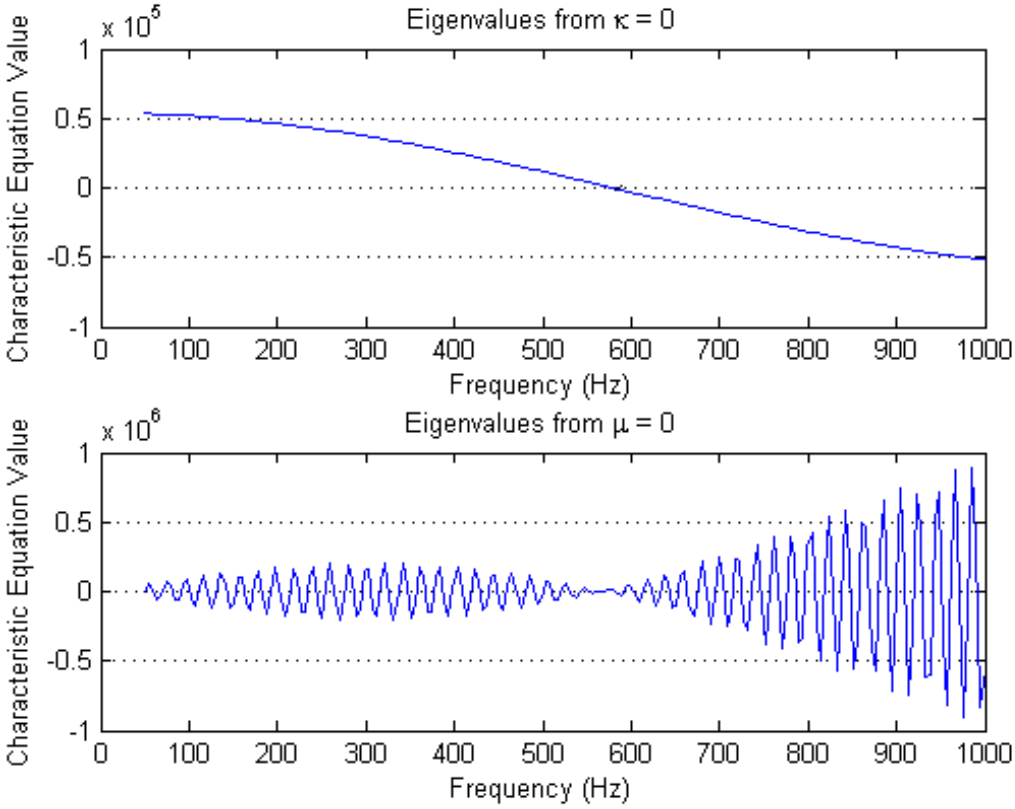

Figure 4.2: This figure shows the soil and air eigenvalue plots, respectively, for the two-layer waveguide.

or

$$\kappa_{s,n} \approx z_a \sqrt{\left[(2n-1)\frac{\pi}{2z_s}\right]^2 - k_s^2 + k_a^2}.$$

for $n \in \mathbb{N}$. Resonances occur when $\kappa_{s,n}$ ceases to be evanescent and when $\kappa_{s,n} \to 0$. Denote these as *E-resonances* and *Z-resonances*. An E-resonance occurs when $\kappa_{s,n} = k_a z_a$. This results in

$$k_s = \frac{2\pi f}{c_{p,s}} = (2n-1)\frac{\pi}{2\left|z_s\right|} \to f = c_{p,s}\frac{(2n-1)}{4\left|z_s\right|}.$$

Similarly, a Z-resonance occurs when $\kappa_{s,n} = 0$, which gives

$$f_n = (2n-1)\frac{c_a c_s}{4\left|z_s\right|\sqrt{c_a^2 - c_s^2}}.$$

The location of the E-resonances and Z-resonances are shown in Figure (4.2). Note that in this project, the input values that generated each graph are listed in the appendix.

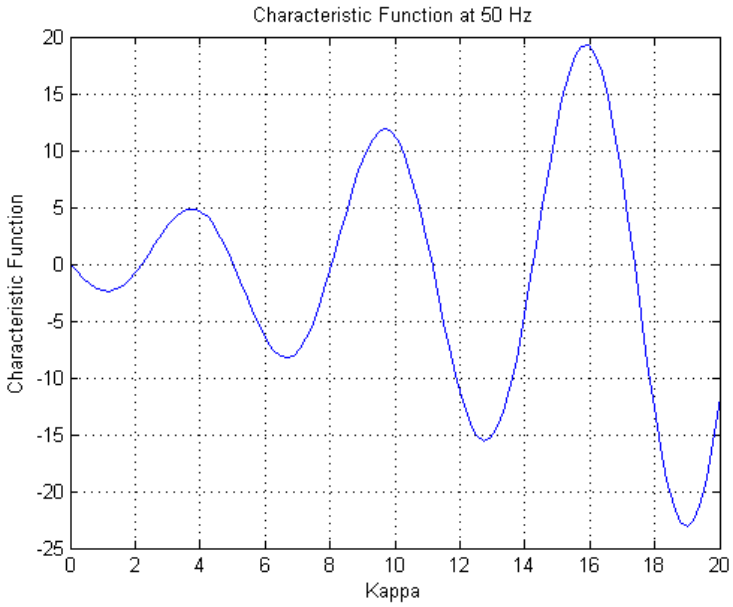

Figure 4.3: The first six eigenvalues for the depth condition. The κ values are limited from 0 to 20 in this graphic, for demonstration purposes. The zeros of the characteristic function determine the eigenvalues.

Eigenvalue Plots

Figure (4.3) shows a plot of the characteristic function (eqn. 4.19) at $f = 50$ Hz. The eigenvalues in this plot are the E-resonances. Figure (4.3) indicates the first of the κ eigenvalues occurs at approximately 2.2, a second eigenvalue of 5.3, and subsequent eigenvalues occurring at intervals of approximately π. A MATLAB^{TM} program based on the secant method of finding zeros of a function was written, since the secant method converges quickly when the interval containing a zero is known.[7] The eigenvalues depend upon the frequency. Figure (4.4) shows that the eigenvalues are quite sensitive to frequency. Note, however, that the spacing of the values of interest for κ remains at intervals of approximately π. Although there are exceptions to this spacing, the secant method has been highly effective in finding the κ which result in zeros of the eigenfunction.

Orthogonality of the Depth Condition

Using a Sturm-Liouville argument, which is outlined in Appendix (A), the eigenfunctions described in equation (4.18) were confirmed to be orthogonal. The weight function, as defined in Appendix (A), is

$$\chi(z) = \begin{cases} \rho_s & \text{when } 0 < z \leq z_a \\ \rho_a & \text{when } z_s \leq z < 0 \end{cases}$$

[7] [17], pg. 70.

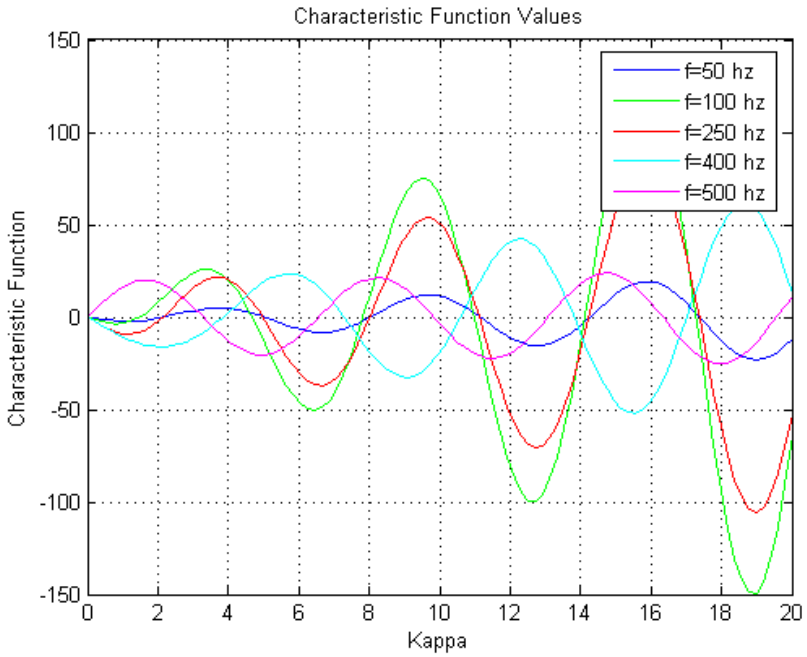

Figure 4.4: Eigenvalues for the depth condition at multiple frequencies, demonstrating the eigenfunction dependence on frequency.

4.2 Insertion of a Point Source

Insertion of a point source, also known as a unit impulse, in the upper waveguide layer leads to the boundary value problem

$$\nabla^2 p + k^2 p = -\frac{1}{r}\delta(r - r_0)\,\delta(\theta - \theta_0)\,\delta(z - z_0). \tag{4.20}$$

The Dirac delta "function", $\delta(x)$, is a mathematical representation of a function equal to ∞ at $x = 0$, and is equal to 0 for all other values.[8] In other words,

$$\delta(x - x_i) = \begin{cases} 0 & x \neq x_i \\ \infty & x = x_i \end{cases} \tag{4.21}$$

Additionally, the delta function has the property that the integral of a function, $f(x)$, multiplied by a delta function $\delta(x - x_0)$, over the interval (a, b) (assuming that $a \leq x_0 \leq b$)

$$\int_a^b f(x)\,\delta(x - x_0) = f(x_0). \tag{4.22}$$

Let $p(r, \theta, z) = \sum_{m=0}^{\infty}\sum_{n=1}^{\infty} F_{mn}(r)\,G_m(\theta)\,Z_n(z)$. Then $\nabla^2 p$ in cylindrical coordinates is represented by

$$\begin{aligned}\nabla^2 p &= \sum_{m=0}^{\infty}\sum_{n=1}^{\infty}\left[F''_{mn}(r) + \frac{1}{r}F'_{mn}(r)\right]G_m(\theta)\,Z_n(z) \\ &\quad -\frac{n^2}{r^2}F_{mn}(r)\,G_m(\theta)\,Z_n(z) + F_{mn}(r)\,G_m(\theta)\left[-\left(k^2 - \mu\right)Z_n(z)\right].\end{aligned}$$

Substitution into eqn (4.20) yields

$$\begin{aligned}&\sum_{m=0}^{\infty}\sum_{n=1}^{\infty}\left[F''_{mn}(r) + \frac{1}{r}F'_{mn}(r) - \frac{m^2}{r^2}F_{mn}(r) + \mu_n F_{mn}(r)\right]G_m(\theta)\,Z_n(z) \\ = \;& -\frac{1}{r}\delta(r - r_0)\,\delta(\theta - \theta_0)\,\delta(z - z_0).\end{aligned}$$

Multiplying by $G_k(\theta)\,\chi(z)\,Z_l(z)\,m$, integrating to use the orthogonality of the angular and depth equations, and using the properties of delta functions (eqns. (4.21) and (4.22)) gives

$$\begin{aligned}&\left(F''_{kl}(r) + \frac{1}{r}F'_{kl}(r) - \frac{m^2}{r^2}F_{kl}(r) + \mu_n F_{kl}(r)\right)\int_{-\pi}^{\pi} G_k(\theta)^2\,d\theta\int_{z_s}^{z_a}\chi(z)\,Z_l(z)^2\,dz \\ = \;& -\frac{1}{r}\delta(r - r_0)\,G_k(\theta_0)\,\chi(z_0)\,Z_l(z_0).\end{aligned}$$

[8] [11], pg. 392.

Letting

$$C_{kl} = \frac{G_k(\theta_0)\,\chi(z_0)\,Z_l(z_0)}{\int_{-\pi}^{\pi} G_k(\theta)^2\,d\theta \int_{z_s}^{z_a} \chi(z)\,Z_l(z)^2\,dz}$$

results in

$$rF''_{kl}(r) + F'_{kl}(r) + \left(r\mu_n - \frac{m^2}{r}\right) F_{kl}(r) = -C_{kl}\delta(r - r_0).$$

The equation above can be rewritten as

$$\frac{\partial}{\partial r}\left(rF'_{kl}(r)\right) + \left(r\mu_n - \frac{m^2}{r}\right) F_{kl}(r) = -C_{kl}\delta(r - r_0). \tag{4.23}$$

and integrating from $r_0 - \varepsilon$ to $r_0 + \varepsilon$ gives

$$\begin{aligned} & (r_0+\varepsilon)\,F'_{kl}(r_0+\varepsilon) - (r_0-\varepsilon)\,F'_{kl}(r_0-\varepsilon) + \int_{r_0-\varepsilon}^{r_0+\varepsilon}\left(r\mu_n - \frac{m^2}{r}\right) F_{kl}(r)\,dr \\ = \;& -C_{kl} \end{aligned}$$

Letting $\varepsilon \to 0$ and requiring that $F_{kl}(r)$ be continuous at $r = r_0$ gives the conditions

$$F_{kl}(r_0+) = F_{kl}(r_0-) \tag{4.24}$$

$$F'_{kl}(r_0+) - F'_{kl}(r_0-) = -\frac{1}{r_0}C_{kl}$$

Except at $r = r_0$, equation (4.23) is just Bessel's equation. Thus

$$G_{kl}(r) = \begin{cases} A_{kl}J_k\left(\sqrt{\mu_l}r\right), & 0 \le r < r_0 \\ B_{kl}H_k^{(1)}\left(\sqrt{\mu_l}r\right), & r_0 < r \end{cases}$$

is bounded at the origin and satisfies the Sommerfeld Radiation Condition.[9] Bessel functions of the first kind satisfy boundedness at the origin. The Sommerfeld Radiation Condition states that

$$\lim_{r\to\infty} \sqrt{r}\left(\frac{\partial}{\partial r}\mathbf{w} - ik\mathbf{w}\right) = 0.$$

Type 1 Hankel functions satisfy the radiation condition. Additionally, the Hankel function of the first kind indicates waves propagating outward from the source, which represents the physical reality. The conditions expressed in (4.24) require

$$A_{kl}J_k\left(\sqrt{\mu_l}r_0\right) - B_{kl}H_k^{(1)}\left(\sqrt{\mu_l}r_0\right) = 0$$

$$A_{kl}\sqrt{\mu_l}J'_k\left(\sqrt{\mu_l}r_0\right) - B_{kl}\sqrt{\mu_l}H_k^{(1)\prime}\left(\sqrt{\mu_l}r_0\right) = -\frac{1}{r_0}C_{kl}.$$

[9] [25], Ch. 6.32.

Solving for A_{kl} and B_{kl} results in

$$A_{kl} = -\frac{\frac{1}{r_0} C_{kl} H_k^{(1)}\left(\sqrt{\mu_l} r_0\right)}{-\sqrt{\mu_l} H_k^{(1)\prime}\left(\sqrt{\mu_l} r_0\right) J_k\left(\sqrt{\mu_l} r_0\right) + \sqrt{\mu_l} H_k^{(1)}\left(\sqrt{\mu_l} r_0\right) J_k'\left(\sqrt{\mu_l} r_0\right)} \tag{4.25}$$

$$B_{kl} = -\frac{\frac{1}{r_0} C_{kl} J_k\left(\sqrt{\mu_l} r_0\right)}{-\sqrt{\mu_l} H_k^{(1)\prime}\left(\sqrt{\mu_l} r_0\right) J_k\left(\sqrt{\mu_l} r_0\right) + \sqrt{\mu_l} H_k^{(1)}\left(\sqrt{\mu_l} r_0\right) J_k'\left(\sqrt{\mu_l} r_0\right)}.$$

According to the Handbook of Mathematical Functions[10], particularly,

$$C_m'(z) = \frac{-z C_{m+1}(z) + m C_m(z)}{z} \tag{4.26}$$

and

$$H_{k+1}^{(1)}(z) H_k^{(2)}(z) - H_{k+1}^{(2)}(z) H_k^{(1)}(z) = -\frac{4i}{\pi z}, \tag{4.27}$$

the denominator of equation (4.25) simplifies to

$$-\sqrt{\mu_l} H_k^{(1)\prime}\left(\sqrt{\mu_l} r_0\right) J_k\left(\sqrt{\mu_l} r_0\right) + \sqrt{\mu_l} H_k^{(1)}\left(\sqrt{\mu_l} r_0\right) J_k'\left(\sqrt{\mu_l} r_0\right) = -\frac{2i}{\pi r_0}.$$

Thus

$$A_{kl} = -\frac{\frac{1}{r_0} C_{kl} H_k^{(1)}\left(\sqrt{\mu_l} r_0\right)}{-\frac{2i}{\pi r_0}} = -\frac{i\pi}{2} C_{kl} H_k^{(1)}\left(\sqrt{\mu_l} r_0\right)$$

$$B_{kl} = -\frac{\frac{1}{r_0} C_{kl} J_k\left(\sqrt{\mu_l} r_0\right)}{-\frac{2i}{\pi r_0}} = -\frac{i\pi}{2} C_{kl} J_k\left(\sqrt{\mu_l} r_0\right).$$

Noting

$$\int_{-\pi}^{\pi} G_0(\theta)^2 \, d\theta = 2\pi, \text{ when } G_0(\theta) = 1$$

$$\int_{-\pi}^{\pi} G_m(\theta)^2 \, d\theta = \pi, \text{ when } G_m(\theta) = \cos(m\theta), \ \sin(m\theta)$$

gives

$$C_{0n} = \frac{\chi(z_0) Z_n(z_0)}{2\pi \int_{z_s}^{z_a} \chi(z) Z_n(z)^2 \, dz}$$

$$C_{mn} = \frac{G_m(\theta_0) \chi(z_0) Z_n(z_0)}{\pi \int_{z_s}^{z_a} \chi(z) Z_n(z)^2 \, dz}, G_m(\theta) = \cos(m\theta), \ \sin(m\theta).$$

[10] [2], pg. 362, eqn. (9.1.27).

Thus, for $r < r_0$

$$\begin{aligned} p(r,\theta,z) &= \sum_{n=1}^{\infty} -\frac{i}{4\Phi_n} H_0^{(1)}\left(\sqrt{\mu_n} r_0\right) J_0\left(\sqrt{\mu_n} r\right) \chi(z_0) Z_n(z_0) Z_n(z) \\ &\quad + \sum_{m=1}^{\infty}\sum_{n=1}^{\infty} -\frac{i}{2\Phi_n} \left(H_m^{(1)}\left(\sqrt{\mu_n} r_0\right) J_m\left(\sqrt{\mu_n} r\right) \cos(m\theta_0)\cos(m\theta)\right. \\ &\quad \left. + H_m^{(1)}\left(\sqrt{\mu_n} r_0\right) J_m\left(\sqrt{\mu_n} r\right) \sin(m\theta_0)\sin(m\theta)\right) \chi(z_0) Z_n(z_0) Z_n(z) \end{aligned} \tag{4.28}$$

$$\begin{aligned} &= \sum_{n=1}^{\infty} -\frac{i}{4\Phi_n} H_0^{(1)}\left(\sqrt{\mu_n} r_0\right) J_0\left(\sqrt{\mu_n} r\right) \chi(z_0) Z_n(z_0) Z_n(z) \\ &\quad + \sum_{m=1}^{\infty}\sum_{n=1}^{\infty} -\frac{i}{2\Phi_n} H_m^{(1)}\left(\sqrt{\mu_n} r_0\right) J_m\left(\sqrt{\mu_n} r\right) \cos(m(\theta_0-\theta)) \\ &\quad \times \chi(z_0) Z_n(z_0) Z_n(z) \end{aligned}$$

and for $r > r_0$

$$\begin{aligned} p(r,\theta,z) &= \sum_{n=1}^{\infty} -\frac{i}{4\Phi_n} H_0^{(1)}\left(\sqrt{\mu_n} r\right) J_0\left(\sqrt{\mu_n} r_0\right) \chi(z_0) Z_n(z_0) Z_n(z) \\ &\quad + \sum_{m=1}^{\infty}\sum_{n=1}^{\infty} -\frac{i}{2\Phi_n} H_m^{(1)}\left(\sqrt{\mu_n} r\right) J_m\left(\sqrt{\mu_n} r_0\right) \cos(m(\theta_0-\theta)) \chi(z_0) Z_n(z_0) Z_n(z) \end{aligned} \tag{4.29}$$

where $\Phi_n = \int_{z_s}^{z_a} \chi(z) Z_n(z)^2 \, dz$.

Velocity in the z-direction is given by

$$\begin{aligned} w_z &= -\frac{i}{\omega\rho}(\partial_z p) \\ &= -\frac{i}{\omega\rho}\left[\sum_{n=1}^{\infty} -\frac{i}{4\Phi_n} H_0^{(1)}\left(\sqrt{\mu_n} r_0\right) J_0\left(\sqrt{\mu_n} r\right) \chi(z_0) Z_n(z_0) Z_n'(z)\right. \\ &\quad \left. + \sum_{m=1}^{\infty}\sum_{n=1}^{\infty} -\frac{i}{2\Phi_n} H_m^{(1)}\left(\sqrt{\mu_n} r_0\right) J_m\left(\sqrt{\mu_n} r\right) \cos(m(\theta_0-\theta)) \chi(z_0) Z_n(z_0) Z_n'(z)\right] \end{aligned} \tag{4.30}$$

when $r < r_0$, and

$$\begin{aligned} w_z &= -\frac{i}{\omega\rho}\left[\sum_{n=1}^{\infty} -\frac{i}{4\Phi_n} H_0^{(1)}\left(\sqrt{\mu_n} r\right) J_0\left(\sqrt{\mu_n} r_0\right) \chi(z_0) Z_n(z_0) Z_n'(z)\right. \\ &\quad + \sum_{m=1}^{\infty}\sum_{n=1}^{\infty} -\frac{i}{2\Phi_n} H_m^{(1)}\left(\sqrt{\mu_n} r\right) J_m\left(\sqrt{\mu_n} r_0\right) \cos(m(\theta_0-\theta)) \\ &\quad \left. \times \chi(z_0) Z_n(z_0) Z_n'(z)\right] \end{aligned}$$

when $r > r_0$. Note that these results are comparable with similar models found in the literature.[11]

[11] [9], [6], [12], [23].

Chapter 5

MATLAB^{TM} User Interface for the Two Layer Waveguide

A user interface, featuring an experimental and laboratory input, was created from the equations for the Two Layer Waveguide. Specific instructions for the user interface are included, as well as the theoretical background for the transition of the soil properties to the porous representation.

5.1 Instructions for the Soil Resonance User Interface

The soil resonance user interface is designed to aid experimental physicists in predicting soil resonances in field experiments, where equipment is limited, and in laboratory settings, with more precisely defined measurements and analysis tools. The field experiment case ("basic module"), which utilizes atmospheric temperature and humidity and relies on more qualitative measures for soil type, moisture, and compactness, is designed for rough predictions based on previous data. The laboratory case ("advanced module") uses precise laboratory tests to determine the density and sound speed through the air and soil.

5.1.1 General Instructions for the User Interface

1. Upon obtaining the User Interface files, save the files and note their location.
2. Open MATLAB^{TM}.
3. In the "Current Directory" script next to the help icon (a yellow ?), select the file directory where the Interface files are stored.
4. Type "gui" into the "Command Window".

5.1.2 Instructions for Use of the Basic Module

1. To select the basic module, press enter when presented with the advanced selection.
2. Enter the ambient temperature in degrees Celsius.
3. Enter the ambient humidity in decimal form.
4. Select the appropriate soil type which most closely describes the soil in the experiment. Select only the numbers given, decimal values are not acceptable.
5. Approximate the soil moisture on a scale of 1 to 5, with 1 being very dry soil, to 5 being very moist soil.
6. Approximate the packing of the soil on a scale of 1 to 4, with 1 being very loose soil, and 4 being very compact soil.

5.1.3 Instructions for Use of the Advanced Module

1. To select the advanced module, press any number followed by enter when presented with the advanced selection.
2. Enter the speed of sound in the atmosphere. (Default - 343 m/s). To select the default value, press enter without entering a value. Default values are available for all advanced menu entries. An explanation of the chosen default value follows in the "Theoretical Background" section below.
3. Enter the speed of shear sound waves in the soil. (Default - 210.31 m/s)
4. Enter the speed of compressional sound waves in the soil. (Default - 647 m/s)
5. Enter the flow resistivity of the soil[1]. (Default - 0 $\frac{Pa \times s}{m^2}$)
6. Enter the density of the atmosphere. (Default - 1.205 $\frac{kg}{m^3}$)
7. Enter the tolerance of the secant method computation. (Default - 5e-5)

5.1.4 General Instructions Following the Basic or Advanced Module

1. Enter the depth of the porous soil (above bedrock) AS A NEGATIVE VALUE. For example, if the depth of the soil before hitting bedrock is 0.175 meters, the depth would be entered as "-0.175".
2. Enter the position of the source as a vector. See Figure (5.1) below for further clarification.

[1] [3], pg. 175.

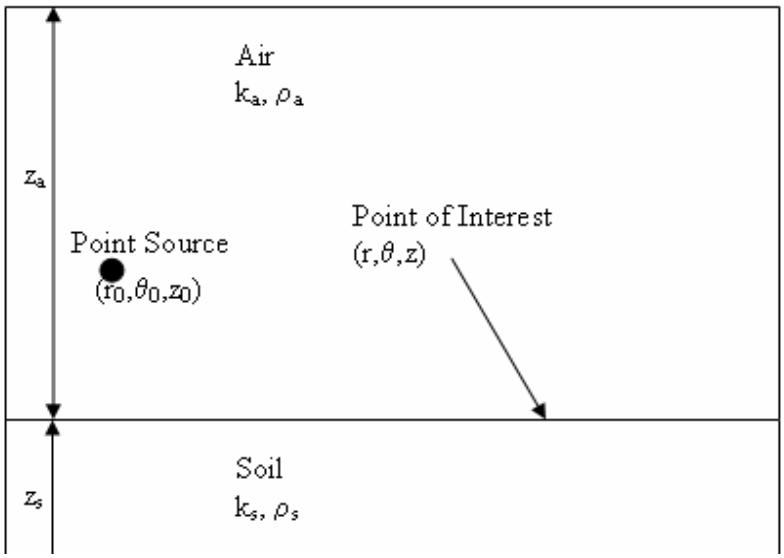

Figure 5.1: The physical representation of the numerical entry quantities for source and position of the two-layer waveguide user interface.

3. If interested in a frequency - pressure plot, enter the range of frequencies of interest as a vector (ie, if a frequency sweep from 100-200 is desired, enter [100,200]. If a depth - pressure plot is of interest, press enter. Then enter the depth range of interest (in the same format as the frequency sweep), press enter and enter the frequency of interest.

5.2 Theoretical Background

The theoretical background necessary to write the programs devised for the numerical implementation is described in this section. The background presented here is applicable for the numerical implementation shown throughout this paper.

5.2.1 The Basic Module

The ambient temperature is used to approximate the density of the air and the sound speed through the air. Density was determined using data from E. Sengpiel[2], and sound speed was found using the formula[3]

$$c_{a,T} = 331.4 + 0.6 \times T_{amb} \left({}^0\mathrm{C}\right).$$

[2] [24]
[3] [24]

Soil Type in User Interface	Soil Type in Oelze Paper
Sand	Plainfield Soil
Silt	Sable Soil
Clay	Drummer Soil
Organic Matter	Adrian Soil

Figure 5.2: This table shows the user interface soil labels with the soil labels from the original paper by Oelze et al[6].

Humidity also affects sound speed and density. The atmospheric density was adjusted by

$$\rho_a = \rho_{a,T}(1 + H)/(1 + 1.609H),^4$$

where $\rho_{a,T}$ is the density from the temperature data, and H is the humidity percentage. The sound speed through the air is determined from

$$c_a = c_{a,T} + 0.6Hc_{a,T}.^5$$

The soil type and composition entries are compared to data collected by Oelze et al.[6] The soil labels are contained in table (5.2). The exact percentage of composition is also available in the Oelze paper.[7]

5.2.2 The Advanced Module

The default values for density and speed in each medium are from data collected by Dr. D. Keith Wilson and Dr. H. Cudney in a dry, desert - like environment. The default $\sigma = 0$ was chosen for simplicity. Finally, the tolerance for the secant method is a reasonable value for the data.

[4][26]
[5][24]
[6][8], pg. 792.
[7][8], pg. 789.

Chapter 6

Numerical Analysis of the Two Layer Waveguide Problem

A MATLAB^{TM} program was devised to calculate the pressure and velocity described in equations (4.28) and (4.30). The program and its supporting commands can be found in the appendix. There were many reasons behind writing the program for the simple, two layer waveguide problem. The program will provide the basic structure for future programs involving more complicated problems, and will allow the development of solutions to anticipated problems. Additionally, the effects of numerical selection for the atmospheric height (z_a) and rigid soil depth (z_s) need to be investigated to analyze their contribution to the pressure and velocity. Assumptions for the variables for each graphic are as follows (unless otherwise stated): $\sigma = 0, c_s = 160, c_a = 330, z_s = -1, z_a = 500$. The value for σ was chosen for simplicity, c_s, c_a and z_s are appropriate for the environment of interest, and z_a was computationally determined.

6.1 Determining Resonances for the Two Layer Waveguide Problem

Equation (4.28) describes the pressure at a point (r, θ, z). Resonant frequencies, or resonances, are the frequencies at which there are large amplitude oscillations. Thus, resonances are indicated by large deviations in pressure caused by the acoustic wave. Resonances in Figure (6.1) occur at $f \approx 136, 228, 319, 412$ Hz. In context of the two layer waveguide problem, resonances indicate that the soil surface oscillates at maximum amplitude at these frequencies. The direction of the peak (up or down) is not significant, it is connected to constructive and destructive interference. Should landmine detection be attempted at low soil depths (before hitting bedrock), Figure (6.1) suggests that resonances detected in the range of $f \approx 136, 228, 319, 412$ Hz are probably soil resonances, instead of mine resonances. Figure (6.2) compares the effect of deeper soil on resonant effects of the rigid substrate. It is reasonable that resonances existing at a depth of 1 meter would not be as apparent or appear at all in deeper soil, due to greater attenuation with distance. In fact, there are more resonances in deeper soil, but these resonances occur at broader frequencies in shallow

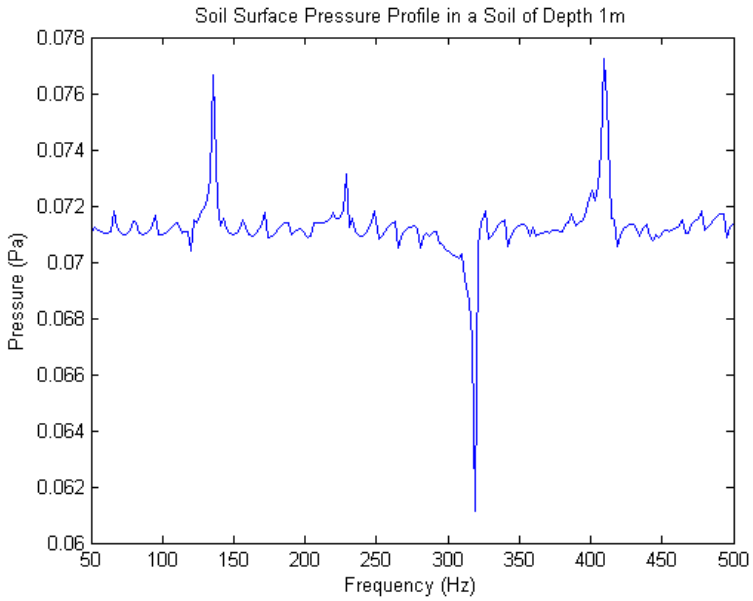

Figure 6.1: Graphical representation used to find resonances. The resonances of the two-layer waveguide occur from the soil layer, and differ with depth.

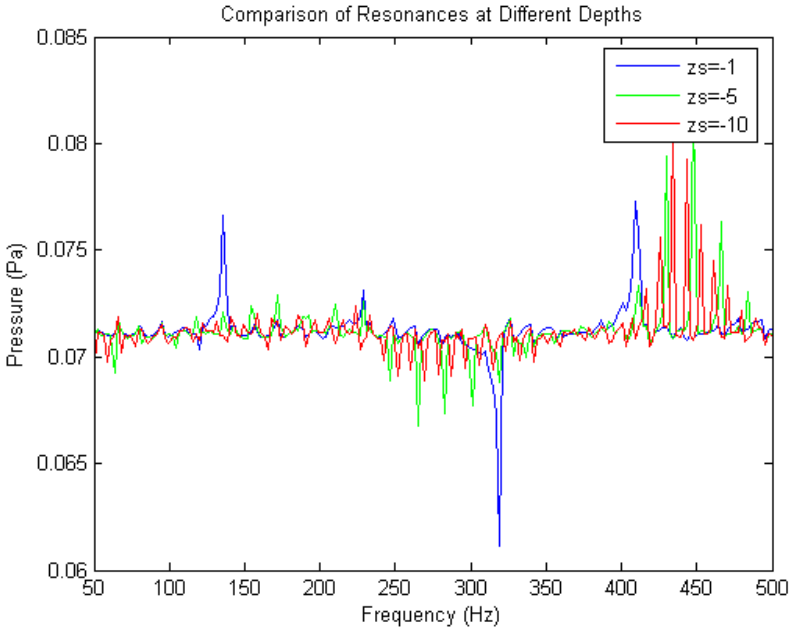

Figure 6.2: Graphical representation of resonances demonstrating the effect of soil depth.

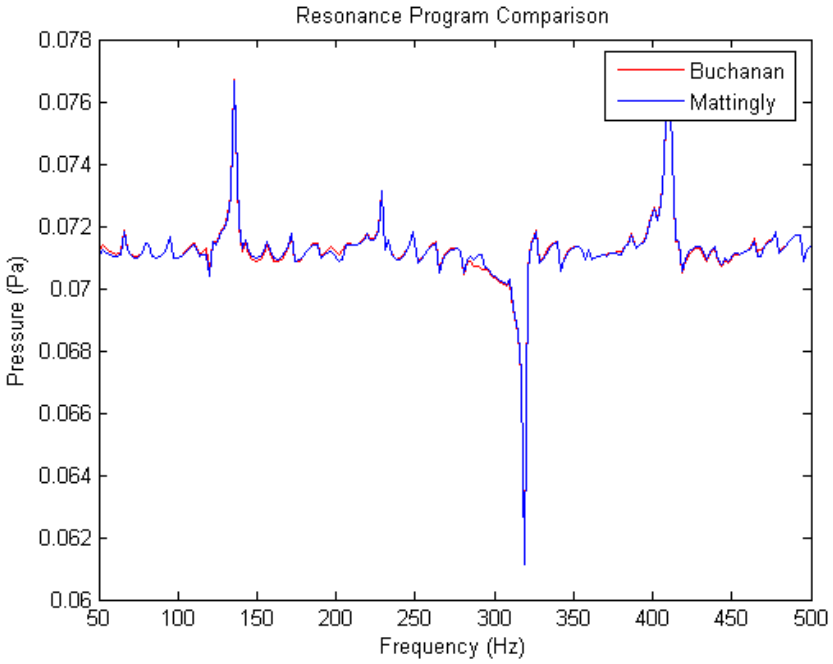

Figure 6.3: Comparison of two independantly written programs for the two-layer waveguide problem.

soil. The peaks at approximately $f = 450$ are believed to be resonances which happen to occur at the frequencies used for the calculation. Note that the resonances in the deeper soil are narrower than the shallow depth (z_s) resonances. To ensure accuracy in programming, both Mattingly and Buchanan wrote independent codes. There is a slight disagreement in the curves, due to MATLAB^{TM}'s computation of the depth condition, which was written in two different, equivalent ways by the programmers.

6.2 Selection of σ

According to Morse and Ingard[1], σ is the pressure drop required to force a unit flow through the material. If the value for σ is too high, the resonances will not appear, since the flow resistance is too high. Similarly, if the flow resistance is too low, the model will not match the physical reality. Figure (6.4) shows the effects of low and high values of σ.

[1] [22], pg. 253.

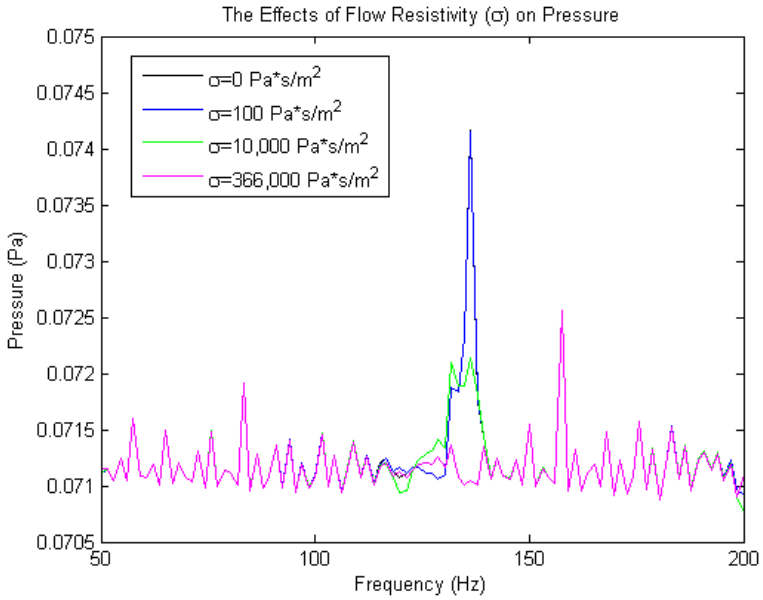

Figure 6.4: This graph demonstrates the effect of σ on pressure. Note that resonances do not appear when σ is very high.

6.3 Selection of z_a

The effects of the numerical selection for the atmospheric height (z_a) were considered. The appropriate value for z_a will not show significant deviation from much larger values, and its behavior will be consistent with the larger values. z_a needs to be as small as possible to maximize the computational efficiency of the program. The receiver height versus pressure graph, Figure (6.5), allows comparison of the different values for z_a. After investigation, an appropriate value for z_a is 500 meters. The pressures recorded at 500 meters closely resemble the pressures recorded at 800 meters over the span of 100 hertz, as shown in Figure (6.6). Lower values for z_a, as show in Figure (6.5), show noticeable deviation from $z_a = 500$ m. For example, the next lower value of $z_a = 200$ m (in red) does not closely resemble the behavior of $z_a = 800$ m, particularly at the resonant frequency, $f = 128$ Hz.

6.4 Effects of z_s

The considerations for the depth of the soil is entirely dependent on the operating environment. The rigid soil depth physically represents the depth at which the porous soil layer interfaces with a more dense (bedrock-type) soil that reflects most of the acoustic energy. This soil depth is also dependant on soil type. In Figure (6.7), a dry soil environment, the resonant effects are very distinguished when compared to Figure (6.8), a moist soil environment. The effects of moisture

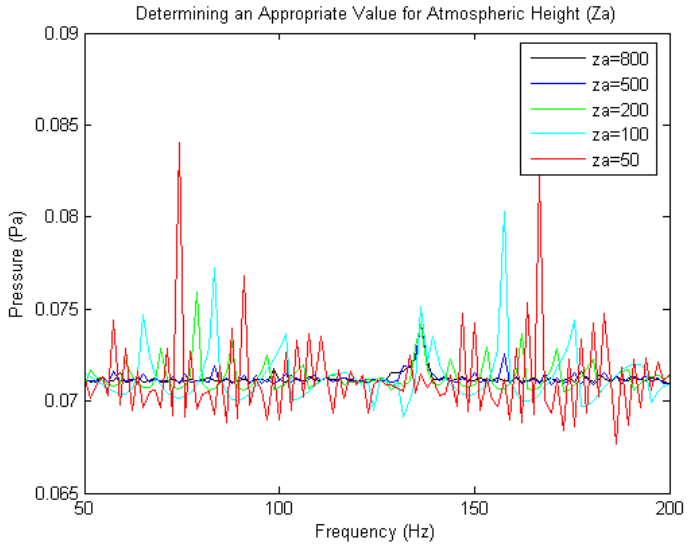

Figure 6.5: Graphical representation of the effect of z_a on the pressure placed on the mine. The optimal value for z_a will approximate z_a at much larger values, while remaining computationally efficient.

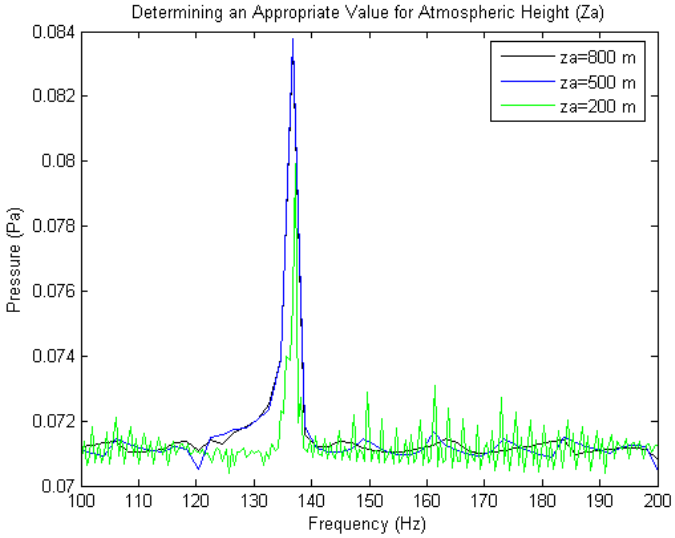

Figure 6.6: Graphical representation of the effect of z_a on the pressure at $z = 0$. This graphic shows the comparison for the hypothesized optimal value for z_a (500 m), approximating z_a at much larger values (800 m).

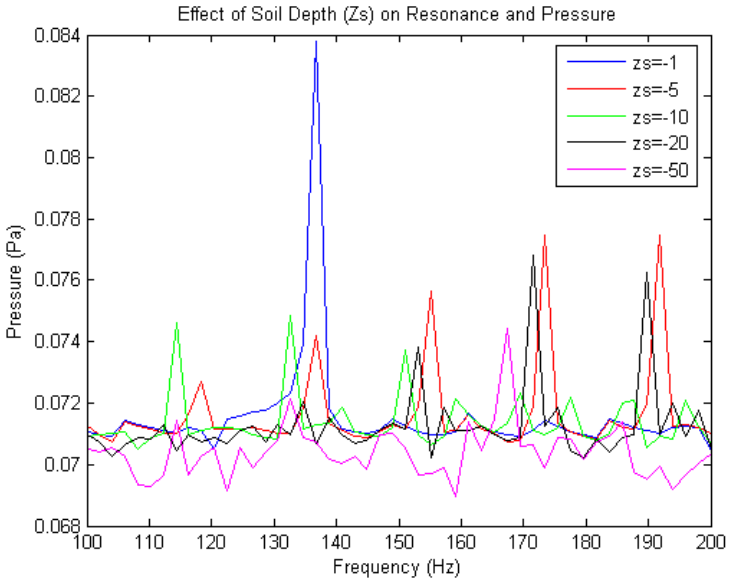

Figure 6.7: Graphical representation of the effect of z_s on the pressure placed on the mine. This graphic shows the comparison for depth of the bedrock layers in a sandy soil environment.

are incorporated into the soil sound speed, c_s.[2] Smaller pressures are recorded in the moist soil environment, and the resonances are barely distinguishable. This mathematical finding makes physical sense: a moist soil is more dense, causing more attenuation in the sound wave, which results in lower pressure differences and decreased resonant effects. σ remained at zero for the computation presented below, but future analysis of different soils will need to include different σ, which is clearly effected by soil type. Values suggested in a soil sound speed paper[3] are being examined for their relevance to this problem.

[2] [8], pg. 792.
[3] [8], pg. 792.

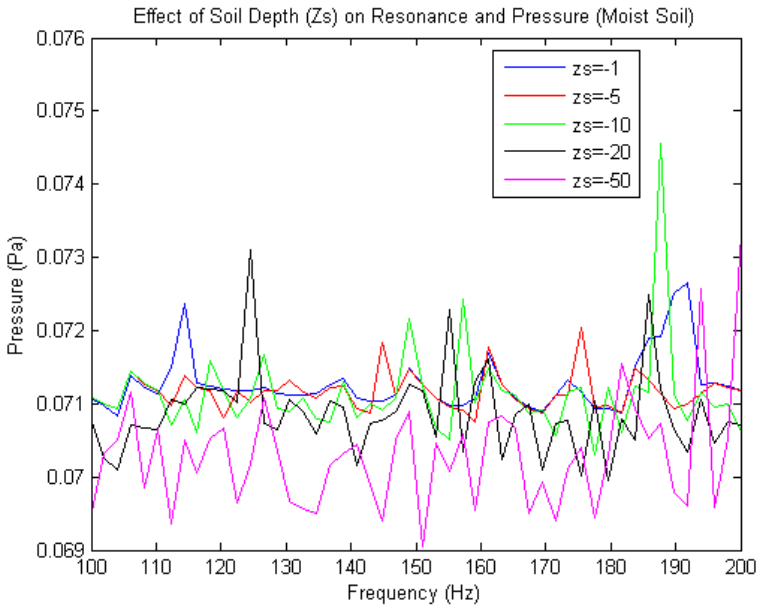

Figure 6.8: Graphical representation of the effect of z_s on the acoustic pressure. This graphic shows the comparison for depth of the bedrock layers in a mixed soil environment. (The computations in this graphic considered only a change in sound speed, since the values for σ have yet to be validated.

Chapter 7

Solution of the Membrane Problem

Figure (7.1) represents the membrane problem, which consists of the top plate of the landmine imbedded in the rigid substrate from the waveguide of the two layer waveguide problem. While the functions outside the imaginary cylinder remain identical to those from the two layer waveguide problem (see eqns. (4.28) and (4.29)), the equations within the cylinder will be derived in the following 2 chapters.

7.1 Definition of the Green's Function

Suppose now that a membrane occupies the region $D = \{(r, \theta) : r \leq a\}$. The equation for the motion of a damped membrane subject to an external pressure $p(r, \theta, t)$ is

$$T\nabla^2 u - \beta\partial_t u + p = \rho\partial_{tt} u.$$

where T is the tension of the membrane and ρ is its density. If the external pressure is time-harmonic $p(r, \theta, t) = p(r, \theta) e^{-i\omega t}$ and the membrane is fixed at the boundary, then

$$\nabla^2 u + k^2 u = -\frac{1}{T} p$$

$$u(a, \theta) = 0$$

with $k^2 = (\rho\omega^2 + i\beta\omega)/T$. Let $\mathcal{G}(r, \theta, r', \theta')$ denote the Green's function for the problem, that is,

$$\nabla^2_{(r,\theta)} \mathcal{G} + k^2 \mathcal{G} = -\frac{1}{r} \delta(r - r') \delta(\theta - \theta') \tag{7.1}$$

$$\mathcal{G}(a, \theta, r', \theta') = 0, \mathcal{G}(r, \theta, r', \theta') = \mathcal{G}(r', \theta', r, \theta)$$

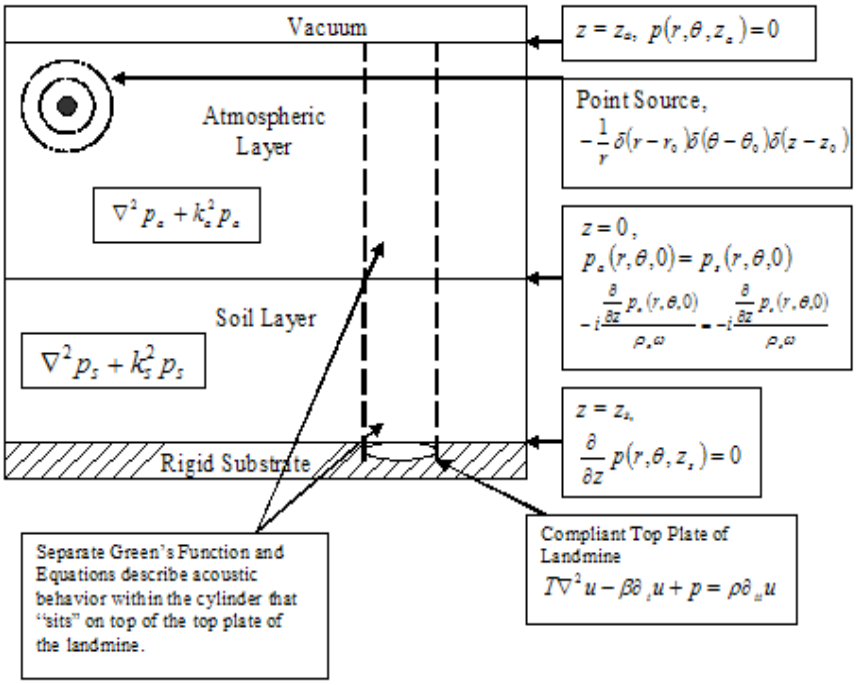

Figure 7.1: A mathematical schematic of the membrane problem in cylindrical coordinates displaying this paper's notation. T is the tension of the membrane, which will be examined for the case of the plastic landmine.

Note that

$$\begin{aligned}
&\int_0^a\int_{-\pi}^{\pi}\left[\mathcal{G}\left(r,\theta,r',\theta'\right)\nabla^2 u\left(r,\theta\right)-u\nabla^2_{(r,\theta)}\mathcal{G}\left(r,\theta,r',\theta'\right)\right]rd\theta dr\\
=&\int_0^a\int_{-\pi}^{\pi}\left[-\mathcal{G}\left(r,\theta,r',\theta'\right)\left(k^2u\left(r,\theta\right)+\frac{1}{T}p\left(r,\theta\right)\right)\right.\\
&\left.+\left(k^2\mathcal{G}\left(r,\theta,r',\theta'\right)+\frac{1}{r}\delta\left(r-r'\right)\delta\left(\theta-\theta'\right)\right)u\left(r,\theta\right)\right]rd\theta dr\\
=&-\frac{1}{T}\int_0^a\int_{-\pi}^{\pi}\mathcal{G}\left(r,\theta,r',\theta'\right)p\left(r,\theta\right)rd\theta dr+u\left(r',\theta'\right).
\end{aligned}$$

Since $\nabla\cdot\left(u\nabla v\right)=\nabla u\cdot\nabla v+u\nabla^2 v$, the divergence theorem gives

$$\begin{aligned}
&\int_0^a\int_{-\pi}^{\pi}\left[\mathcal{G}\left(r,\theta,r',\theta'\right)\nabla^2 u\left(r,\theta\right)-u\nabla^2_{(r,\theta)}\mathcal{G}\left(r,\theta,r',\theta'\right)\right]rd\theta dr\\
=&\iint_D\left[\nabla\cdot\left(\mathcal{G}\nabla u\right)-\nabla\mathcal{G}\cdot\nabla u-\left(\nabla\cdot\left(u\nabla\mathcal{G}-\nabla\mathcal{G}\cdot\nabla u\right)\right)\right]dA\\
=&\int_{\partial D}\left[\mathcal{G}\nabla u\cdot n-u\nabla\mathcal{G}\cdot n\right]ds=0
\end{aligned}$$

in view of the boundary conditions. Thus, the solution to the non-homogeneous membrane problem is

$$u\left(r,\theta\right)=\frac{1}{T}\int_0^a\int_{-\pi}^{\pi}\mathcal{G}\left(r,\theta,r',\theta'\right)p\left(r',\theta'\right)r'd\theta' dr' \tag{7.2}$$

7.2 Determination of the Green's Function

It remains to find the Green's function. In polar coordinates,

$$\frac{1}{r}\partial_r\left(r\partial_r\mathcal{G}\right)+\frac{1}{r^2}\partial_{\theta\theta}\mathcal{G}+k^2\mathcal{G}=0$$

except at $\left(r,\theta\right)=\left(r',\theta'\right)$. Seeking solutions of the form $\Theta\left(r,\theta\right)=F\left(r\right)G\left(\theta\right)$ gives

$$\frac{\frac{1}{r}\left(rF'\left(r\right)\right)'}{F\left(r\right)}+\frac{1}{r^2}\frac{G''\left(\theta\right)}{G\left(\theta\right)}+k^2=0$$

$$-\frac{r\left(rF'\left(r\right)\right)'}{F\left(r\right)}-k^2r^2=\frac{G''\left(\theta\right)}{G\left(\theta\right)}=-\lambda$$

From equations (4.7) and (4.8) the problem

$$G''\left(\theta\right)+\lambda G\left(\theta\right)=0$$

$$G\left(-\pi\right)=G\left(\pi\right),G'\left(-\pi\right)=G'\left(\pi\right)$$

has the solution

$$\lambda_m = m^2, m = 0, 1, 2, ...$$
$$G_0 = 1, G_m(\theta) = \cos(m\theta), \sin(m\theta).$$

The problem for $F(r)$ is

$$r(rF'(r))' + \left(k^2r^2 - m^2\right)F(r) = 0$$
$$F(a) = 0$$

Substituting a solution of the form $\mathcal{G}(r,\theta) = \sum_{m=0}^{\infty} F_m(r) G_m(\theta)$ into the Laplacian gives

$$\begin{aligned}
&\frac{1}{r}\partial_r(r\partial_r\mathcal{G}) + \frac{1}{r^2}\partial_{\theta\theta}\mathcal{G} \\
= &\sum_{m=0}^{\infty} \frac{1}{r}\frac{d}{dr}(rF_m'(r)) G_m(\theta) + \frac{1}{r^2}F_m(r) G_m''(\theta) \\
= &\sum_{m=0}^{\infty} \left(F_m''(r) + \frac{1}{r}F_m'(r)\right) G_m(\theta) - \frac{m^2}{r^2}F_m(r) G_m(\theta)
\end{aligned}$$

Substituting this into (7.1) gives

$$\begin{aligned}
&\sum_{m=0}^{\infty} \left(F_m''(r) + \frac{1}{r}F_m'(r)\right) G_m(\theta) - \frac{m^2}{r^2}F_m(r) G_m(\theta) + k^2F_m(r) G_m(\theta) \\
= &-\frac{1}{r}\delta(r - r')\delta(\theta - \theta')
\end{aligned}$$

$$\sum_{m=0}^{\infty} \left(rF_m''(r) + F_m'(r) + \left(k^2r - \frac{m^2}{r}\right)F_m(r)\right) G_m(\theta) = -\delta(r - r')\delta(\theta - \theta')$$

Multiplying by $G_{m'}(\theta)$ and integrating gives

$$\begin{aligned}
&\left(rF_{m'}''(r) + F_{m'}'(r) + \left(k^2r - \frac{m'^2}{r}\right)F_{m'}(r)\right) \int_{-\pi}^{\pi} G_{m'}(\theta)^2 d\theta \\
= &-\delta(r - r') G_{m'}(\theta') \\
&rF_{m'}''(r) + F_{m'}'(r) + \left(k^2r - \frac{m'^2}{r}\right)F_{m'}(r) = -D_{m'}\delta(r - r') \qquad (7.3)
\end{aligned}$$

where

$$D_{m'} = \frac{G_{m'}(\theta')}{\int_{-\pi}^{\pi} G_{m'}(\theta')^2 d\theta}.$$

Integrating from $r_0 - \varepsilon$ to $r_0 + \varepsilon$ gives

$$\begin{aligned}
&(r' + \varepsilon)F_{m'}'(r' + \varepsilon) - (r' - \varepsilon)F_{m'}'(r' - \varepsilon) + \int_{r'-\varepsilon}^{r'+\varepsilon} \left(k^2r - \frac{m'^2}{r}\right)F_{m'}(r) dr \\
= &-D_{m'}
\end{aligned}$$

Letting $\varepsilon \to 0$ and requiring that $F_{m'}(r)$ be continuous at $r = r'$ gives the conditions

$$F_{m'}(r'+) = F_{m'}(r'-) \tag{7.4}$$

$$F'_{kl'}(r'+) - F'_{kl'}(r'-) = -\frac{1}{r'} D_{m'}$$

Except at $r = r'$, (7.3) is just Bessel's equation. Since the solution must be bounded at $r = 0$,

$$F_m(r) = \begin{cases} A_{m'} J_{m'}(kr) & 0 \le r < r' \\ B_{m'} J_{m'}(kr) + C_{m'} Y_{m'}(kr) & r_0 < r \le a \end{cases}$$

The Hankel Function is replaced by its identity, the sum of Bessel Functions of the first and second kind, for simplification of adherence to the boundary conditions. The jump conditions and the boundary condition gives

$$A_{m'} J_{m'}(kr') - B_{m'} J_{m'}(kr') - C_{m'} Y_{m'}(kr') = 0$$

$$kA_{m'} J'_{m'}(kr') - kB_{m'} J'_{m'}(kr') - kC_{m'} Y'_{m'}(kr') = -\frac{1}{r'} D_{m'} \tag{7.5}$$

$$B_{m'} J_{m'}(ka) + C_{m'} Y_{m'}(ka) = 0$$

Thus, the system to be solved is

$$\begin{bmatrix} J_{m'}(kr') & -J_{m'}(kr') & -Y_{m'}(kr') \\ J'_{m'}(kr') & -J'_{m'}(kr') & -Y'_{m'}(kr') \\ 0 & J_{m'}(ka) & Y_{m'}(ka) \end{bmatrix} \begin{bmatrix} A_{m'} \\ B_{m'} \\ C_{m'} \end{bmatrix} = \begin{bmatrix} 0 \\ -\frac{1}{kr'} D_{m'} \\ 0 \end{bmatrix}$$

The determinant of the coefficient matrix is

$$\begin{aligned} & -J_{m'}(ka) \begin{vmatrix} J_{m'}(kr') & -Y_{m'}(kr') \\ J'_{m'}(kr') & -Y'_{m'}(kr') \end{vmatrix} \\ & +Y_{m'}(ka) \begin{vmatrix} J_{m'}(kr') & -J_{m'}(kr') \\ J'_{m'}(kr') & -J'_{m'}(kr') \end{vmatrix} \\ = \; & -J_{m'}(ka) \left(-J_{m'}(kr') Y'_{m'}(kr') + J'_{m'}(kr') Y_{m'}(kr') \right) \end{aligned}$$

From equations (4.26) and (4.27):

$$\begin{aligned} = \; & -\left(\frac{-kr' Y_{m'+1}(kr') + m' Y_{m'}(kr')}{kr'} \right) J_{m'}(kr') \\ & +Y_{m'}(kr') \left(\frac{-kr' J_{m'+1}(kr') + m' J_{m'}(kr')}{kr'} \right) \end{aligned}$$

$$= Y_{m'+1}(kr') J_{m'}(kr') - \frac{m' Y_{m'}(kr')}{kr'} J_{m'}(kr') - Y_{m'}(kr') J_{m'+1}(kr') + Y_{m'}(kr') \frac{m' J_{m'}(kr')}{kr'}$$

$$= Y_{m'+1}(kr') J_{m'}(kr') - Y_{m'}(kr') J_{m'+1}(kr')$$

By Abramowitz and Stegun[1]

$$J_{\nu+1}(z)\,Y_v(z) - J_\nu(z)\,Y_{v+1}(z) = -\frac{2}{\pi(z)}$$

so our equation yields:

$$= -\frac{2}{\pi(kr')}$$

Thus, by Cramer's Rule

$$A_{m'} = -\frac{\pi(kr')}{2J_{m'}(ka)}\begin{vmatrix} 0 & -J_{m'}(kr') & -Y_{m'}(kr') \\ -\frac{1}{kr'}D_{m'} & -J'_{m'}(kr') & -Y'_{m'}(kr') \\ 0 & J_{m'}(ka) & Y_{m'}(ka) \end{vmatrix}$$

$$= -\left(-\frac{\pi(kr')}{2J_{m'}(ka)}\left(-\frac{1}{kr'}D_{m'}\right)\begin{vmatrix} -J_{m'}(kr') & -Y_{m'}(kr') \\ J_{m'}(ka) & Y_{m'}(ka) \end{vmatrix}\right)$$

$$= -\frac{\pi(kr')}{2J_{m'}(ka)}\left(\frac{1}{kr'}D_{m'}\right)\left(-J_{m'}(kr')\,Y_{m'}(ka) + Y_{m'}(kr')\,J_{m'}(ka)\right)$$

$$= -\frac{\pi}{2J_{m'}(ka)}\left(D_{m'}\right)\left(-J_{m'}(kr')\,Y_{m'}(ka) + Y_{m'}(kr')\,J_{m'}(ka)\right)$$

Similarly,

$$B_{m'} = -\frac{\pi(kr')}{2J_{m'}(ka)}\begin{vmatrix} J_{m'}(kr') & 0 & -Y_{m'}(kr') \\ J'_{m'}(kr') & -\frac{1}{kr'}D_{m'} & -Y'_{m'}(kr') \\ 0 & 0 & Y_{m'}(ka) \end{vmatrix}$$

$$= \frac{\pi}{2J_{m'}(ka)}D_{m'}J_{m'}(kr')\,Y_{m'}(ka)$$

$$C_{m'} = -\frac{\pi(kr')}{2J_{m'}(ka)}\begin{vmatrix} J_{m'}(kr') & -J_{m'}(kr') & 0 \\ J'_{m'}(kr') & -J'_{m'}(kr') & -\frac{1}{kr'}D_{m'} \\ 0 & J_{m'}(ka) & 0 \end{vmatrix}$$

$$= -\frac{\pi}{2J_{m'}(ka)}D_{m'}J_{m'}(kr')\,J_{m'}(ka) = -\frac{\pi}{2}D_{m'}J_{m'}(kr')$$

Noting that

$$D_0 = \frac{G_0(\theta')}{\int_{-\pi}^{\pi} G_0(\theta')^2\,d\theta} = \frac{1}{2\pi}$$

$$D_m = \frac{G_m(\theta')}{\int_{-\pi}^{\pi} G_m(\theta')^2\,d\theta} = \frac{G_m(\theta')}{\pi}, G_m(\theta') = \cos(\theta'), \sin(\theta')$$

[1] [2], pg. 362, eqn. (9.1.16).

gives

$$\begin{aligned}
\Theta(r,\theta,r',\theta') &= F_0(r) + \sum_{m=1}^{\infty} F_m(r)\, G_m(\theta) \\
&= \frac{1}{4J_0(ka)} \left(J_0(kr')\, Y_0(ka) - J_0(ka)\, Y_0(kr')\right) J_0(kr) \\
&\quad + \sum_{m=1}^{\infty} \frac{1}{2J_m(ka)} \left(J_m(kr')\, Y_m(ka) - J_m(ka)\, Y_m(kr')\right) \\
&\quad \times J_m(kr) \cos(m\theta) \cos(m\theta') \\
&\quad + \sum_{m=1}^{\infty} \frac{1}{2J_m(ka)} \left(J_m(kr')\, Y_m(ka) - J_m(ka)\, Y_m(kr')\right) \\
&\quad \times J_m(kr) \sin(m\theta) \sin(m\theta') \\
&= \frac{1}{4J_0(ka)} \left(J_0(kr')\, Y_0(ka) - J_0(ka)\, Y_0(kr')\right) J_0(kr) \\
&\quad + \sum_{m=1}^{\infty} \frac{1}{2J_m(ka)} \left(J_m(kr')\, Y_m(ka) - J_m(ka)\, Y_m(kr')\right) \\
&\quad \times J_m(kr) \cos(m(\theta - \theta'))
\end{aligned}$$

for $r < r'$ and

$$\begin{aligned}
\Theta(r,\theta,r',\theta') &= F_0(r) + \sum_{m=1}^{\infty} F_m(r)\, G_m(\theta) \\
&= \frac{1}{4J_0(ka)} J_0(kr')\, Y_0(ka)\, J_0(kr) - \frac{1}{4} J_0(kr')\, Y_0(kr) \\
&\quad + \sum_{m=1}^{\infty} \frac{1}{2J_m(ka)} \left(Y_m(ka)\, J_m(kr) - Y_m(kr)\, J_m(ka)\right) \\
&\quad \times J_m(kr') \cos(m(\theta - \theta'))
\end{aligned}$$

for $r > r'$.

Returning to (7.2)

$$\begin{aligned} u(r,\theta) &= \frac{1}{T}\int_0^a\int_{-\pi}^{\pi}\mathcal{G}(r,\theta,r',\theta')\,p(r',\theta')\,r'd\theta'dr' \\ &= \frac{1}{T}\int_0^r\int_{-\pi}^{\pi}\left[\frac{1}{4J_0(ka)}J_0(kr')\,Y_0(ka)\,J_0(kr)-\frac{1}{4}J_0(kr')\,Y_0(kr)\right. \\ &\quad +\sum_{m=1}^{\infty}\frac{1}{2J_m(ka)}\left(Y_m(ka)\,J_m(kr)-Y_m(kr)\,J_m(ka)\right)J_m(kr') \\ &\quad \left.\times\cos\left(m\left(\theta-\theta'\right)\right)\right]p(r',\theta')\,r'd\theta'dr' \\ &\quad +\frac{1}{T}\int_0^r\int_{-\pi}^{\pi}\left[\frac{1}{4J_0(ka)}\left(J_0(kr')\,Y_0(ka)-J_0(ka)\,Y_0(kr')\right)J_0(kr)\right. \\ &\quad +\sum_{m=1}^{\infty}\frac{1}{2J_m(ka)}\left(J_m(kr')\,Y_m(ka)-J_m(ka)\,Y_m(kr')\right)J_m(kr) \\ &\quad \left.\times\cos\left(m\left(\theta-\theta'\right)\right)\right]p(r',\theta')\,r'd\theta'dr' \end{aligned} \tag{7.6}$$

7.3 Comparison with Mathews and Walker

Mathews and Walker[2] approach the similar non-homogeneous membrane problem

$$\nabla^2_{(r,\theta)}\widetilde{\mathcal{G}}+k^2\widetilde{\mathcal{G}}=\frac{1}{r}\delta(r-r')\,\delta(\theta-\theta')$$

with jump boundary conditions

$$\begin{gathered} A_{m'}J_{m'}(kr')-B_{m'}J_{m'}(kr')-C_{m'}Y_{m'}(kr')=0 \\ kA_{m'}J'_{m'}(kr')-kB_{m'}J'_{m'}(kr')-kC_{m'}Y'_{m'}(kr')=\frac{1}{r'}D_{m'} \\ B_{m'}J_{m'}(ka)+C_{m'}Y_{m'}(ka)=0. \end{gathered} \tag{7.7}$$

The Green's Function is then

$$\widetilde{\mathcal{G}}=\begin{cases}\displaystyle\sum_m A_m J_m(kr)\cos(m\theta) & (r<r') \\ \displaystyle\sum_m B_m\left[J_m(kr)Y_m(ka)-Y_m(kr)\,J_m(ka)\right]\cos(m\theta) & (r>r')\end{cases}$$

where

$$A_m=\frac{1}{2\varepsilon_m J_m(ka)}\left[J_m(ka)\,Y_m(kr')-Y_m(ka)\,J_m(kr')\right]$$

$$B_m=\frac{-J_m(kr')}{2\varepsilon_m J_m(ka)}$$

[2][20], pg. 273.

and

$$\varepsilon_m = \begin{cases} 2 & \text{if } m' = 0 \\ 1 & \text{if } m' > 0 \end{cases}$$

Therefore, for $r < r'$,

$$\begin{aligned} \widetilde{\mathcal{G}} &= \sum_m A_m J_m(kr) \cos(m\theta) \\ &= \frac{1}{4J_0(ka)} \left[J_0(ka) Y_0(kr') - Y_0(ka) J_0(kr') \right] J_0(kr) \\ &\quad + \sum_m \frac{1}{2J_m(ka)} \left[J_m(ka) Y_m(kr') - Y_m(ka) J_m(kr') \right] \\ &\quad \times J_m(kr) \cos(m\theta) \end{aligned}$$

while for $r > r'$,

$$\begin{aligned} \widetilde{\mathcal{G}} &= \sum_m B_m \left[J_m(kr) Y_m(ka) - Y_m(kr) J_m(ka) \right] \cos(m\theta) \\ &= \frac{-J_0(kr')}{4J_0(ka)} \left[J_0(kr) Y_0(ka) - Y_0(kr) J_0(ka) \right] \\ &\quad + \sum_m \frac{-J_m(kr')}{2J_m(ka)} \left[J_m(kr) Y_m(ka) - Y_m(kr) J_m(ka) \right] \cos(m\theta) \end{aligned}$$

The solution in Mathews and Walker is identical to the solution presented in this paper, with the exception of a negative sign in each portion (due to the absence of the negative sign preceding $\frac{1}{r'}$ in equation (7.7)).

Chapter 8

Membrane Imbedded in a Rigid Substrate

Let $D = \{(r,\theta) : r \leq a\}$ be the area occupied by a membrane with a point source located at (r_0, θ_0, z_0), $a < r_0$ and an atmosphere satisfying a pressure release condition at $z = z_a$. From equations (4.28) and (4.29), the incident pressure is

$$p_i(r,\theta,z) = \begin{cases} \sum_{m=0}^{\infty}\sum_{n=1}^{\infty} -\frac{i}{2\varepsilon_m \Phi_n} H_m^{(1)}\left(\sqrt{\mu_n} r_0\right) J_m\left(\sqrt{\mu_n} r\right) & r < r_0 \\ \times \cos\left(m\left(\theta_0 - \theta\right)\right) \chi(z_0) Z_n(z_0) Z_n(z), & \\ \sum_{m=0}^{\infty}\sum_{n=1}^{\infty} -\frac{i}{2\varepsilon_m \Phi_n} H_m^{(1)}\left(\sqrt{\mu_n} r\right) J_m\left(\sqrt{\mu_n} r_0\right) & r > r_0 \\ \times \cos\left(m\left(\theta_0 - \theta\right)\right) \chi(z_0) Z_n(z_0) Z_n(z), & \end{cases}$$

where

$$\varepsilon_m = \begin{cases} 2 & m = 0 \\ 1 & m > 0 \end{cases}.$$

Total pressure is the sum of the incident pressure field, p_{inc}, and the scattered pressure field, p_{scat}, thus $p = p_{inc} + p_{scat}$. p_{scat} must also satisfy the boundary value problem

$$\nabla^2 p + k^2 p = 0$$

$$\frac{\partial}{\partial z} p(r,\theta,z_s) = 0, r > a \tag{8.1}$$

$$p(r,\theta,z_a) = 0. \tag{8.2}$$

$$p(r,\theta,0+) = p(r,\theta,0-) \tag{8.3}$$

$$-i\frac{\frac{\partial}{\partial z} p(r,\theta,0+)}{\rho_a \omega} = -i\frac{\frac{\partial}{\partial z} p(r,\theta,0-)}{\rho_s \omega} \tag{8.4}$$

Again, equation (8.4) is derived from the time-harmonic assumption on the conservation of momentum equation (eqn. (3.4)). Solutions are of the form

$$\begin{aligned} p_{scat}(r,\theta,z) &= \sum_{m=0}^{\infty}\sum_{n=1}^{\infty} H_m^{(1)}\left(\sqrt{\mu_n} r\right)\left(C_{mn}\cos(m\theta) + D_{mn}\sin(m\theta)\right) Z_n(z), \\ r &> a, \end{aligned}$$

where μ_n are the eigenvalues from Problem two layer waveguide (eqn. 4.18). Above the membrane, total pressure is given by

$$\begin{aligned} p(r,\theta,z) &= \sum_{m=0}^{\infty}\sum_{n=1}^{\infty} J_m\left(\sqrt{\zeta_{mn}}r\right)\left(A_{mn}\cos(m\theta)+B_{mn}\sin(m\theta)\right)\phi_{mn}(z), \qquad (8.5)\\ r &< a, \end{aligned}$$

where the eigenvalues ζ_{mn} and the eigenfunctions $\phi_{mn}(z)$ are to be determined.

At the interface $r=a$ the continuity conditions

$$p_{scat}(a+,\theta,z)+p_{inc}(a+,\theta,z)=p(a-,\theta,z) \qquad (8.6)$$

$$\partial_r p_{scat}(a+,\theta,z)+\partial_r p_{inc}(a+,\theta,z)=\partial_r p(a-,\theta,z)$$

are imposed. At $z=z_s$ continuity of velocity gives, in the case of the time-harmonic oscillations,

$$-i\omega u(r,\theta)=\frac{1}{i\omega\rho_s}\partial_z p(r,\theta,z_s),\ r<a \qquad (8.7)$$

where u is the vertical displacement of the membrane and ρ_s is the density of the soil.

8.1 Solution of the Problem

8.1.1 The Eigenvalue Problem

The eigenfunctions in the atmosphere $\phi_{mn,a}(z)$ satisfy the equations

$$\phi''_{mn,a}(z)+\left(k_a^2-\zeta\right)\phi_{mn,a}(z)=0$$

$$\phi_{mn,a}(z_a)=0$$

The differential equation has solution

$$\phi_{mn,a}(z)=E\cos(\Omega_a z)+F\sin(\Omega_a z),$$

where

$$\Omega_a^2=k_a^2-\zeta.$$

The pressure release condition (eqn. (8.2)) gives

$$E\cos(\Omega_a z_a)+F\sin(\Omega_a z_a)=0$$

$$E\cos(\Omega_a z_a)=-F\sin(\Omega_a z_a).$$

Note that $\phi_{mn,a}(z)$ becomes $E_1\sin(\Omega_a(z-z_a))$ for some E_1. The eigenfunctions in the soil satisfy the equations

$$\phi''_{mn,s}(z)+\left(k_s^2-\zeta\right)\phi_{mn,s}(z)=0$$

The differential equation has solution

$$\phi_{mn,s}(z) = K\cos(\Omega_s z) + L\sin(\Omega_s z),$$

where

$$\Omega_s^2 = k_s^2 - \zeta.$$

Note that equation (8.1) does not apply, since for $\phi_{mn,s}$, $r \leq a$.The atmosphere-soil interface condition (eqn. (8.3)) on pressure implies

$$-E_1\sin(\Omega_a(z_a)) = K$$

and continuity of velocity (eqn. (8.4)) gives

$$-i\frac{\Omega_a(\cos(\Omega_a z_a))}{\rho_a\omega} = -i\frac{\Omega_s L}{\rho_s\omega}$$

Substitution into $\phi_{mn,a}(z)$ yields

$$\phi_{mn,a}(z) = E_1\sin(\Omega_a(z - z_a))$$

and $\phi_{mn,s}(z)$ is

$$\phi_{mn,s}(z) = E_1\left(\frac{\rho_s\Omega_a}{\rho_a\Omega_s}\cos(\Omega_a z_a)\sin(\Omega_s z) - \sin(\Omega_a z_a)\cos(\Omega_s z)\right)$$

Thus, the eigenfunctions have the form

$$\phi_{mn}(z) = \begin{cases} \sin(\Omega_a(z - z_a)) & 0 \leq z \leq z_a \\ \frac{\rho_s\Omega_a}{\rho_a\Omega_s}\cos(\Omega_a z_a)\sin(\Omega_s z) - \sin(\Omega_a(z_a))\cos(\Omega_s z) & z_s \leq z < 0 \end{cases}.$$

From (7.6) the response of the membrane to an external pressure, p_e, is

$$\begin{aligned} u(r,\theta) &= \frac{1}{2T}\int_0^r\int_{-\pi}^{\pi}\sum_{m=0}^{\infty}\frac{1}{\varepsilon_m J_m(ka)}\left(Y_m(ka)J_m(kr) - Y_m(kr)J_m(ka)\right) \\ &\quad\times J_m(kr')\cos(m(\theta-\theta'))p_e(r',\theta')\,r'd\theta'dr' \\ &\quad+\frac{1}{2T}\int_r^a\int_{-\pi}^{\pi}\sum_{m=0}^{\infty}\frac{1}{\varepsilon_m J_m(ka)}\left(J_m(kr')Y_m(ka) - J_m(ka)Y_m(kr')\right) \\ &\quad\times J_m(kr)\cos(m(\theta-\theta'))p_e(r',\theta')\,r'd\theta'dr' \\ &= \frac{1}{2T}\sum_{m=0}^{\infty}\frac{1}{\varepsilon_m J_m(ka)}\left(Y_m(ka)J_m(kr) - Y_m(kr)J_m(ka)\right) \\ &\quad\times\int_0^r J_m(kr')\int_{-\pi}^{\pi}\cos(m(\theta-\theta'))p_e(r',\theta')\,d\theta'r'dr' \\ &\quad+\frac{1}{2T}\sum_{m=0}^{\infty}\frac{J_m(kr)}{\varepsilon_m J_m(ka)}\int_r^a\left(J_m(kr')Y_m(ka) - J_m(ka)Y_m(kr')\right) \\ &\quad\times\int_{-\pi}^{\pi}\cos(m(\theta-\theta'))p_e(r',\theta')\,d\theta'r'dr'. \end{aligned} \tag{8.8}$$

Since in this problem $p_e(r',\theta') = p(r',\theta',z_s)$ where p is given by (8.5),

$$\begin{aligned}
&\int_{-\pi}^{\pi} \cos(m(\theta-\theta'))\, p_e(r',\theta')\, d\theta' \\
= &\int_{-\pi}^{\pi} \sum_{m'=0}^{\infty}\sum_{n=1}^{\infty} J_{m'}\left(\sqrt{\zeta_{mn}}r'\right)\left(A_{m'n}\cos(m'\theta') + B_{m'n}\sin(m'\theta')\right) \\
&\times\phi_{mn}(z_s)\cos(m(\theta-\theta'))\, d\theta' \\
= &\ \varepsilon_m \pi \sum_{n=1}^{\infty} J_m\left(\sqrt{\zeta_{mn}}r'\right)\left(A_{mn}\cos(m\theta) + B_{mn}\sin(m\theta)\right) \\
&\times\left(\cos(\Omega_a z_a)\cos(\Omega_s z_s) - \frac{\rho_s\Omega_a}{\rho_a\Omega_s}\sin(\Omega_a z_a)\sin(\Omega_s z_s)\right)
\end{aligned}$$

in which case equation (8.8) becomes

$$\begin{aligned}
u(r,\theta) = &\frac{\pi}{2T}\sum_{m=0}^{\infty}\sum_{n=1}^{\infty}\frac{1}{J_m(ka)}\left(Y_m(ka)J_m(kr) - Y_m(kr)J_m(ka)\right) \\
&\times\left(A_{mn}\cos(m\theta) + B_{mn}\sin(m\theta)\right)\int_0^r J_m(kr')\, J_m\left(\sqrt{\zeta_{mn}}r'\right) r'dr' \\
&\times\left(\frac{\rho_s\Omega_a}{\rho_a\Omega_s}\cos(\Omega_a z_a)\sin(\Omega_s z_s) - \sin(\Omega_a z_a)\cos(\Omega_s z_s)\right) \\
&+\frac{\pi}{2T}\sum_{m=0}^{\infty}\sum_{n=1}^{\infty}\frac{J_m(kr)}{J_m(ka)}\left(A_{mn}\cos(m\theta) + B_{mn}\sin(m\theta)\right) \\
&\times\int_r^a \left(J_m(kr')Y_m(ka) - J_m(ka)Y_m(kr')\right) J_m\left(\sqrt{\zeta_{mn}}r'\right) r'dr' \\
&\times\left(\frac{\rho_s\Omega_a}{\rho_a\Omega_s}\cos(\Omega_a z_a)\sin(\Omega_s z_s) - \sin(\Omega_a z_a)\cos(\Omega_s z_s)\right)
\end{aligned}$$

According to MAPLE™

$$\begin{aligned}
&\left(Y_m(ka)J_m(kr) - Y_m(kr)J_m(ka)\right)\int_0^r J_m(kr')\, J_m\left(\sqrt{\zeta_{mn}}r'\right) r'dr' \\
&+J_m(kr)\int_r^a \left(J_m(kr')Y_m(ka) - J_m(ka)Y_m(kr')\right) J_m\left(\sqrt{\zeta_{mn}}r'\right) r'dr' \\
= &\frac{k}{k^2-\zeta_{mn}}\left(\begin{array}{c} rJ_m(ka)\, J_m\left(\sqrt{\zeta_{mn}}r\right)\left[J_m(kr)Y_{m+1}(kr) - J_{m+1}(kr)Y_m(kr)\right] \\ +aJ_m(kr)\, J_m\left(\sqrt{\zeta_{mn}}a\right)\left[J_{m+1}(ka)Y_m(ka) - J_m(ka)Y_{m+1}(ka)\right]\end{array}\right) \\
= &\frac{2}{\pi\left(k^2-\zeta_{mn}\right)}\left(J_m(kr)\, J_m\left(\sqrt{\zeta_{mn}}a\right) - J_m(ka)\, J_m\left(\sqrt{\zeta_{mn}}r\right)\right)
\end{aligned}$$

where the identity[1]

$$J_{m+1}(z)Y_m(z) - J_m(z)Y_{m+1}(z) = \frac{2}{\pi z}$$

[1] [2], pg. 362, eqn. (9.1.16).

has been used. Thus,

$$\begin{aligned} u(r,\theta) &= \frac{1}{T}\sum_{m=0}^{\infty}\sum_{n=1}^{\infty}\frac{1}{(k^2-\zeta_{mn})J_m(ka)}\left(A_{mn}\cos(m\theta)+B_{mn}\sin(m\theta)\right) \\ &\quad\times\left(J_m(kr)\,J_m\left(\sqrt{\zeta_{mn}}a\right)-J_m(ka)\,J_m\left(\sqrt{\zeta_{mn}}r\right)\right) \\ &\quad\times\left(\frac{\rho_s\Omega_a}{\rho_a\Omega_s}\cos(\Omega_a z_a)\sin(\Omega_s z_s)-\sin(\Omega_a z_a)\cos(\Omega_s z_s)\right) \end{aligned}$$

and from equation (8.5)

$$\begin{aligned} \partial_z p(r,\theta,z_s) &= \sum_{m=0}^{\infty}\sum_{n=1}^{\infty}J_m\left(\sqrt{\zeta_{mn}}r\right)\left(A_{mn}\cos(m\theta)+B_{mn}\sin(m\theta)\right) \\ &\quad\times\left(\frac{\rho_s\Omega_a}{\rho_a}\cos(\Omega_a z_a)\cos(\Omega_s z_s)+\Omega_s\sin(\Omega_a z_a)\sin(\Omega_s z_s)\right) \end{aligned}$$

and equation (8.7) becomes

$$\begin{aligned} &\frac{\rho_s\omega^2}{T}\sum_{m=0}^{\infty}\sum_{n=1}^{\infty}\frac{1}{(k^2-\zeta_{mn})J_m(ka)}\left(A_{mn}\cos(m\theta)+B_{mn}\sin(m\theta)\right) \\ &\times\left(J_m(kr)\,J_m\left(\sqrt{\zeta_{mn}}a\right)-J_m(ka)\,J_m\left(\sqrt{\zeta_{mn}}r\right)\right) \\ &\times\left(\frac{\rho_s\Omega_a}{\rho_a\Omega_s}\cos(\Omega_a z_a)\sin(\Omega_s z_s)-\sin(\Omega_a z_a)\cos(\Omega_s z_s)\right) \\ =\ &\sum_{m=0}^{\infty}\sum_{n=1}^{\infty}J_m\left(\sqrt{\zeta_{mn}}r\right)\left(A_{mn}\cos(m\theta)+B_{mn}\sin(m\theta)\right) \\ &\times\left(\frac{\rho_s\Omega_a}{\rho_a}\cos(\Omega_a z_a)\cos(\Omega_s z_s)+\Omega_s\sin(\Omega_a z_a)\sin(\Omega_s z_s)\right). \end{aligned}$$

Equating the coefficients of the trigonometric functions gives

$$\begin{aligned} &\frac{\rho_a\omega^2}{T}\sum_{n=1}^{\infty}\frac{1}{(k^2-\zeta_{mn})J_m(ka)} \\ &\times A_{mn}\left(J_m(kr)\,J_m\left(\sqrt{\zeta_{mn}}a\right)-J_m(ka)\,J_m\left(\sqrt{\zeta_{mn}}r\right)\right) \\ &\times\left(\frac{\rho_s\Omega_a}{\rho_a\Omega_s}\cos(\Omega_a z_a)\sin(\Omega_s z_s)-\sin(\Omega_a z_a)\cos(\Omega_s z_s)\right) \\ =\ &\sum_{n=1}^{\infty}J_m\left(\sqrt{\zeta_{mn}}r\right)A_{mn} \\ &\times\left(\frac{\rho_s\Omega_a}{\rho_a}\cos(\Omega_a z_a)\cos(\Omega_s z_s)+\Omega_s\sin(\Omega_a z_a)\sin(\Omega_s z_s)\right) \end{aligned}$$

with the same equation for B_{mn}. Multiplying by $rJ_m\left(\sqrt{\zeta_{mn}}r\right)$ and integrating from 0 to a gives

$$\begin{aligned}
&\frac{\rho_s\omega^2}{T}\sum_{n=1}^{\infty}\frac{1}{\left(k^2-\zeta_{mn}\right)J_m\left(ka\right)}A_{mn}\\
&\times\left(\frac{\rho_s\Omega_a}{\rho_a\Omega_s}\cos\left(\Omega_a z_a\right)\sin\left(\Omega_s z_s\right)-\sin\left(\Omega_a z_a\right)\cos\left(\Omega_s z_s\right)\right)\\
&\times\left(J_m\left(\sqrt{\zeta_{mn}}a\right)\int_0^a rJ_m\left(kr\right)J_m\left(\sqrt{\zeta_{mn}}r\right)dr-J_m\left(ka\right)\int_0^a rJ_m^2\left(\sqrt{\zeta_{mn}}r\right)dr\right)\\
=\;&\sum_{n=1}^{\infty}\int_0^a rJ_m^2\left(\sqrt{\zeta_{mn}}r\right)dr A_{mn}\\
&\times\left(\frac{\rho_s\Omega_a}{\rho_a}\cos\left(\Omega_a z_a\right)\cos\left(\Omega_s z_s\right)+\Omega_s\sin\left(\Omega_a z_a\right)\sin\left(\Omega_s z_s\right)\right).
\end{aligned}$$

Requiring the A_{mn} to be arbitrary gives the characteristic equations

$$\begin{aligned}
&-\frac{\rho_s\omega^2}{T}\frac{1}{\left(k^2-\zeta_{mn}\right)J_m\left(ka\right)}\\
&\times\left(\frac{\rho_s\Omega_a}{\rho_a\Omega_s}\cos\left(\Omega_a z_a\right)\sin\left(\Omega_s z_s\right)-\sin\left(\Omega_a z_a\right)\cos\left(\Omega_s z_s\right)\right)\\
&\times\left(J_m\left(\sqrt{\zeta_{mn}}a\right)\int_0^a rJ_m\left(kr\right)J_m\left(\sqrt{\zeta_{mn}}r\right)dr-J_m\left(ka\right)\int_0^a rJ_m^2\left(\sqrt{\zeta_{mn}}r\right)dr\right)\\
=\;&\int_0^a rJ_m^2\left(\sqrt{\zeta_{mn}}r\right)dr\\
&\times\left(\frac{\rho_s\Omega_a}{\rho_a}\cos\left(\Omega_a z_a\right)\cos\left(\Omega_s z_s\right)+\Omega_s\sin\left(\Omega_a z_a\right)\sin\left(\Omega_s z_s\right)\right),
\end{aligned}$$

for $m=0,1,2,3...$ Define $I_1=\int_0^a rJ_m\left(kr\right)J_m\left(\sqrt{\zeta_{mn}}r\right)dr$ and $I_2=\int_0^a rJ_m^2\left(\sqrt{\zeta_{mn}}r\right)dr=\frac{a^2}{2}\left[J_m^2\left(\sqrt{\zeta_{mn}}a\right)+J_{m+1}^2\left(\sqrt{\zeta_{mn}}a\right)\right]$. According to MAPLE™,

$$\begin{aligned}
I_1&=\int_0^a rJ_m\left(kr\right)J_m\left(\sqrt{\zeta_{mn}}r\right)dr\\
&=\frac{a}{\zeta_{mn}-k^2}\left[\sqrt{\zeta_{mn}}J_m\left(ka\right)J_{m+1}\left(\sqrt{\zeta_{mn}}a\right)-kJ_{m+1}\left(ka\right)J_m\left(\sqrt{\zeta_{mn}}a\right)\right]\\
I_2&=\int_0^a rJ_m^2\left(\sqrt{\zeta_{mn}}r\right)dr=\frac{a^2}{2}\left[J_m^2\left(\sqrt{\zeta_{mn}}a\right)+J_{m+1}^2\left(\sqrt{\zeta_{mn}}a\right)\right]\\
&\quad-\frac{a}{\sqrt{\zeta_{mn}}}\left(mJ_{m+1}\left(\sqrt{\zeta_{mn}}a\right)J_m\left(\sqrt{\zeta_{mn}}a\right)\right)
\end{aligned}$$

which results in

$$\begin{aligned} & -\frac{\rho_s\omega^2}{T}\frac{1}{\left(k^2-\zeta_{mn}\right)J_m\left(ka\right)} \\ & \times\left(\frac{\rho_s\Omega_a}{\rho_a\Omega_s}\cos\left(\Omega_a z_a\right)\sin\left(\Omega_s z_s\right)-\sin\left(\Omega_a z_a\right)\cos\left(\Omega_s z_s\right)\right) \\ & \times\left(J_m\left(\sqrt{\zeta_{mn}}a\right)I_1-J_m\left(ka\right)I_2\right)-I_2 \\ & \times\left(\frac{\rho_s\Omega_a}{\rho_a}\cos\left(\Omega_a z_a\right)\cos\left(\Omega_s z_s\right)+\Omega_s\sin\left(\Omega_a z_a\right)\sin\left(\Omega_s z_s\right)\right) \\ = \;& 0, m=0,1,2,3... \end{aligned}$$

Change of variables for analysis of the characteristic equation in MATLAB™ requires that $\tau_{mn} = z_a\sqrt{k_a^2-\zeta_{mn}}$, which implies that $\zeta_{mn} = k_a^2 - \left(\frac{\tau_{mn}}{z_a}\right)^2$. This ensures the eigenvalues, τ_{mn}, will be approximately evenly spaced, similar to the change of variables from the two-layer waveguide. The characteristic equation therefore becomes

$$\begin{aligned} & -\frac{\rho_s\omega^2}{T}\frac{1}{\left(k^2-\zeta_{mn}\right)J_m\left(ka\right)} \\ & \times\left(\frac{\rho_s\tau_{mn}}{z_a\rho_a\sqrt{k_s^2-\zeta_{mn}}}\cos\left(\tau_{mn}\right)\sin\left(z_s\sqrt{k_s^2-\zeta_{mn}}\right)-\sin\left(\tau_{mn}\right)\cos\left(z_s\sqrt{k_s^2-\zeta_{mn}}\right)\right) \\ & \times\left(J_m\left(\sqrt{\zeta_{mn}}a\right)I_1-J_m\left(ka\right)I_2\right)+I_2 \\ & \times\left(\frac{\rho_s\tau_{mn}}{z_a\rho_a}\cos\left(\tau_{mn}\right)\cos\left(z_s\sqrt{k_s^2-\zeta_{mn}}\right)+\sqrt{k_s^2-\zeta_{mn}}\sin\left(\tau_{mn}\right)\sin\left(z_s\sqrt{k_s^2-\zeta_{mn}}\right)\right) \\ = \;& 0, m=0,1,2,3... \end{aligned} \tag{8.9}$$

8.1.2 Predicting Resonances

Consider equation (8.9). Substitution of Ω_s results in

$$\begin{aligned} & -\frac{\rho_s\omega^2}{T}\frac{1}{\left(k^2-\zeta_{mn}\right)J_m\left(ka\right)} \\ & \times\left(\frac{\rho_s\tau_{mn}}{z_a\rho_a\Omega_s}\cos\left(\tau_{mn}\right)\sin\left(z_s\Omega_s\right)-\sin\left(\tau_{mn}\right)\cos\left(z_s\Omega_s\right)\right) \\ & \times\left(J_m\left(\sqrt{\zeta_{mn}}a\right)I_1-J_m\left(ka\right)I_2\right)+I_2 \\ & \times\left(\frac{\rho_s\tau_{mn}}{z_a\rho_a}\cos\left(\tau_{mn}\right)\cos\left(z_s\Omega_s\right)+\sqrt{k_s^2-\zeta_{mn}}\sin\left(\tau_{mn}\right)\sin\left(z_s\Omega_s\right)\right) \\ = \;& 0, m=0,1,2,3... \end{aligned}$$

For a Z-resonance ($\tau \to 0$), assuming $\rho_a \ll \rho_s$,

$$-\frac{\rho_s\omega^2}{T}\frac{1}{(k^2-k_a^2)}\sin\left(z_s\sqrt{k_s^2-k_a^2}\right)\left(J_0\left(k_a a\right)I_1 - J_0\left(ka\right)I_2\right)$$
$$+J_0\left(ka\right)I_2\left(\cos\left(z_s\sqrt{k_s^2-k_a^2}\right)\right)=0$$

with

$$I_1 = \frac{a}{k_a^2-k^2}\left(k_a J_0\left(ka\right)J_1\left(k_a a\right) - kJ_1\left(ka\right)J_0\left(k_a a\right)\right)$$

and

$$I_2 = \frac{a^2}{2}\left(J_0^2\left(k_a a\right)+J_1^2\left(k_a a\right)\right) - \frac{a}{k_a}\left(mJ_1\left(k_a a\right)J_0\left(k_a a\right)\right).$$

For an E-resonance ($\zeta_{mn} \to 0$),

$$-\frac{\rho_s\omega^2}{T}\left(\sin\left(z_s k_s\right)\right)\left(\frac{J_1\left(ka\right)}{k} - J_0\left(ka\right)\frac{a}{2}\right) - k_s k^2 J_0\left(ka\right)\frac{a}{2}\cos\left(z_s k_s\right)=0.$$

Recall that $\tau = z_a\sqrt{k_a^2-\zeta_{mn}}$, and ζ represents the resonant properties of the membrane. These equations are plotted over a broad range of frequencies for the Sabatier parameters (fig (8.1)).

8.1.3 The Radial Continuity Conditions

The first of the radial continuity conditions (8.6) gives

$$\begin{aligned}
&\sum_{m=0}^{\infty}\sum_{n=1}^{\infty}H_m^{(1)}\left(\sqrt{\mu_n}a\right)\left(C_{mn}\cos\left(m\theta\right)+D_{mn}\sin\left(m\theta\right)\right)Z_n\left(z\right)\\
&+\sum_{m=0}^{\infty}\sum_{n=1}^{\infty}-\frac{i}{2\varepsilon_m\Phi_n}H_m^{(1)}\left(\sqrt{\mu_n}r_0\right)J_m\left(\sqrt{\mu_n}a\right)\cos\left(m\left(\theta_0-\theta\right)\right)\\
&\times\chi\left(z_0\right)Z_n\left(z_0\right)Z_n\left(z\right)\\
=&\sum_{m=1}^{\infty}\sum_{n=1}^{\infty}J_m\left(\sqrt{\zeta_{mn}}a\right)\left(A_{mn}\cos\left(m\theta\right)+B_{mn}\sin\left(m\theta\right)\right)\phi_{mn}\left(z\right)
\end{aligned}$$

where

$$\phi_{mn}\left(z\right)=\begin{cases}\sin\left(\Omega_a\left(z-z_a\right)\right) & 0\le z\le z_a\\ \frac{\rho_s\Omega_a}{\rho_a\Omega_s}\cos\left(\Omega_a z_a\right)\sin\left(\Omega_s z\right)-\sin\left(\Omega_a\left(z_a\right)\right)\cos\left(\Omega_s z\right) & z_s\le z<0\end{cases}.$$

The second of the radial continuity conditions (8.6) gives

$$\begin{aligned}
&\sum_{m=0}^{\infty}\sum_{n=1}^{\infty}\sqrt{\mu_n}H_m^{(1)\prime}\left(\sqrt{\mu_n}a\right)\left(C_{mn}\cos\left(m\theta\right)+D_{mn}\sin\left(m\theta\right)\right)Z_n\left(z\right)\\
&+\sum_{m=0}^{\infty}\sum_{n=1}^{\infty}-\frac{i\sqrt{\mu_n}}{2\varepsilon_m\Phi_n}H_m^{(1)}\left(\sqrt{\mu_n}r_0\right)J_m'\left(\sqrt{\mu_n}a\right)\cos\left(m\left(\theta_0-\theta\right)\right)\chi\left(z_0\right)Z_n\left(z_0\right)Z_n\left(z\right)\\
=&\sum_{m=1}^{\infty}\sum_{n=1}^{\infty}\sqrt{\zeta_{mn}}J_m'\left(\sqrt{\zeta_{mn}}a\right)\left(A_{mn}\cos\left(m\theta\right)+B_{mn}\sin\left(m\theta\right)\right)\phi_{mn}\left(z\right).
\end{aligned}$$

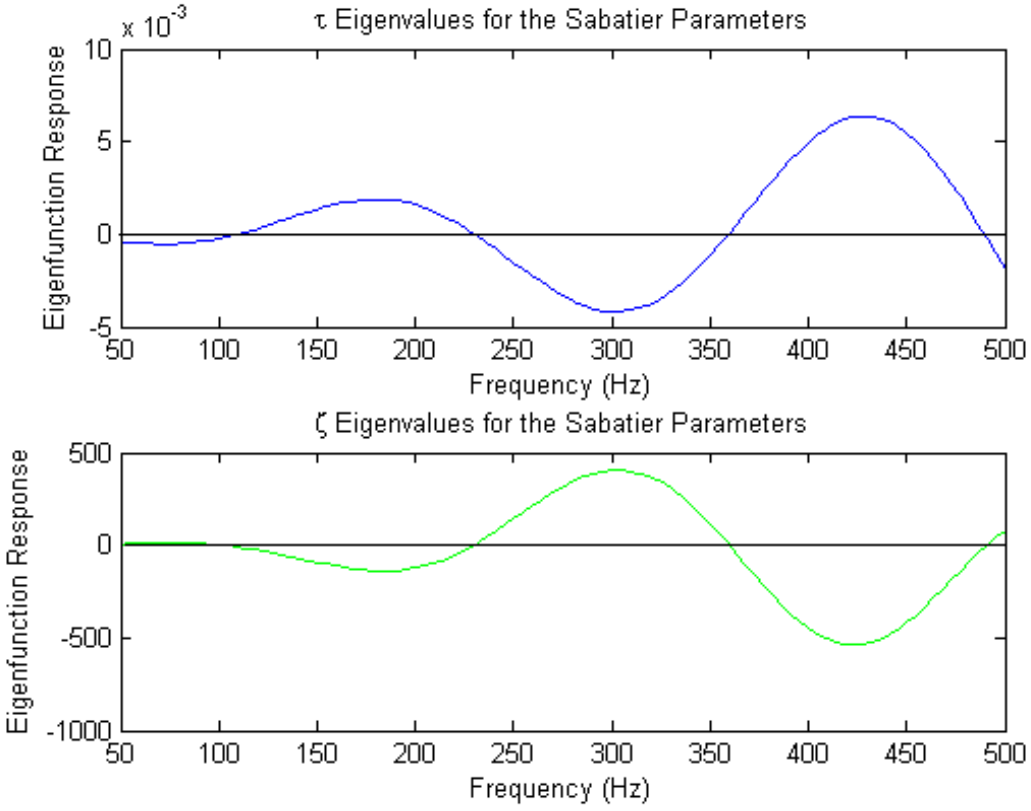

Figure 8.1: Eigenvalues of the Membrane Problem. The eigenvalues corresponding to frequencies are determined from the zero crossings.

Equating the coefficients of the trigonometric functions gives

$$\begin{aligned}
&\sum_{n=1}^{\infty} J_m\left(\sqrt{\zeta_{mn}}a\right)\phi_{mn}(z)\,A_{mn} - H_m^{(1)}\left(\sqrt{\mu_n}a\right)Z_n(z)\,C_{mn} \\
= \;& -\frac{i}{2\varepsilon_m\Phi_n}H_m^{(1)}\left(\sqrt{\mu_n}r_0\right)J_m\left(\sqrt{\mu_n}a\right)\cos(m\theta_0)\,\chi(z_0)\,Z_n(z_0)\,Z_n(z)
\end{aligned}$$

$$\begin{aligned}
&\sum_{n=1}^{\infty} J_m\left(\sqrt{\zeta_{mn}}a\right)\phi_{mn}(z)\,B_{mn} - H_m^{(1)}\left(\sqrt{\mu_n}a\right)Z_n(z)\,D_{mn} \\
= \;& -\frac{i}{2\varepsilon_m\Phi_n}H_m^{(1)}\left(\sqrt{\mu_n}r_0\right)J_m\left(\sqrt{\mu_n}a\right)\sin(m\theta_0)\,\chi(z_0)\,Z_n(z_0)\,Z_n(z)
\end{aligned}$$

$$\begin{aligned}
&\sum_{n=1}^{\infty} \sqrt{\zeta_{mn}}J_m'\left(\sqrt{\zeta_{mn}}a\right)\phi_{mn}(z)\,A_{mn} - \sqrt{\mu_n}H_m^{(1)\prime}\left(\sqrt{\mu_n}a\right)Z_n(z)\,C_{mn} \\
= \;& -\frac{i\sqrt{\mu_n}}{2\varepsilon_m\Phi_n}H_m^{(1)}\left(\sqrt{\mu_n}r_0\right)J_m'\left(\sqrt{\mu_n}a\right)\cos(m\theta_0)\,\chi(z_0)\,Z_n(z_0)\,Z_n(z)
\end{aligned}$$

$$\begin{aligned}
&\sum_{n=1}^{\infty} \sqrt{\zeta_{mn}}J_m'\left(\sqrt{\zeta_{mn}}a\right)\phi_{mn}(z)\,B_{mn} - \sqrt{\mu_n}H_m^{(1)\prime}\left(\sqrt{\mu_n}a\right)Z_n(z)\,D_{mn} \\
= \;& -\frac{i\sqrt{\mu_n}}{2\varepsilon_m\Phi_n}H_m^{(1)}\left(\sqrt{\mu_n}r_0\right)J_m'\left(\sqrt{\mu_n}a\right)\sin(m\theta_0)\,\chi(z_0)\,Z_n(z_0)\,Z_n(z)\,.
\end{aligned}$$

If $\theta_0 = 0$ it suffices to consider the cosine equations. Multiplying by χZ_n and integrating on z from z_s to z_a and using the orthogonality of the Z_n gives

$$\begin{aligned}
&\sum_{l=1}^{\infty} J_m\left(\sqrt{\zeta_l}a\right)I_{mnl}A_{ml} - \Phi_n H_m^{(1)}\left(\sqrt{\mu_n}a\right)C_{mn} \\
= \;& -\Phi_n\frac{i}{2\varepsilon_m\Phi_n}H_m^{(1)}\left(\sqrt{\mu_n}r_0\right)J_m\left(\sqrt{\mu_n}a\right)\chi(z_0)\,Z_n(z_0)
\end{aligned}$$

$$\begin{aligned}
&\sum_{l=1}^{\infty} \sqrt{\zeta_l}J_m'\left(\sqrt{\zeta_l}a\right)I_{mnl}A_{ml} - \Phi_n\sqrt{\mu_n}H_m^{(1)\prime}\left(\sqrt{\mu_n}a\right)C_{mn} \\
= \;& -\Phi_n\frac{i\sqrt{\mu_n}}{2\varepsilon_m\Phi_n}H_m^{(1)}\left(\sqrt{\mu_n}r_0\right)J_m'\left(\sqrt{\mu_n}a\right)\chi(z_0)\,Z_n(z_0)
\end{aligned}$$

where, according to MAPLE™,

$$\begin{aligned}
\Phi_n &= \int_{z_s}^{z_a}\chi(z)\,Z_n(z)^2\,dz = \int_{z_s}^{0}\rho_a Z_{s,n}(z)^2\,dz + \int_{0}^{z_a}\rho_s Z_{a,n}(z)^2\,dz \\
&= -\frac{\rho_a z_s}{2\alpha}\sin(\xi_n)^2(\cos(\alpha_n)\sin(\alpha_n)+\alpha_n) + \frac{\rho_s z_a}{2\xi_n}\cos(\alpha_n)^2(-\cos(\xi_n)\sin(\xi_n)+\xi_n)
\end{aligned}$$

$$\begin{aligned} I_{mnl} &= \int_{z_s}^{z_a} \chi(z)\,\phi_{ml}(z)\,Z_n(z)\,dz = \int_{z_s}^{0} \rho_a \phi_{ml,s}(z)\,Z_{n,s}(z)\,dz + \int_{0}^{z_a} \rho_s \phi_{ml,a}(z)\,Z_{n,a}(z)\,dz \\ &= \frac{\sin(\xi_n)\,z_s}{z_a\left(-\iota_{mn}^2+\alpha_n^2\right)} \begin{pmatrix} -z_s\rho_s\tau_{mn}\cos(\iota_{mn})\cos(\tau_{mn}) + z_a\rho_a\alpha_n\sin(\alpha_n)\sin(\tau_{mn}) \\ -\iota_{mn}z_a\rho_a\sin(\iota_{mn})\sin(\tau_{mn}) + z_s\rho_s\tau_{mn}\cos(\alpha_n)\cos(\tau_{mn}) \end{pmatrix} \\ &\quad + \frac{z_a\rho_s\cos(\alpha_n)\left(-\tau_{mn}\cos(\tau_{mn})\sin(\xi_n)+\xi_n\sin(\tau_{mn})\cos(\xi_n)\right)}{\xi_n^2-\tau_{mn}^2} \end{aligned}$$

where

$$\begin{aligned} \xi_n &= z_a\sqrt{k_a^2-\mu_n} \\ \alpha_n &= z_s\sqrt{k_s^2-\mu_n} \\ \tau_{mn} &= z_a\sqrt{k_a^2-\zeta_{mn}} \\ \iota_{mn} &= z_s\sqrt{k_s^2-\zeta_{mn}} \end{aligned}$$

and

$$\mu_n = k_a^2 - \left(\frac{\kappa_n}{z_a}\right)^2.$$

Eliminating C_{mn} gives

$$\begin{aligned} &\sum_{l=1}^{\infty}\left[\sqrt{\mu_n}H_m^{(1)\prime}\left(\sqrt{\mu_n}a\right)J_m\left(\sqrt{\zeta_{lm}}a\right) - \sqrt{\zeta_{lm}}J_m'\left(\sqrt{\zeta_{lm}}a\right)H_m^{(1)}\left(\sqrt{\mu_n}a\right)\right]I_{mnl}A_{ml} \qquad (8.10) \\ = &-\frac{i\sqrt{\mu_n}}{2\varepsilon_m}\chi(z_0)\,Z_n(z_0)\,H_m^{(1)}\left(\sqrt{\mu_n}r_0\right)\begin{bmatrix} H_m^{(1)\prime}\left(\sqrt{\mu_n}a\right)J_m\left(\sqrt{\mu_n}a\right) \\ -J_m'\left(\sqrt{\mu_n}a\right)H_m^{(1)}\left(\sqrt{\mu_n}a\right)\end{bmatrix}. \end{aligned}$$

Equation (8.10) is an infinite dimensional linear system for A_{ml}. In computing A_{ml}, the infinite limit will be replaced by a sufficiently high value, N, to form a finite dimensional system. This is one of the equations that will be programmed into MATLAB™ to solve the Membrane Problem. Note that $\mathcal{C}_v'(z) = -\mathcal{C}_{v+1}(z) + \frac{v}{z}\mathcal{C}_v(z)$, if $\mathcal{C}$ is a Bessel or Hankel Function.[2] For simplicity, rewrite equation (8.10), defining the first and second lines.

$$\begin{aligned} &\sum_{l=1}^{\infty}\left[\sqrt{\mu_n}H_m^{(1)\prime}\left(\sqrt{\mu_n}a\right)J_m\left(\sqrt{\zeta_{lm}}a\right) - \sqrt{\zeta_{lm}}J_m'\left(\sqrt{\zeta_{lm}}a\right)H_m^{(1)}\left(\sqrt{\mu_n}a\right)\right]I_{mnl}A_{ml} \qquad (8.11) \\ = &-\frac{i\sqrt{\mu_n}}{2\varepsilon_m}\chi(z_0)\,Z_n(z_0)\,H_m^{(1)}\left(\sqrt{\mu_n}r_0\right)\left[H_m^{(1)\prime}\left(\sqrt{\mu_n}a\right)J_m\left(\sqrt{\mu_n}a\right) - J_m'\left(\sqrt{\mu_n}a\right)H_m^{(1)}\left(\sqrt{\mu_n}a\right)\right] \qquad (8.12) \end{aligned}$$

The bracketed portion of line (8.12) can be rewritten

$$\begin{aligned} &H_m^{(1)\prime}\left(\sqrt{\mu_n}a\right)J_m\left(\sqrt{\mu_n}a\right) - J_m'\left(\sqrt{\mu_n}a\right)H_m^{(1)}\left(\sqrt{\mu_n}a\right) \\ = &\left(-H_{m+1}^{(1)}\left(\sqrt{\mu_n}a\right) + \frac{m}{\sqrt{\mu_n}a}H_m^{(1)}\left(\sqrt{\mu_n}a\right)\right)J_m\left(\sqrt{\mu_n}a\right) \\ &-H_m^{(1)}\left(\sqrt{\mu_n}a\right)\left(-J_{m+1}\left(\sqrt{\mu_n}a\right) + \frac{m}{\sqrt{\mu_n}a}J_m\left(\sqrt{\mu_n}a\right)\right) \end{aligned}$$

[2] [2], pg. 361.

Combining like terms yields

$$\begin{aligned} &= J_m\left(\sqrt{\mu_n}a\right)\left(-H^{(1)}_{m+1}\left(\sqrt{\mu_n}a\right)+\frac{m}{\sqrt{\mu_n}a}H^{(1)}_m\left(\sqrt{\mu_n}a\right)-\frac{m}{\sqrt{\mu_n}a}H^{(1)}_m\left(\sqrt{\mu_n}a\right)\right) \\ &\quad +J_{m+1}\left(\sqrt{\mu_n}a\right)H^{(1)}_m\left(\sqrt{\mu_n}a\right) \\ &= J_{m+1}\left(\sqrt{\mu_n}a\right)H^{(1)}_m\left(\sqrt{\mu_n}a\right)-J_m\left(\sqrt{\mu_n}a\right)H^{(1)}_{m+1}\left(\sqrt{\mu_n}a\right) \end{aligned} \tag{8.13}$$

The bracketed portion of line (8.11) can be rewritten

$$\begin{aligned} &\sqrt{\mu_n}H^{(1)\prime}_m\left(\sqrt{\mu_n}a\right)J_m\left(\sqrt{\zeta_{lm}}a\right)-\sqrt{\zeta_{lm}}J'_m\left(\sqrt{\zeta_{lm}}a\right)H^{(1)}_m\left(\sqrt{\mu_n}a\right) \\ &= \sqrt{\mu_n}\left(-H^{(1)}_{m+1}\left(\sqrt{\mu_n}a\right)+\frac{m}{\sqrt{\mu_n}a}H^{(1)}_m\left(\sqrt{\mu_n}a\right)\right)J_m\left(\sqrt{\zeta_{lm}}a\right) \\ &\quad -\sqrt{\zeta_{lm}}H^{(1)}_m\left(\sqrt{\mu_n}a\right)\left(-J_{m+1}\left(\sqrt{\zeta_{lm}}a\right)+\frac{m}{\sqrt{\zeta_{lm}}a}J_m\left(\sqrt{\zeta_{lm}}a\right)\right) \end{aligned}$$

Combining like terms yields

$$\begin{aligned} &= J_m\left(\sqrt{\zeta_{lm}}a\right) \\ &\quad \times\left(-\sqrt{\mu_n}H^{(1)}_{m+1}\left(\sqrt{\mu_n}a\right)+\sqrt{\mu_n}\frac{m}{\sqrt{\mu_n}a}H^{(1)}_m\left(\sqrt{\mu_n}a\right)-\sqrt{\zeta_{lm}}\frac{m}{\sqrt{\zeta_{lm}}a}H^{(1)}_m\left(\sqrt{\mu_n}a\right)\right) \\ &\quad +\sqrt{\zeta_{lm}}J_{m+1}\left(\sqrt{\zeta_{lm}}a\right)H^{(1)}_m\left(\sqrt{\mu_n}a\right) \\ &= \sqrt{\zeta_{lm}}J_{m+1}\left(\sqrt{\zeta_{lm}}a\right)H^{(1)}_m\left(\sqrt{\mu_n}a\right)-\sqrt{\mu_n}J_m\left(\sqrt{\zeta_{lm}}a\right)H^{(1)}_{m+1}\left(\sqrt{\mu_n}a\right) \end{aligned} \tag{8.14}$$

Lines (8.13) and (8.14) were entered into the formula for A_{mn}. Therefore,

$$\begin{aligned} &\sum_{l=1}^{\infty}\left[\sqrt{\zeta_{lm}}J_{m+1}\left(\sqrt{\zeta_{lm}}a\right)H^{(1)}_m\left(\sqrt{\mu_n}a\right)-\sqrt{\mu_n}J_m\left(\sqrt{\zeta_{lm}}a\right)H^{(1)}_{m+1}\left(\sqrt{\mu_n}a\right)\right]I_{mnl}A_{ml} \\ &= -\frac{i\sqrt{\mu_n}}{2\varepsilon_m}\chi\left(z_0\right)Z_n\left(z_0\right)H^{(1)}_m\left(\sqrt{\mu_n}r_0\right)\left[\begin{array}{c} J_{m+1}\left(\sqrt{\mu_n}a\right)H^{(1)}_m\left(\sqrt{\mu_n}a\right) \\ -J_m\left(\sqrt{\mu_n}a\right)H^{(1)}_{m+1}\left(\sqrt{\mu_n}a\right)\end{array}\right]. \end{aligned}$$

The C_{mn} are then given by

$$C_{mn}=\frac{\sum_{l=1}^{\infty}J_m\left(\sqrt{\zeta_l}a\right)I_{mnl}A_{ml}}{\Phi_nH^{(1)}_m\left(\sqrt{\mu_n}a\right)}-\frac{iH^{(1)}_m\left(\sqrt{\mu_n}r_0\right)J_m\left(\sqrt{\mu_n}a\right)\chi\left(z_0\right)Z_n\left(z_0\right)}{2\varepsilon_m\Phi_nH^{(1)}_m\left(\sqrt{\mu_n}a\right)}.$$

Velocity in the atmosphere is

$$\begin{aligned} w &= \frac{1}{i\omega\rho_a}\partial_z p \\ &= \frac{1}{i\omega\rho_a}\sum_{m=0}^{\infty}\sum_{n=1}^{\infty}J_m\left(\sqrt{\zeta_{mn}}r\right)A_{mn}\cos\left(m\theta\right)\phi'_{mn}\left(z\right), r<a \end{aligned} \tag{8.15}$$

where

$$\phi_{mn}(z) = \sin(\Omega_a(z - z_a)).$$

and

$$\phi'_{mn}(z) = \Omega_a \cos(\Omega_a(z - z_a)).$$

Chapter 9

Membrane Analysis and Comparison with Sabatier[1]

9.1 Membrane Analysis

In this section, the blue line in each graph represents the Sabatier parameters. All other colors are variations on the indicated parameter. Note that the Sabatier parameters are $z_s = -0.175$ m, $c_a = 340$ m/s, $\rho_a = 1.2\ \frac{kg}{m^3}$, $c_{comp,s} = 160$ m/s, $c_{shear,s} = 75$ m/s, and $\rho_s = 1400\ \frac{kg}{m^3}$.

9.1.1 Termination of the Infinite Sum

In order to obtain reasonable solutions, it is necessary to extend the solution in equation (8.15) to at least the first soil eigenvalue. This eigenvalue results from equation (4.18), particularly from the $\cos z_s\sqrt{k_s^2-\mu}$ in the first line. Since $\cos(x) = 0$ when $x = \frac{(2n-1)\pi}{2}$, $z_s\sqrt{k_s^2-\mu} = \frac{(2n-1)\pi}{2}$. Therefore, $\mu = k_s^2 - \left(\frac{(2n-1)\pi}{2z_s}\right)^2 \rightarrow \kappa = z_a\sqrt{k_a^2 - k_s^2 + \left(\frac{(2n-1)\pi}{2z_s}\right)^2}$. Since the first soil resonance is of interest, $n = 1$, and $\kappa = z_a\sqrt{k_a^2 - k_s^2 + \left(\frac{\pi}{2z_s}\right)^2}$. With the appropriate substitutions made, $\kappa = 500\sqrt{\left(\frac{2\pi f}{c_a}\right)^2 - \left(\frac{2\pi f\left(2\pi f + i\frac{\sigma}{\rho_p}\right)}{c_{ss}^2}\right) + \left(\frac{\pi}{2z_s}\right)^2}$. To ensure that the first resonance is completely accounted for, $\kappa + 1000$ will be used to terminate the infinite sum. Figure (9.1) represents early and late termination of the sum, around this predicted value, for the first mechanical resonance for the Sabatier parameters.

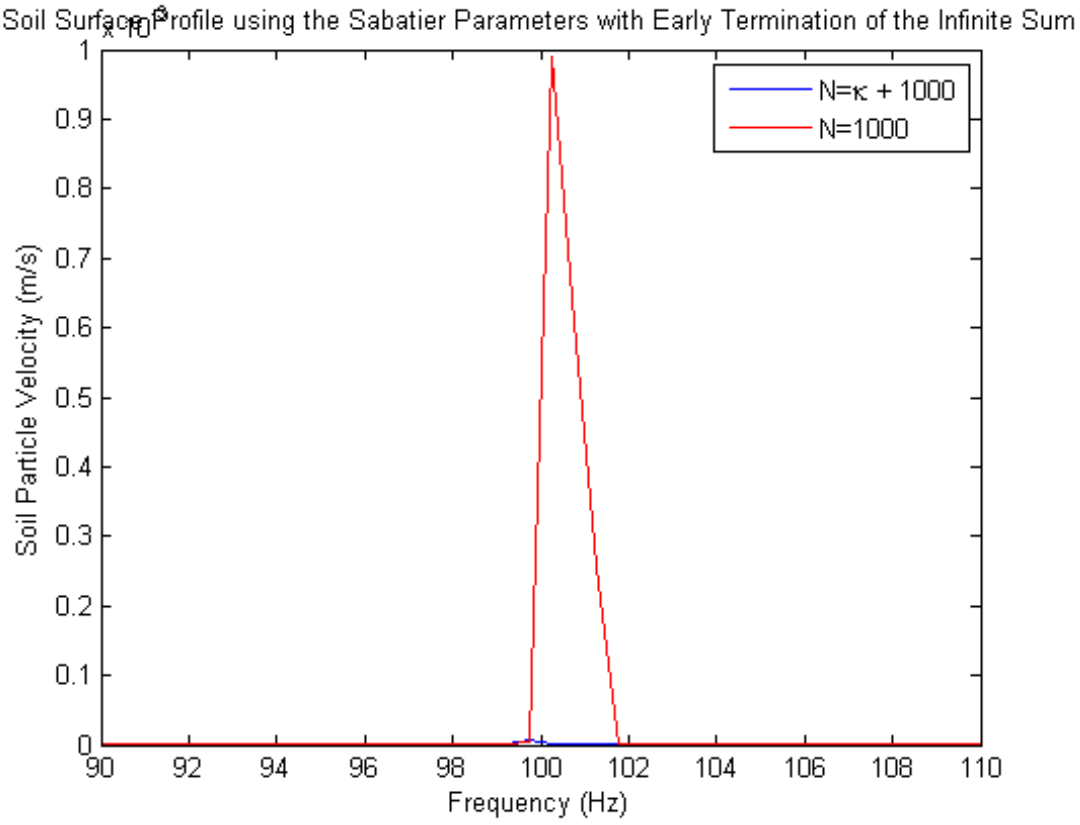

Figure 9.1: This figure represents the effects of early termination of the infinite sum. Note the exaggeration and unreasonable difference in magnitude between the resonance. The vertical scale is 1×10^{-3}.

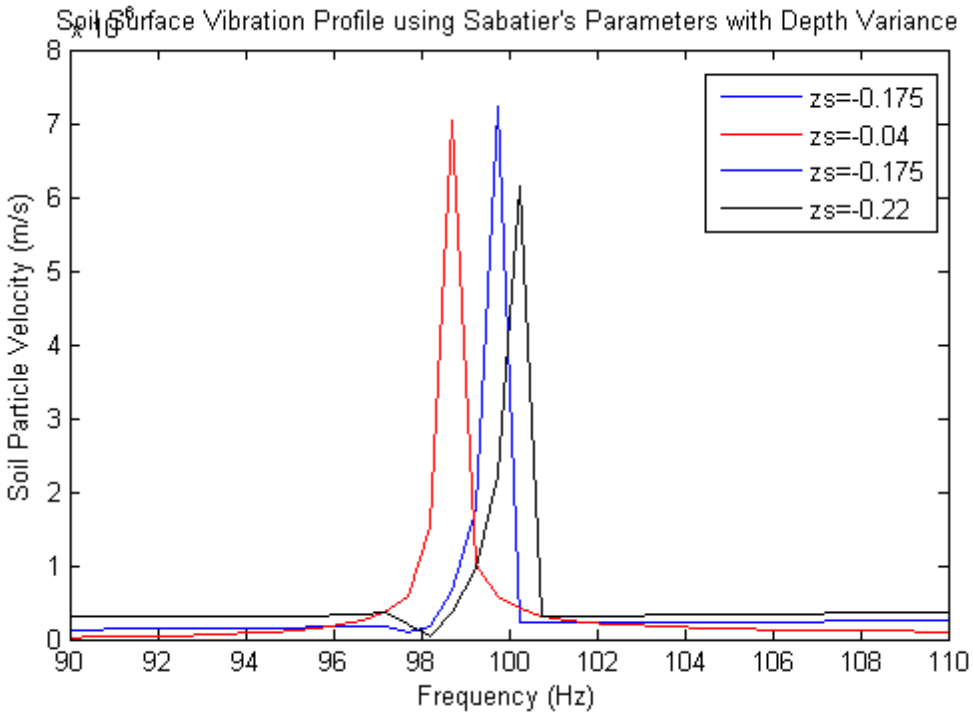

Figure 9.2: This graphic shows how increasing the depth results in much weaker mechanical and acoustic resonances. Note how the resonances change with depth. The vertical scale is 1×10^{-6}. The units of z_s are meters.

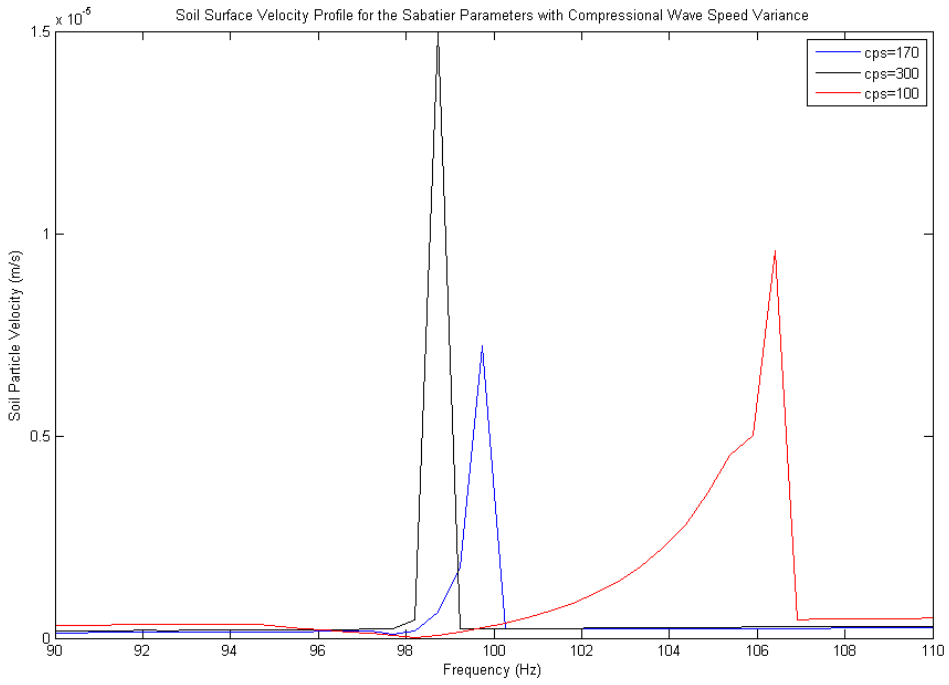

Figure 9.3: Results of varying the compressional wave speed within the Sabatier parameters. The units of $c_{p,s}$ are m/s.

9.1.2 Variance of Parameters

Depth of Mine Detection Limitations

As seen in Figure (9.2), as depth increases, the mechanical resonance moves to the right and decreases in strength. If the large mechanical resonance disappears, the acoustical resonance is also very hard to detect. The resonance of the mine itself is much stronger than the acoustic resonance. Resonances at larger depths are soil resonances, and can be predicted from the two-layer waveguide. According to Sabatier, landmines are usually buried less than 10 centimeters (.1 m) from the soil surface. As indicated by Figure (9.2), the soil particle velocity plots are more precise at shallow depths.

Soil Variations

Compressional sound speed (fig. (9.3)) affects the curvature, location, and magnitude of the resonance. Larger values for compressional sound speed move the resonances to the left, and decrease the curvature of the leading part of the resonance. There does not appear to be any correlation

[1] [27]

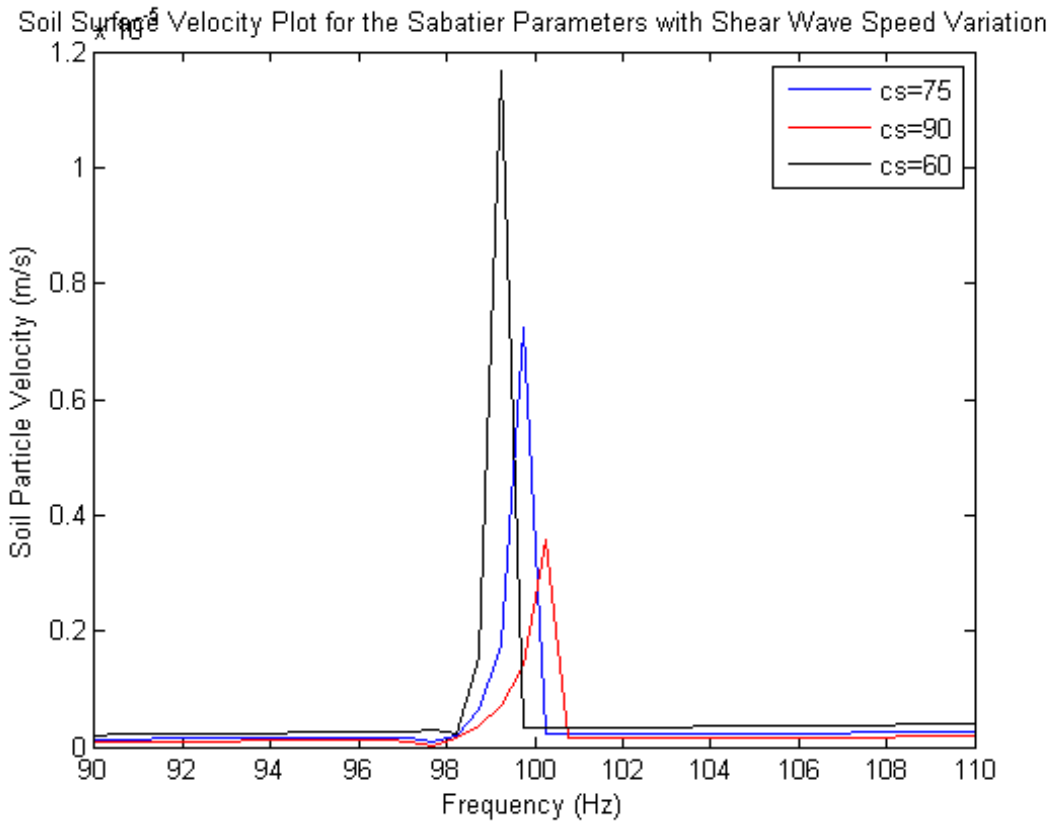

Figure 9.4: Results of varying the shear wave speed within the Sabatier parameters. The units of c_s are m/s. The vertical scale is 1×10^{-5}.

between large and small values with magnitude; however, magnitude does show some dependence on compressional wave speed. Note that Sabatier suggests a value of 160 $\frac{m}{s}$, while experiments from Dr. D. Keith Wilson and Dr. Harley Cudney of the US Army Corps of Engineers suggest values may be as high as 647$\frac{m}{s}$ in shallow desert soil. With such a large variance in soil parameters, ascertaining the effect of sound speed on the profiles is a very important step in predicting the landmine resonances.

According to Figure (9.4), larger values of shear sound speed appear to move the resonance to the right, and decrease the intensity of the soil velocity response.

Similarly, the density of the soil appears to have significant effect (fig. (9.5)). This parameter seems to adjust resonance width, amplitude, and a slight shift in the resonant frequency. The only apparent correlation is between the magnitude of ρ_p and the resonance shift: small ρ_p appear to the right of larger values for ρ_p. Sabatier suggests a value of 1400$\frac{kg}{m^3}$, while the experimental data from Wilson and Cudney suggest 1600 $\frac{kg}{m^3}$. Note that $\rho_s = \rho_p + \frac{i\sigma}{\omega}$, and that the ρ_p was altered by changing ρ_s; the value given the key for the graph.

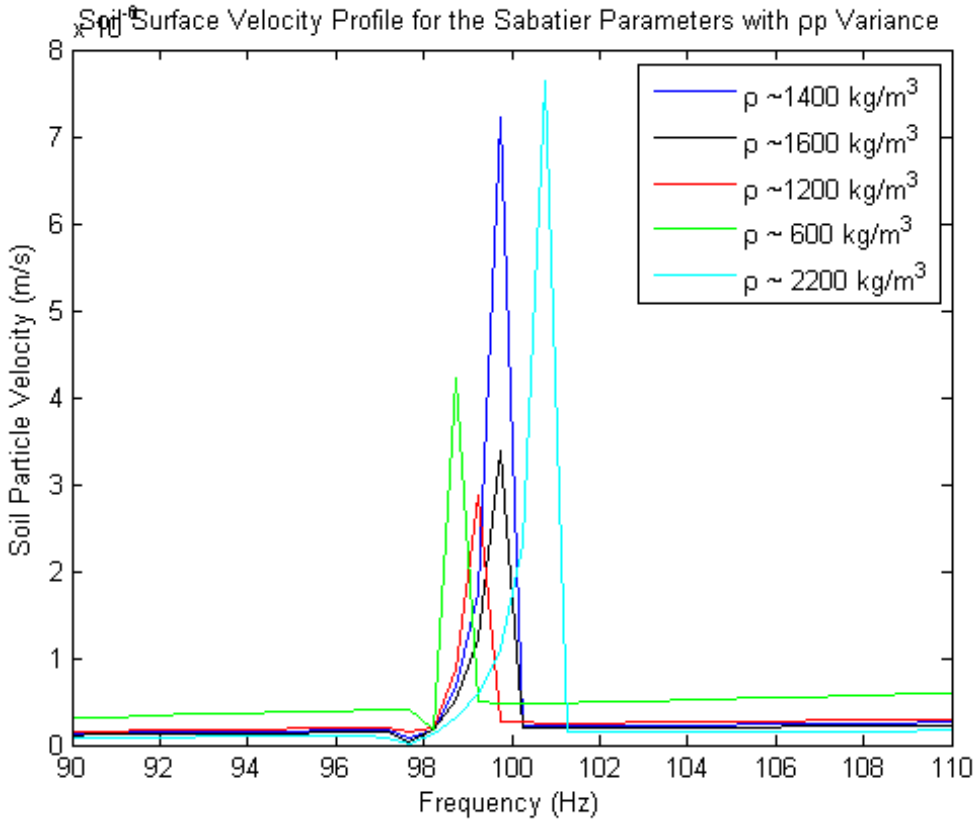

Figure 9.5: This graphic demonstrates the sensitivity of the soil particle velocity to changes in ρ_p.The vertical scale is 1×10^{-6}.

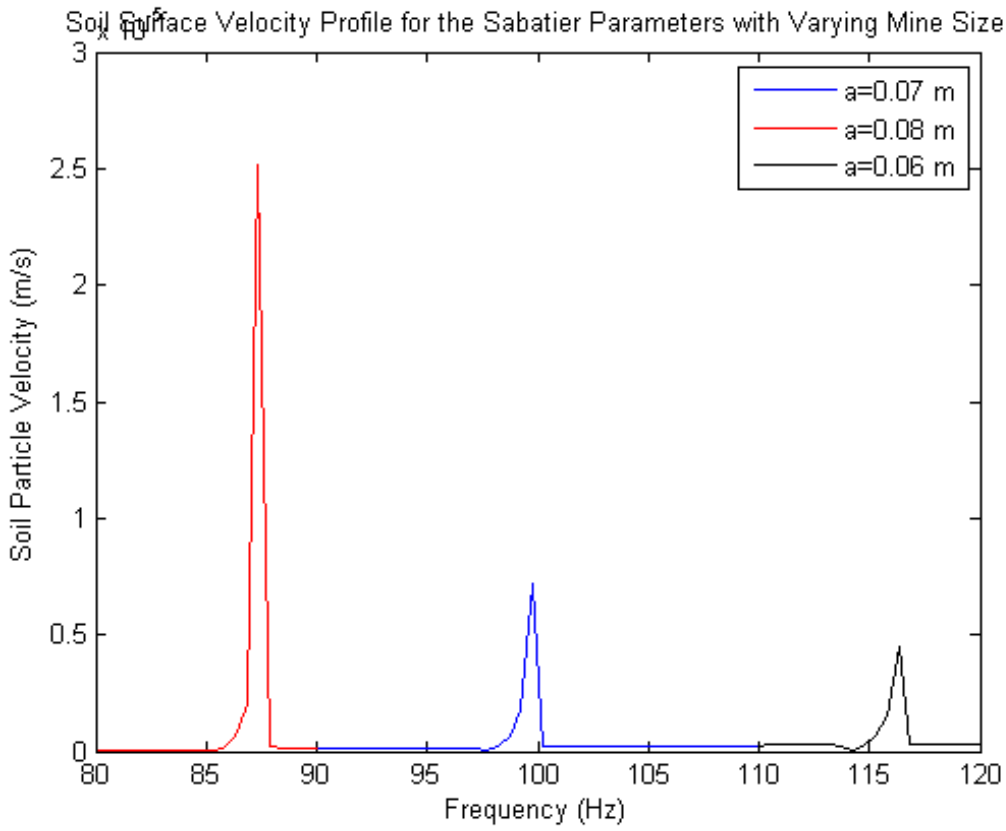

Figure 9.6: This profile shows the effect of the size of the mine with regard to the resonance. Note even small changes in the radius a seem to have large effects. The vertical scale is 1×10^{-5}.

9.1.3 Membrane Variation

The membrane density and tension are difficult quantities to assign since they are particular to each landmine. Since this model is based on the VS 1.6 Anti-Tank mine, a brief discussion of the selection process for ρ_m follows in the discussion on the comparison with Sabatier's model. However, this discussion suggests that either the mechanical resonance or exact parameters with regard to both tension and density must be known for accurate detection.

The size of the landmine also affects detectability. The VS 1.6 is approximately the size of a dinner plate, with a radius of 7 centimeters (.07 m). However, the smaller the mine, the smaller the amplitude of the resonances, making the mine harder to detect. This is shown in Figure (9.6). Note that small changes (not even order of magnitude changes) have a large effect on the resonant frequencies.

9.2 Comparison with Sabatier's Findings

9.2.1 The Sabatier - Waxler - Velea Paper[7]

In *An Effective Fluid Model for Landmine Detection using Acoustic to Seismic Coupling*, Sabatier et. al create a "right circular waveguide with rigid walls, [which] contains air in the upper half, soil in the lower half, and a buried mine placed concentrically on the waveguide's axis."[8] Using a mass-spring problem analogy, Sabatier then uses a "brute force numerical scheme"[9] to solve the pressure equation, using the same boundary conditions as this project. The paper from Sabatier et al. does not consider the scattering effects of the mine or soil for an incident acoustic or seismic wave; whereas this project has included the scattering effects.

The Sabatier parameters refer to the properties used by Sabatier in his research. The first parameter described is the depth of the buried mine, referred to as z_s in this project, at 3 inches, or 0.075 meters. The mine's radius is next mentioned, referred to as a in this project, and assigned a value of 0.07 meters. The frequency sweep that Sabatier performs ranges from $f = 80 - 300$ Hz. Finally, the air and soil parameters that Sabatier uses are listed as $c_a = 340$ m/s, $\rho_a = 1.2\ \frac{kg}{m^3}$, $c_s = 160$ m/s, and $\rho_s = 1400\ \frac{kg}{m^3}$.

9.2.2 Selection of ρ_m, the Density of the Membrane

The selection of ρ_m, along with other variables, determines the resonances for the soil-membrane system. Sabatier's model of the system as a mass-spring damper lists parameters specific to the mass and spring that cannot be easily translated into values for this project. Expecting that the mechanical resonance should occur at approximately 100 Hz, reasonable approximations are made from the mathematical equations for ρ_m. From equation (8.9), a mechanical resonance occurs when $J_0(ka) = 0$, where $k \in \mathbb{R}$. Recall that $k = \sqrt{\frac{\rho_m\omega^2 + i\beta_m\omega}{T}}$ is actually complex, where ω is the angular frequency ($\omega = 2\pi f$), β_m accounts for the damping, and T is the tension. The first zero of the Bessel function occurs when $ka = 2.405$.[11] If $a = .07$ m, as in Sabatier's experiment, then $k = 34.3571 \approx \sqrt{\frac{\rho_m\omega^2}{T}}$. Sabatier's parameters are assumed for the other variables to be $\omega = 2\pi\,(100)$ Hz, $\beta_m = 1000$ N-s/m, and $T = 2,000,000$ kg/s^2, then $\rho_m = 5980.04 \approx 6000$ kg/m^3.

9.2.3 Comparison with Sabatier's Work

A mechanical resonance is defined as "the resonant frequencies of any mechanical system for which the input mechanical reactance goes to zero."[12] The mechanical system refers to the land-mine itself, explaining the narrow band response observed in this paper's frequency response graph.

[7] [27]
[8] [27], pg. 1993.
[9] [27], pg. 1996.
[11] [5], pg. x.
[12] [18], pg. 48.

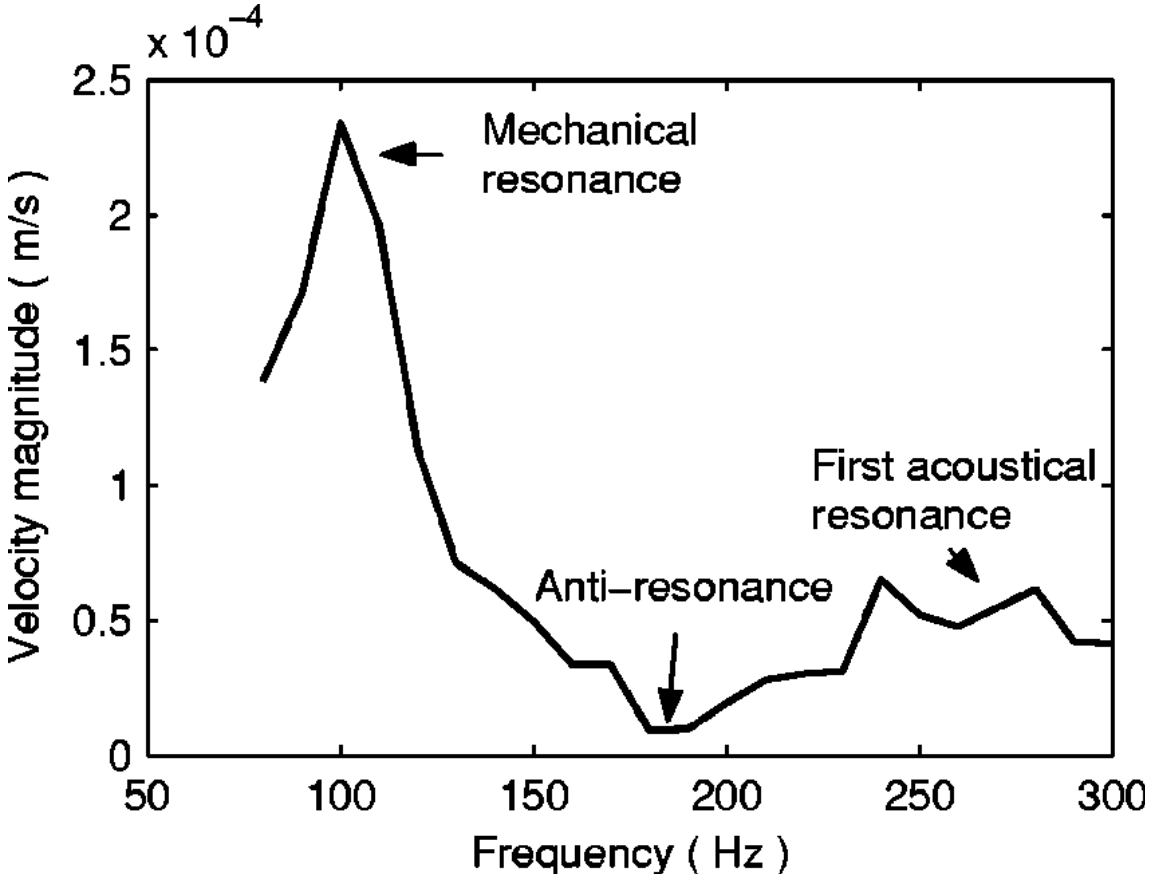

Figure 9.7: Sabatier's measured values in a soil surface velocity plot. Note the increments are approximately 10 Hz.

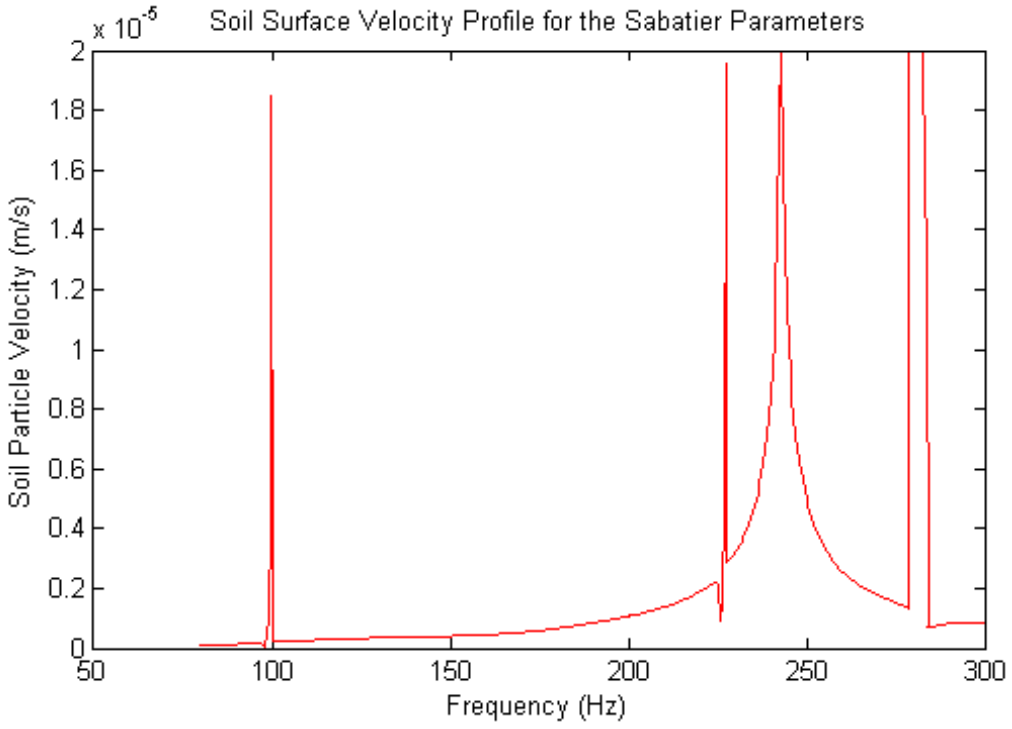

Figure 9.8: Predictions based on the theoretical solution presented in this paper for Sabatier's parameters.

Man-made objects, like a landmine case, tend to have a relatively narrow band response due to the highly organized molecular structure of the solid material when compared with the granular and significantly more random structure of the soil particles. This higher quality factor "Q" response allows acoustic to seismic landmine detection to remain fairly accurate (in discriminating detections from false alarms) in even rocky soil, where conventional detection techniques fail. Note the common resonance in the Sabatier plot (fig. (9.7)) and this project's plot (fig. (9.8)) at approximately 100 Hz.

The anti-resonance is the frequencies which result in a local minimum for the frequency response plot. This can be compared to the destructive interference between two propagating waves. Sabatier claims the anti-resonance occurs from 180-210 Hz, while the data from this paper suggests anti-resonances occur precisely before the mechanical resonances.

The prediction also suggests a second mechanical resonances for the membrane at approximately 230 Hz.

There appears to be a peak in Sabatier's work near $f = 240$ Hz that is unlabeled. This is a soil resonance, predicted by the two-layer waveguide problem in this paper (see fig. (9.9)). The same soil resonance is observed in the plot from this project's derivation.

The first acoustical resonance is term defined by Sabatier to be the frequency at which "the layer of soil between the top of the mine and the surface of the soil"[16] vibrates at maximum amplitude. This resonance occurs very clearly in Sabatier's graph at approximately $f = 280$ Hz. However, according to Figure (9.9), the second soil resonance occurs at this same frequency.

[16][27], pg. 1994.

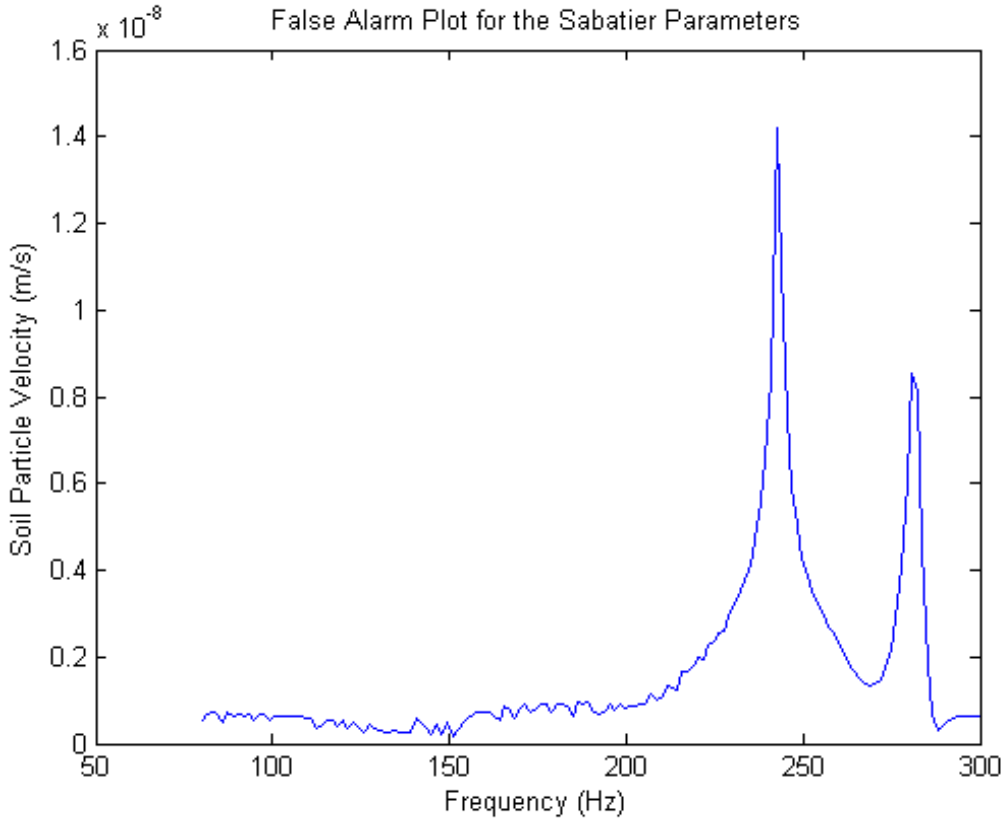

Figure 9.9: This plot shows the predicted soil resonances for the false alarm case, generated from the two-layer waveguide using the Sabatier parameters.

Chapter 10

COMSOL^{TM} Advances

COMSOL^{TM} is a sophisticated multiphysics program which employs the finite element method to solve very complicated problems of multiple equations very quickly. The finite element method discretize the domain into smaller areas, and solves the equations over these small areas. For clarification, an example is included in Figure (10.1). COMSOL^{TM} is well-known for its selective meshing technique, which permits the user to use rough meshing in less important parts of the diagram, and fine meshing in important parts of the diagram. The diagram used to calculate these results, along with its selective meshing, is shown in Figure (10.1). For the two-layer waveguide, the two-dimensional axially symmetric, time harmonic pressure acoustics module is used. The Bessel panel and loudspeaker tutorials suggested the spherical geometry developed in Figure (10.2) to represent the two-layer waveguide. The Bessel panel tutorial was chosen because of its implementation of the delta function.From the data obtained in the solution, shown as the subplot within Figure (10.2), multiple post-processing options are available. Of particular interest for this problem are the radial distance versus pressure plots, an example of which is shown in Figure (10.3).

Unfortunately, COMSOL^{TM} has not produced results that agree with the two-layer waveguide results. The main problem appears to be the implementation of the delta function in COMSOL^{TM}.

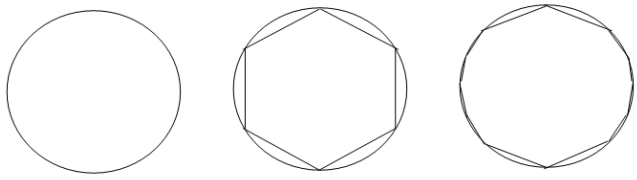

Figure 10.1: The illustration above demonstrates how the Finite Element Method would calculate the perimeter of a circle. The middle circle would be considered a rough mesh, while the circle on the right would give a more accurate solution.

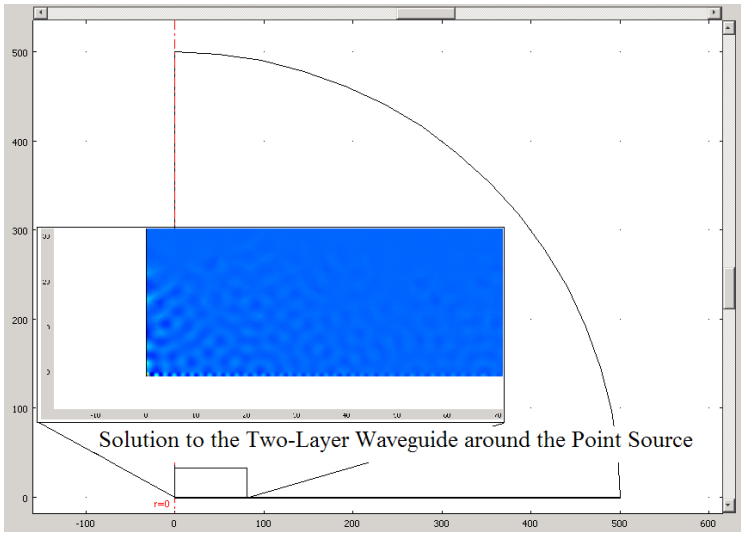

Figure 10.2: This diagram shows the geometry of the COMSOL model drafted for the two-layer waveguide. A quarter circle with a radius of 500 representing the atmospheric layer was placed atop a rectangle of depth 1 meter. Appropriate boundary conditions were selected, and the solution in the location around the point source is shown as an insert.

The source in the problem plotted in Figure (10.3) was at $r_0 = 0$, so the highest pressure should logically appear at $r \approx 0$. The COMSOL™ solution is still being worked on, and hopefully a result matching the MATLAB™ computed two-layer waveguide will be obtained.

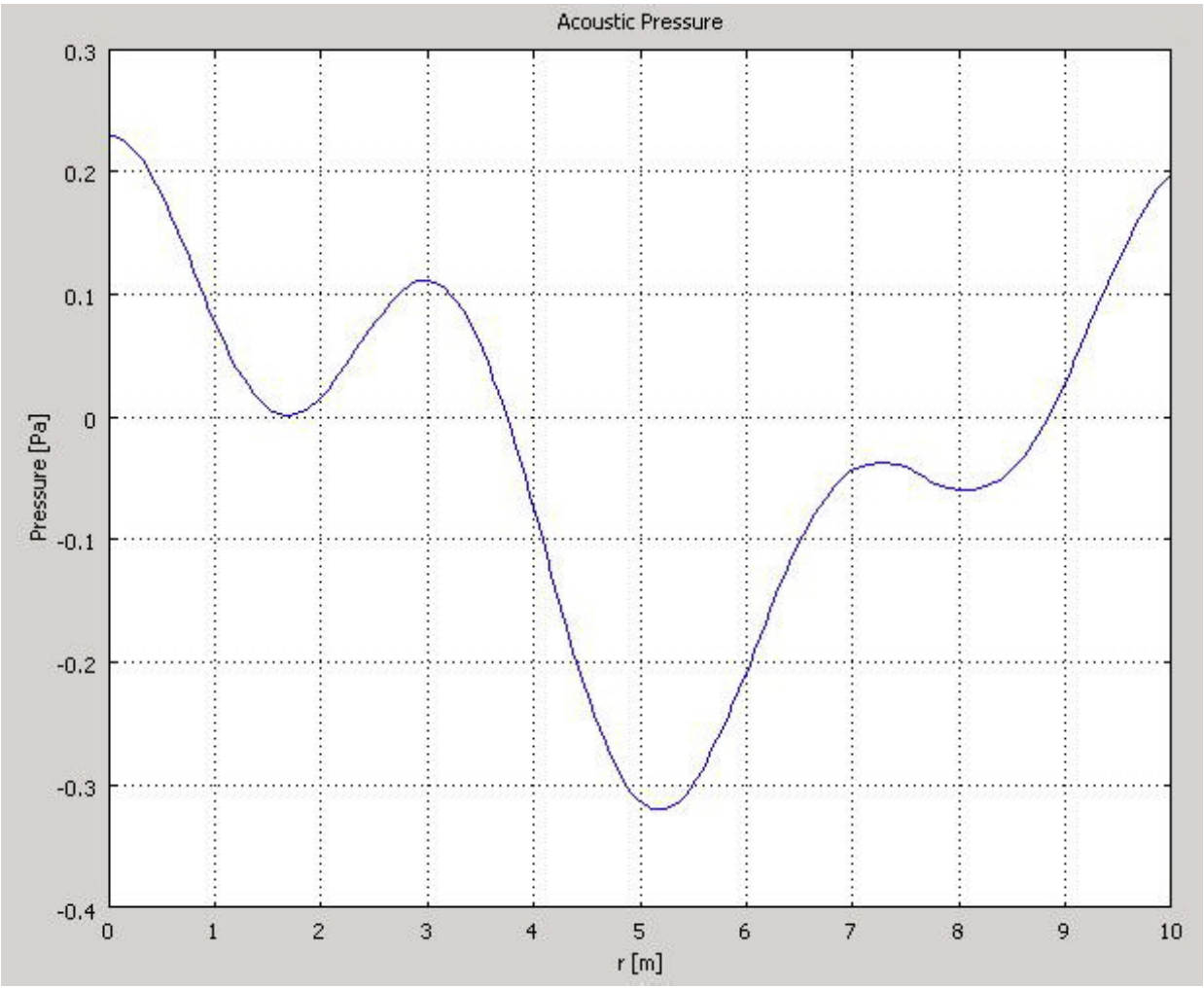

Figure 10.3: An example of a radial distance versus pressure plot for the two-layer waveguide.

Bibliography

[1] *Interview with SPC Daniel P. Staciak, USA, 2d Battalion, 87th Inf, 3rd Brigade, 10th Mountian Division*. Deployment from 05 February, 2006 - 25 May, Afganistan, 2007.

[2] M. Abramowitz and I. Stegun, editors. *Handbook of Mathematical Functions*. Dover, New York, 1965.

[3] K. Attenborough, S. Taherzadeh, H. Bass, R. Raspet, G. Becker, A. Gudesen, A. Chrestman, G. Daigle, A. L'Esperance, Y. Gabillet, K. Gilbert, Y. Li, M. White, P. Naz, J. Noble, and H. van Hoof. Benchmark cases for outdoor sound propagation models. *J. Acoust. Soc. Am.*, 97(1):173–191, 1995.

[4] P. Bergmann. The wave equation in a medium with a variable index of refraction. *J. Acoust. Soc. Am.*, 17:329–333, 1946.

[5] F. Bowman. *Introduction to Bessel Functions*. Dover Publications Inc., New York, 1958.

[6] C. Boyles. *Acoustic Waveguides*. John Wiley and Sons, New York, 1984.

[7] M. Croll. *The History of Landmines*. Pen and Sword Books, Ltd., Barnsley, Great Britian, 1998.

[8] M. O. R. Darmody and W. O'Brien. Measurement of attenuation and speed of sound in soils. *Soil Sci. Soc. Am. J.*, 66:788–796, 2002.

[9] G. Frisk. *Ocean and Seabed Acoustics*. Prentice Hall, Englewood Cliffs, New Jersey, 1994.

[10] E. Gossard. *Waves in the Atmosphere*. Elsevier, Amsterdam, 1975.

[11] R. Haberman. *Applied Partial Differential Equations*. Pearson Education, Inc., Boston, 2004.

[12] R. Hackman. Acoustical scattering in an inhomogeneous waveguide:theory. *J. Acoust. Soc. Am.*, 80:1447–1458, 1986.

[13] N. Haskell. Asymptotic approximation for the normal modes in sound channel wave propagation. *J. Appl. Phys.*, 22:157–168, 1951.

[14] A. Healey and W. Webber. Sensors for the detection of land-based munitions. *Defense Technical Information Center - Naval Postgraduate School, Monterey, California*, 1995.

[15] C. Hines. Atmospheric gravity waves: A new toy for the wave theorist. *Radio Sci.*, 69:375–380, 1965.

[16] F. Ingenito. Scattering from an object in a stratified medium. *J. Acoust. Soc. Am.*, 82:2051–2059, 1987.

[17] A. Kharab and R. Guenther. *An Introduction to Numerical Methods*. Chapman and Hall, London, 2006.

[18] A. C. L.E. Kinsler, A.R. Frey and J. Sanders. *Fundamentals of Acoustics, 4th Edition*. John Wiley and Sons, New York, 2000.

[19] J. MacDonald, J. Lockwood, J. McFee, T. Altshuler, T. Broach, L. Carin, R. Harmon, C. Rappaport, W. Scott, and R. Weaver. *Alternatives for Landmine Detection*. RAND Science and Technology Policy Institute, Santa Monica, California, 2003.

[20] J. Mathews and R. Walker, editors. *Mathematical Methods of Physics*. Addison Wesley, Boston, 1971.

[21] R. McGrath. *Landmines and Unexploded Ordnance: A Resource Book*. Pluto Press, London, 2000.

[22] P. Morse and K. Ingard. *Theoretical Acoustics*. Princeton University Press, Princeton, New Jersy, 1968.

[23] F. I. N. Makris and W. Kuperman. Detection of a submerged object insonified by surface noise in an ocean waveguide. *J. Acoust. Soc. Am.*, 96(3):1703–1724, 1994.

[24] E. Sengpiel. *für Mikrofonaufnahmetechnik und Tonstudiotechnik - Microphone for Recording Technique and Recording Studio Technology*. online at sengpielaudio.com, University of the Arts, Berlin.

[25] A. Sommerfeld, editor. *Partial Differential Equations of Physics*. Academic Press, New York, 1964.

[26] E. Toolbox. *Density of Dry Air, Water Vapor, and Moist Humid Air*. online at engineeringtoolbox.com, The Engineering Toolbox.

[27] D. Velea, R. Waxler, and J. Sabatier. An effective fluid model for landmine detection using acoustic to seismic coupling. *J. Acoust. Soc. Am.*, 115(5):1993–2002, 2004.

[28] N. Youngblood. *The Development of Mine Warfare*. Praeger Security International, Westport, Conneticut, 2006.

[29] C. Zwikker and C. Kosten. *Sound Absorbing Materials*. Elsevier Publishing Corp., New York, 1949.

Appendix A

Orthogonality Proofs

A.1 Orthogonality of the Eigenfunctions

The generic Sturm-Liouville Differential Equation in the z coordinate is represented by

$$\frac{\partial}{\partial z}\left(p\left(z\right)\frac{\partial Z}{\partial z}\right)+\left[\lambda\chi\left(z\right)+q\left(z\right)\right]Z=0. \tag{A.1}$$

In the case of the two layer waveguide problem,

$$Z_a''\left(z\right)+\left(-\mu+k_a^2\right)Z_a\left(z\right)=0$$

$$Z_s''\left(z\right)+\left(-\mu+k_s^2\right)Z_s\left(z\right)=0$$

$p\left(z\right)=1$, $\lambda=-\mu$, and $q\left(z\right)=\begin{cases} k_a^2 & 0<z\leq z_a \\ k_s^2 & z_a\leq z<0 \end{cases}$, to obtain the $Z\left(z\right)=\begin{cases} Z_a & 0<z\leq z_a \\ Z_s & z_s\leq z<0 \end{cases}$ function. Let Z_m and Z_n be eigenfunctions of the depth equation ($Z\left(z\right)$). The following proof implies that eigenfunctions Z_m and Z_n of the Sturm-Liouville equation are orthogonal on (a,b) with respect to the weight function $\chi\left(z\right)$ if

$$\int_a^b Z_m\left(z\right)\left(p\left(z\right)Z_n'\left(z\right)\right)'dz+\int_a^b q\left(z\right)Z_m\left(z\right)Z_n\left(z\right)dz+\lambda_n\int_a^b\chi\left(z\right)Z_m\left(z\right)Z_n\left(z\right)dz=0. \tag{A.2}$$

In the case of the two layer waveguide problem, the condition above refers to the two intervals of $(z_s,0)$ and $(0,z_a)$, written as

$$\int_{z_s}^0 Z_{s,m}\left(z\right)Z_{s,n}''\left(z\right)dz+\int_{z_s}^0 k_s^2 Z_{s,m}\left(z\right)Z_{s,n}\left(z\right)dz-\mu_n\int_{z_s}^0\chi\left(z\right)Z_{s,m}\left(z\right)Z_{s,n}\left(z\right)dz=0$$

$$\int_0^{z_a} Z_{a,m}\left(z\right)Z_{a,n}''\left(z\right)dz+\int_0^{z_a} k_a^2 Z_{a,m}\left(z\right)Z_{a,n}\left(z\right)dz-\mu_n\int_0^{z_a}\chi\left(z\right)Z_{a,m}\left(z\right)Z_{a,n}\left(z\right)dz=0.$$

Using integration by parts on the first integral of both conditions gives

$$\int_a^b Z_m(z)\left(p(z)\,Z_n'(z)\right)'dz = Z_m(z)\,p(z)\,Z_n'(z)\,|_a^b - \int_a^b p(z)\,Z_m'(z)\,Z_n'(z)\,dz$$

or, in the specific cases presented in this paper,

$$\int_{z_s}^0 Z_{s,m}(z)\,Z_{s,n}''(z)\,dz = Z_{s,m}(z)\,Z_{s,n}'(z)\,|_{z_s}^0 - \int_{z_s}^0 Z_{s,m}'(z)\,Z_{s,n}'(z)\,dz$$

$$\int_0^{z_a} Z_{a,m}(z)\,Z_{a,n}''(z)\,dz = Z_{a,m}(z)\,Z_{a,n}'(z)\,|_0^{z_a} - \int_0^{z_a} Z_{a,m}'(z)\,Z_{a,n}'(z)\,dz.$$

The governing boundary conditions are that $Z(z_a)=0$, $Z_a(0)=Z_s(0)$, $\rho_s Z_a'(0)=\rho_a Z_s'(0)$ and $Z'(z_s)=0$. Therefore,

$$Z_{s,m}(z)\,Z_{s,n}'(z)\,|_{z_s}^0 = Z_{s,m}(0)\,Z_{s,n}'(0) - Z_{s,m}(z_s)\,Z_{s,n}'(z_s) = Z_{s,m}(0)\,Z_{s,n}'(0)$$

$$\begin{aligned} Z_{a,m}(z)\,Z_{a,n}'(z)\,|_0^{z_a} &= Z_{a,m}(z_a)\,Z_{a,n}'(z_a) - Z_{a,m}(0)\,Z_{a,n}'(0) = -Z_{a,m}(0)\,Z_{a,n}'(0) \\ &= -\frac{\rho_a}{\rho_s} Z_{s,m}(0)\,Z_{s,n}'(0). \end{aligned}$$

So,

$$Z_{s,m}(0)\,Z_{s,n}'(0) - \int_{z_s}^0 Z_{s,m}'(z)\,Z_{s,n}'(z)\,dz + \int_{z_s}^0 k_s^2 Z_{s,m}(z)\,Z_{s,n}(z)\,dz - \mu_n \int_{z_s}^0 \chi(z)\,Z_{s,m}(z)\,Z_{s,n}(z)\,dz = 0$$

$$\begin{aligned} 0 &= -Z_{a,m}(0)\,Z_{a,n}'(0) - \int_0^{z_a} Z_{a,m}'(z)\,Z_{a,n}'(z)\,dz \\ &\quad + \int_0^{z_a} k_a^2 Z_{a,m}(z)\,Z_{a,n}(z)\,dz - \mu_n \int_0^{z_a} \chi(z)\,Z_{a,m}(z)\,Z_{a,n}(z)\,dz. \end{aligned}$$

Switching m and n gives

$$\begin{aligned} 0 &= Z_{s,n}(0)\,Z_{s,m}'(0) - \int_{z_s}^0 Z_{s,n}'(z)\,Z_{s,m}'(z)\,dz \\ &\quad + \int_{z_s}^0 k_s^2 Z_{s,n}(z)\,Z_{s,m}(z)\,dz - \mu_m \int_{z_s}^0 \chi(z)\,Z_{s,n}(z)\,Z_{s,m}(z)\,dz \end{aligned}$$

$$\begin{aligned} 0 &= -Z_{a,n}(0)\,Z_{a,m}'(0) - \int_0^{z_a} Z_{a,n}'(z)\,Z_{a,m}'(z)\,dz \\ &\quad + \int_0^{z_a} k_a^2 Z_{a,n}(z)\,Z_{a,m}(z)\,dz - \mu_m \int_0^{z_a} \chi(z)\,Z_{a,n}(z)\,Z_{a,m}(z)\,dz. \end{aligned}$$

Subtracting the two equations, respectively, results in

$$Z_{s,m}(0) Z'_{s,n}(0) - Z_{s,n}(0) Z'_{s,m}(0) - (\mu_n - \mu_m) \int_{z_s}^{0} \chi(z) Z_{s,n}(z) Z_{s,m}(z) dz = 0$$

$$-Z_{a,m}(0) Z'_{a,n}(0) + Z_{a,n}(0) Z'_{a,m}(0) - (\mu_n - \mu_m) \int_{0}^{z_a} \chi(z) Z_{a,n}(z) Z_{a,m}(z) dz = 0.$$

Note that the second equation above is actually

$$-\frac{\rho_a}{\rho_s} \left[Z_{s,m}(0) Z'_{s,n}(0) - Z_{s,n}(0) Z'_{s,m}(0) \right] - (\mu_n - \mu_m) \int_{0}^{z_a} \chi(z) Z_{a,n}(z) Z_{a,m}(z) dz = 0$$

or

$$-Z_{s,m}(0) Z'_{s,n}(0) + Z_{s,n}(0) Z'_{s,m}(0) - \frac{\rho_s}{\rho_a} (\mu_n - \mu_m) \int_{0}^{z_a} \chi(z) Z_{a,n}(z) Z_{a,m}(z) dz = 0$$

so that the first equation added to the equivalent second equation is

$$-(\mu_n - \mu_m) \int_{z_s}^{0} \chi(z) Z_{s,n}(z) Z_{s,m}(z) dz - \frac{\rho_s}{\rho_a} (\mu_n - \mu_m) \int_{0}^{z_a} \chi(z) Z_{a,n}(z) Z_{a,m}(z) dz = 0$$

$$-\rho_a (\mu_n - \mu_m) \int_{z_s}^{0} \chi(z) Z_{s,n}(z) Z_{s,m}(z) dz - \rho_s (\mu_n - \mu_m) \int_{0}^{z_a} \chi(z) Z_{a,n}(z) Z_{a,m}(z) dz = 0$$

$$-(\mu_n - \mu_m) \left[\rho_a \int_{z_s}^{0} \chi(z) Z_{s,n}(z) Z_{s,m}(z) dz + \rho_s \int_{0}^{z_a} \chi(z) Z_{a,n}(z) Z_{a,m}(z) dz \right] = 0.$$

Assuming $\lambda_n \neq \lambda_m$ when $n \neq m$,

$$\int_{z_s}^{z_a} \chi(z) Z_n(z) Z_m(z) = 0$$

where

$$Z_n(z) Z_m(z) = \begin{cases} Z_{a,n}(z) Z_{a,m}(z) dz & \text{when } 0 < z \leq z_a \\ Z_{s,n}(z) Z_{s,m}(z) dz & \text{when } z_s \leq z < 0 \end{cases}$$

implies Z is orthogonal with respect to the weight function

$$\chi(z) = \begin{cases} \rho_s & \text{when } 0 < z \leq z_a \\ \rho_a & \text{when } z_s \leq z < 0 \end{cases}.$$

Appendix B

Additional Proofs

B.1 Explanation of the Exclusion of Gravity from the Conservation of Momentum Equation

The exclusion of the gravity term from the derivation of momentum originates from the following

> Although gravity is always present, it has negligible influence on acoustic disturbances of all but extremely low frequencies, e.g., those of order or less than $\frac{g}{c}$, where g is the acceleration due to gravity and c is the speed of sound; so, for simplicity, the body force term is neglected at the outset. Acoustic-gravity waves [internal waves] (infrasonic waves with frequencies so low as to be strongly affected by gravity) have been a major topic of research during the past two decades but fall outside the scope of an introductory discussion.[1]

Since $c_s = 160\ \mathrm{m/s}$, and $g = 9.8\,\mathrm{m/s^2}$, $\frac{g}{c} = \frac{160\,\mathrm{m/s}}{9.8\,\mathrm{m/s^2}} = 16.327\,\mathrm{Hz} \ll 100\,\mathrm{Hz}$, which is the lowest frequency of interest.

B.2 Proof of the Denominator in equation (4.25) Using *Handbook of Mathematical Functions*[2]

The denominator first reads

$$-\sqrt{\mu_l}H_k^{(1)\prime}\left(\sqrt{\mu_l}r_0\right)J_k\left(\sqrt{\mu_l}r_0\right)+\sqrt{\mu_l}H_k^{(1)}\left(\sqrt{\mu_l}r_0\right)J_k'\left(\sqrt{\mu_l}r_0\right)$$

By Abramowitz and Stegun,[3] the derivative of a Bessel or Hankel function can be simplified into

[1] [4],[13],[15],[10]
[2] [2], pg. 362.
[3] [2], pg. 362, eqn. (9.1.27).

$$-\sqrt{\mu_l}\left(\frac{-\left(\sqrt{\mu_l}r_0\right)H_{k+1}^{(1)}\left(\sqrt{\mu_l}r_0\right)+kH_k^{(1)}\left(\sqrt{\mu_l}r_0\right)}{\sqrt{\mu_l}r_0}\right)J_k\left(\sqrt{\mu_l}r_0\right)$$
$$+\sqrt{\mu_l}H_k^{(1)}\left(\sqrt{\mu_l}r_0\right)\left(\frac{-\left(\sqrt{\mu_l}r_0\right)J_{k+1}\left(\sqrt{\mu_l}r_0\right)+kJ_k\left(\sqrt{\mu_l}r_0\right)}{\sqrt{\mu_l}r_0}\right)$$

Simplifying the denominator of the equation yields

$$\frac{\left(\sqrt{\mu_l}r_0\right)\left[H_{k+1}^{(1)}\left(\sqrt{\mu_l}r_0\right)J_k\left(\sqrt{\mu_l}r_0\right)-H_k^{(1)}\left(\sqrt{\mu_l}r_0\right)J_{k+1}\left(\sqrt{\mu_l}r_0\right)\right]}{r_0}$$
$$+\frac{k\left[H_k^{(1)}\left(\sqrt{\mu_l}r_0\right)J_k\left(\sqrt{\mu_l}r_0\right)-H_k^{(1)}\left(\sqrt{\mu_l}r_0\right)J_k\left(\sqrt{\mu_l}r_0\right)\right]}{r_0}$$

Recognizing that the second part of the equation is zero gives

$$\left(\sqrt{\mu_l}\right)\left[H_{k+1}^{(1)}\left(\sqrt{\mu_l}r_0\right)J_k\left(\sqrt{\mu_l}r_0\right)-H_k^{(1)}\left(\sqrt{\mu_l}r_0\right)J_{k+1}\left(\sqrt{\mu_l}r_0\right)\right]+0$$

Multiplying to use Abramowitz and Stegun,[4]

$$\frac{\sqrt{\mu_l}}{2}\begin{bmatrix} H_{k+1}^{(1)}\left(\sqrt{\mu_l}r_0\right)H_k^{(1)}\left(\sqrt{\mu_l}r_0\right)+H_{k+1}^{(1)}\left(\sqrt{\mu_l}r_0\right)H_k^{(2)}\left(\sqrt{\mu_l}r_0\right) \\ -H_k^{(1)}\left(\sqrt{\mu_l}r_0\right)H_{k+1}^{(1)}\left(\sqrt{\mu_l}r_0\right)-H_k^{(1)}\left(\sqrt{\mu_l}r_0\right)H_{k+1}^{(2)}\left(\sqrt{\mu_l}r_0\right) \end{bmatrix}$$

Applying Abramowitz and Stegun[5] gives

$$\frac{\sqrt{\mu_l}}{2}\left[H_{k+1}^{(1)}\left(\sqrt{\mu_l}r_0\right)H_k^{(2)}\left(\sqrt{\mu_l}r_0\right)-H_k^{(1)}\left(\sqrt{\mu_l}r_0\right)H_{k+1}^{(2)}\left(\sqrt{\mu_l}r_0\right)\right]=\frac{\sqrt{\mu_l}}{2}\left(-\frac{4i}{\pi\sqrt{\mu_l}r_0}\right)=-\frac{2i}{\pi r_0}$$

[4][2], pg. 362, eqn. (9.1.17).
[5][2], pg. 362, eqn. (9.1.17).

Appendix C

Graph Parameters

C.1 Common Values

Note that units have been dropped for the numerical analysis

$z_a = 500$
$c_a = 330$
$\rho_a = 1.168$
$\sigma = 0$
rtol = 5×10^{-5}
$\beta_m = 1000$
$T = 2 \times 10^6$
$a = 0.07$
$m = 0$

C.2 Values for Specific Figures

Figures (4.2) and (8.1):

$z_s = -0.075$
$c_s = 170$
$c_p = 75$
$r_0 = 2$
$z_0 = 2$
$\theta_0 = 0$
$r = 0.0$
$z = 0$
$\theta = 0$

Figures (4.3), (4.4), (6.1), (6.2), (6.3), (6.5), (6.6), (6.7), and (6.4):

$z_s = -1$
$c_s = 160$

$r_0 = 2$
$z_0 = 2$
$\theta_0 = 0$
$r = 0.0$
$z = 0$
$\theta = 0$
Figures (9.1), (9.2), (9.3), (9.4), (9.5), (9.6), and (9.8):
$z_s = -0.175$
$c_s = 170$
$c_p = 75$
$r_0 = 0.2$
$z_0 = 2$
$\theta_0 = 0$
$r = 0.0$
$z = 0$
$\theta = 0$

Appendix D

MATLAB™ Files

D.1 Common Functions

D.1.1 csqrt.m

```
function y=csqrt(z)
    y=sqrt(z);
    iset=find(imag(z)<0);
    y(iset)=-y(iset);
```

D.1.2 eigs4z.m

```
function Z=eigs4z(kap,rhoa,rhos,za,ca,zs,cs,sigma,rhop,f)
    omega=2*pi*f;
    ks=sqrt((omega^2+i*omega*sigma/rhop)/cs^2);
    ka=omega/ca;
    %ps=-i*omega*rhop/(sigma+i*omega*rhop);
    llamb = sqrt(ks^2-ka^2+kap.^2/za^2);
    Z=rhos*(cos(kap).*cos(zs*llamb)).*(kap/za)+rhoa*(sin(kap).*sin(zs*llamb)).*llamb;
```

D.1.3 mu.m

```
function [mu,kappa]=mu(n,ka,rhoa,rhos,za,ca,zs,cs,sigma,rhop,f)
    ftntol=5e-4;
    sectol=5e-4;
    count=1;
    for ii=n
    [kap,fv] = secant(@(kap1) eigs4z(kap1,rhoa,rhos,za,ca,zs,cs,sigma,rhop,f),
    (2*ii-1)*pi/2-pi/8,(2*ii-1)*pi/2+pi/8,sectol);
    if (fv<ftntol)&(real(kap)>(ii-1)*pi)&(real(kap)<ii*pi)
```

```
kappa(count)=kap;
else
k1=(2*ii-1)*pi/2-1.57;
k2=(2*ii-1)*pi/2+1.57;
kapr=linspace(k1,k2,100);
y=real(eigs4z(kapr,rhoa,rhos,za,ca,zs,cs,sigma,rhop,f));
if y(1)>0
I=find(y<0);
else
I=find(y>0);
end
if isempty(I)
if count == 1
kappa(count) = 0;
else
Figure
plot(kapr,y)
error('zero not found')
end
else
[kap,fv]=secant(@(kap1) eigs4z(kap1,rhoa,rhos,za,ca,zs,cs,sigma,rhop,f),
kapr(I(1))-.1,kapr(I(1))+.1,sectol);
kappa(count)=kap;
end
end
count=count+1;
end
if abs(kappa(1))<sectol
kappa=kappa(2:end);
end
mu=ka^2-(kappa/za).^2;
```

D.1.4 rho.m

```
function wrho=rho(z,rhos,rhoa)
    if z>=0
    wrho=rhos;
    else
    wrho=rhoa;
    end
```

D.2 Two-Layer Waveguide Specific Programs

D.2.1 dZn.m

```
function dZ=dZn(z,ka,muv,za,ks,zs)
    if z>=0
    dZ=(ka^2-muv).^(1/2).*sin((ka^2-muv).^(1/2)*za)./cos((ka^2-muv).^(1/2)*za)
    .*sin((ka^2-muv).^(1/2)*z)+(ka^2-muv).^(1/2).*cos((ka^2-muv).^(1/2)*z);
    else
    dZ=sin((ks^2-muv).^(1/2)*zs)./cos((ks^2-muv).^(1/2)*zs).*sin((ka^2-muv).^(1/2)*za)
    ./cos((ka^2-muv).^(1/2)*za).*((ks^2-muv).^(1/2).*cos((ks^2-muv).^(1/2)*zs)
    ./sin((ks^2-muv).^(1/2)*zs).*sin((ks^2-muv).^(1/2)*z)+(ks^2-muv).^(1/2)
    .*cos((ks^2-muv).^(1/2)*z));
    end
```

D.2.2 eigsplot.m

```
za=500; %rough estimate of the upper limit of the problem, units of m
    ca=330; % speed of sound, m/s
    zs=-1; %rough estimate of lower limit of problem, units of m
    cs=160; %Attenborough et al. Attached derivation from Buchanan units m/s
    sigma = 0; %366000;
    rhop = 4150;
    rhoa=1.168; %Wikipedia, density of dry air at std ambient press and temp
    %Density of Air Article, units of kg/m^3
    r0=2;
    z0=2;
    theta0=0;
    NBlock = 250;
    r=1;
    theta=0;
    p=[];
    rtol = 5e-5;
    f=50;
    omega=2*pi*f;
    rhos=rhop+i*sigma/omega;
    kappa=linspace(0,20,100);
    Y=eigs4z(kappa,rhoa,rhos,za,ca,zs,cs,sigma,rhop,f);
    plot(kappa,Y,'b')
```

D.2.3 gui.m

```
disp('Predicted Soil Resonances for Landmine Detection')
    disp('*****************************************************************')
    disp('Effective Fluid Model developed by Mattingly and Buchanan')
    disp(' ')
    disp('This method for determining soil resonances uses linearized Partial')
    disp('Differential Equations to approximate the behavior at the air-soil')
    disp('interface.')
    disp(' ')
    disp('*****************************************************************')
    disp(' ')
    disp('All input values are in the assigned units')
    disp(' ')
    za=500;
    rsp=input('For advanced selections, press any numeric key now');
    if isempty(rsp)
    typ2=input('Enter the ambient temperature (C)');
    if typ2<=-10
    rhoa1=1.341;
    ca1=325.4;
    elseif (typ2>-10)&(typ2<=-5)
    rhoa1=1.316;
    ca1=328.5;
    elseif (typ2>-5)&(typ2<=0)
    rhoa1=1.293;
    ca1=331.5;
    elseif (typ2>0)&(typ2<=5)
    rhoa1=1.269;
    ca1=334.5;
    elseif (typ2>5)&(typ2<=10)
    rhoa1=1.247;
    ca1=337.5;
    elseif (typ2>10)&(typ2<=15)
    rhoa1=1.225;
    ca1=340.5;
    elseif (typ2>15)&(typ2<=20)
    rhoa1=1.204;
    ca1=343.4;
    elseif (typ2>20)&(typ2<=25)
    rhoa1=1.184;
    ca1=346.3;
    elseif (typ2>25)&(typ2<35)
```

```
ca1=349.2;
rhoa1=1.164;
else
rhoa1=1.1;
ca1=331.4+.6*typ2;
end
typ3=input('Enter the humidity in decimal form');
rhoa=rhoa1*(1+typ3)/(1+1.609*typ3);
ca=ca1+typ3*.6*ca1;
typ1=input('Select soil type: 1=sand, 2=silt, 3=clay, 4=organic matter');
typ11=input('Select soil moisture (scale of 1-5, 1=dry, 5=saturated)');
typ12=input('Select soil compaction (scale of 1-4, 1=loose, 4=dense)');
if typ1 == 1
if typ11 == 1
cs=260;
elseif typ11 == 2
if typ12 <3
cs = 138;
else
cs = 103;
end
elseif typ11==3
if typ12 < 3
cs=122;
else
cs=253;
end
else
cs=189;
end
elseif typ1 == 2
if typ11 == 1
if typ12 <3
cs=140;
else
cs=139;
end
elseif typ11 == 2
if typ12 <3
cs = 117;
else
cs = 122;
```

```
end
elseif typ11==3
if typ12 < 3
cs=121;
else
cs=176;
end
else
cs=207;
end
elseif typ1 == 3
if typ11 == 1
if typ12 <3
cs=177;
else
cs=159;
end
elseif typ11 == 2
if typ12 <3
cs = 118;
else
cs = 136;
end
elseif typ11==3
if typ12 < 3
cs=107;
else
cs=245;
end
else
cs=118;
end
elseif typ1 == 4
if typ11 == 1
if typ12 <3
cs=153;
else
cs=121;
end
elseif typ11 == 2
if typ12 <3
cs = 89;
```

```
else
cs = 147;
end
elseif typ11==3
if typ12 < 3
cs=87;
else
cs=86;
end
else
cs=102;
end
else
disp('Error in submission of soil type')
end
cp=270;
sigma=0;
end
rtol = 5e-4;
NBlock = 250;
if ~isempty(rsp)
ca=input('Enter the speed of sound in the atmosphere (m/s)');
if isempty(ca)
ca=343;
end
cp=input('Enter the speed of shear sound waves in the soil (m/s)');
if isempty(cs)
cs=210.31;
end
cs=input('Enter the speed of compressional sound waves in the soil (m/s)');
if isempty(cp)
cp=647;
end
sigma=input('Enter the flow resistivity in the soil (Pa*s/m^2)');
if isempty(sigma)
sigma=0;
end
rhoa=input('Enter the density of the atmosphere (kg/m^3)');
if isempty(rhoa)
rhoa=1.205;
end
rtol=input('Enter the tolerance');
```

```
if isempty(rtol)
rtol=5e-5;
end
end
NBlock=250;
zs=input('Enter the depth of the soil (m)');
if isempty (zs)
zs=-1;
end
AA=input('Enter the position of the source
[radial component, azmuthal component, height component] (m)');
r0=AA(1);
theta0=AA(2);
z0=AA(3);
r=0;
theta=0;
z=0;
CC=input('Enter the frequency range of interest
[lowest frequency,highest frequency] (Hz)');
p=[];
rhop=8.1827e7/(cs^2*.27);
if isempty(CC)
CC=input('Enter the height range of interest [lowest height,highest height] (m)');
f=input('Enter the frequency of interest (Hz)');
cnt = 1;
zrange=linspace(CC(1),CC(2),10);
disp(' Depth(m) Pressure (Pa)')
for z=zrange;
pp(cnt)=press(p,rtol,NBlock,f,sigma,rhop,cs,ca,rhoa,za,zs,z,z0,r,r0,theta,theta0);
disp([z,abs(pp(cnt))])
cnt = cnt+1;
end
plot(zrange,abs(pp),'-m')
hold on
xlabel('Height/Depth Range (m)')
ylabel('Pressure (Pa)')
title('Soil Resonance Predictions - Depth Variation')
end
if ~isempty(CC)
frange=linspace(CC(1),CC(2),10);
cnt = 1;
disp('Frequency(Hz) Pressure(Pa)')
```

```
for f=frange;
pp(cnt)=press(p,rtol,NBlock,f,sigma,rhop,cs,ca,rhoa,za,zs,z,z0,r,r0,theta,theta0);
disp([f,abs(pp(cnt))])
cnt = cnt+1;
end
plot(frange,abs(pp), 'g')
hold on
xlabel('Frequency (Hz)')
ylabel('Pressure (Pa)')
title('Soil Resonance Predictions - Frequency Variation')
end
```

D.2.4 In.m

```
function II=In(ka,ks,rhoa,rhos,za,ca,zs,cs,sigma,rhop,f,muv)
    sqeek=csqrt(ka^2-muv);
    queek=csqrt(ks^2-muv);
    II=1/2*rhos*(-sin(sqeek*za).*cos(sqeek*za)+sqeek*za)./(sqeek.*cos(sqeek*za).^2)+...
    1/2*rhoa*(-queek*zs+queek*zs.*cos(sqeek*za).^2-cos(queek*zs).*sin(queek*zs)+...
    cos(queek*zs).*sin(queek*zs).*cos(sqeek*za).^2
    )./ (cos(queek*zs).^2.*cos(sqeek*za).^2.*queek);
```

D.2.5 press.m

```
function p1=press(p,rtol,NBlock,f,sigma,rhop,cs,ca,rhoa,za,zs,z,z0,r,r0,theta,theta0)
    omega=2*pi*f;
    ks=sqrt((omega^2+i*omega*sigma/rhop)/cs^2);
    ka=omega/ca;
    rhos=1130;%rhop+i*sigma/omega;
    N=0;
    p1=0;
    continN = true;
    while continN
    n=(N+1):(NBlock+N);
    muv = mu(n,ka,rhoa,rhos,za,ca,zs,cs,sigma,rhop,f);
    if muv(1)==ka^2
    muv=muv(2:end);
    end
    II=In(ka,ks,rhoa,rhos,za,ca,zs,cs,sigma,rhop,f,muv);
    p1a=-i./(4*II).*besselh(0,1,(csqrt(muv)*r0)).*besselj(0,(csqrt(muv).*r))
    *rho(z0,rhos,rhoa)
    .*Zn(z0,ka,muv,za,ks,zs).*Zn(z,ka,muv,za,ks,zs);
```

```
p1=p1+sum(p1a);
continM = abs(sum(p1a)/p1) > rtol;
m=1;
while continM
p2a=-i./(2*II).*besselh(m,1,(csqrt(muv)*r0)).*besselj(m,(csqrt(muv).*r))
.*cos(m*(theta-theta0))
*rho(z0,rhos,rhoa).*Zn(z0,ka,muv,za,ks,zs).*Zn(z,ka,muv,za,ks,zs);
p1=p1+sum(p2a);
m=m+1;
continM = abs(sum(p2a)/p1) > rtol;
end
N=N+NBlock;
continN = abs(sum(p1a)/p1) > rtol;
end
```

D.2.6 propforz1.m

```
za=500; %rough estimate of the upper limit of the problem, units of m
ca=340; % speed of sound, m/s
zs=-0.075; %rough estimate of lower limit of problem, units of m
cs=160; %Attenborough et al. Attached derivation from Buchanan units m/s
cp=270;
sigma = 0;
rhoa=1.2; %Wikipedia, density of dry air at std ambient press and temp
%Density of Air Article, units of kg/m^3
r0=2;
z0=2;
theta0=0;
NBlock = 250;
%rrange=linspace(0.01,10,50); %
r=1;
%thetar=linspace(0,90,100);
theta=0;
p=[];
rtol = 5e-5;
rhop=8.1827e7/(cp^2*.27);
f=319;%
%frange=linspace(50,300,300);
z=0;
cnt = 1;
zrange=linspace(-1,5,150);
%for r=rrange
```

```
%for f=frange;
for z=zrange;
%for theta=thetar
omega=2*pi*f;
ks=sqrt((omega.^2+i*omega*sigma/rhop)/cp.^2);
ka=omega/ca;
rhos=1400;
%pp(cnt)=press(p,rtol,NBlock,f,sigma,rhop,cs,ca,rhoa,za,zs,z,z0,r,r0,theta,theta0);
vv(cnt)=
velpl(p,rtol,NBlock,rhos,ca,cs,sigma,f,omega,rhoa,rhop,za,zs,z,z0,r,r0,theta,theta0);
disp([z,abs(vv(cnt))]);%,abs(vv(cnt))])
%disp([z,abs(pp(cnt))])
cnt = cnt+1;
end
plot(zrange,abs(vv),'r')
%plot(rrange,abs(vv), 'g')
%Figure
%plot(frange,abs(pp),'b')
%plot(thetar,abs(pp),'b')
```

D.2.7 secant.m

```
function [x,fval]=secant(f,x0,x1,tol)
    u=feval(f,x0);
    v=feval(f,x1);
    err=abs(x1-x0);
    while (err>tol);
    if (v-u)~=0
    x=x1-v*(x1-x0)/(v-u);
    x0=x1;
    u=v;
    x1=x;
    v=feval(f,x1);
    err=abs(x1-x0);
    else
    x=x1-(x1-x0)/2;
    x0=x1;
    u=v;
    x1=x;
    v=feval(f,x1);
    err=abs(x1-x0);
    end
```

```
    end
    fval=abs(v);
```

D.2.8 velpl.m

```
function v1=
    velpl(p,rtol,NBlock,rhos,ca,cs,sigma,f,omega,rhoa,rhop,za,zs,z,z0,r,r0,theta,theta0)
    omega=2*pi*f;
    ks=sqrt((omega.^2+i*omega*sigma/rhop)/270.^2);
    ka=omega/ca;
    rhos=rhop+i*sigma/omega;
    N=0;
    p1=0;
    continN = true;
    while continN
    n=(N+1):(NBlock+N);
    muv = mu(n,ka,rhoa,rhos,za,ca,zs,cs,sigma,rhop,f);
    if muv(1)==ka^2
    muv=muv(2:end);
    end
    II=In(ka,ks,rhoa,rhos,za,ca,zs,cs,sigma,rhop,f,muv);
    if r<r0
    p1a=-i./(4*II).*besselh(0,1,(csqrt(muv)*r0)).*besselj(0,(csqrt(muv)*r))
    *rho(z0,rhos,rhoa)
    .*Zn(z0,ka,muv,za,ks,zs).*dZn(z,ka,muv,za,ks,zs);
    else
    p1a=-i./(4*II).*besselh(0,1,(csqrt(muv)*r)).*besselj(0,(csqrt(muv)*r0))
    *rho(z0,rhos,rhoa)
    .*Zn(z0,ka,muv,za,ks,zs).*dZn(z,ka,muv,za,ks,zs);
    end
    p1=p1+sum(p1a);
    continM = abs(sum(p1a)/p1) > rtol;
    m=1;
    while continM
    if r<r0
    p2a=-i./(2*II).*besselh(m,1,(csqrt(muv)*r0)).*besselj(m,(csqrt(muv)*r))
    .*cos(m*(theta-theta0))*rho(z0,rhos,rhoa).*Zn(z0,ka,muv,za,ks,zs)
    .*dZn(z,ka,muv,za,ks,zs);
    else
    p2a=-i./(2*II).*besselh(m,1,(csqrt(muv)*r)).*besselj(m,(csqrt(muv)*r0))
    .*cos(m*(theta-theta0))*rho(z0,rhos,rhoa).*Zn(z0,ka,muv,za,ks,zs)
    .*dZn(z,ka,muv,za,ks,zs);
```

```
    end
    p1=p1+sum(p2a);
    m=m+1;
    continM = abs(sum(p2a)/p1) > rtol;
    end
    N=N+NBlock;
    continN = abs(sum(p1a)/p1) > rtol;
    end
    %p=[p, abs(p1)];
    v1=-i./(omega.*rho(z0,rhos,rhoa))*p1;
```

D.2.9 Zn.m

```
function Z=Zn(z,ka,muv,za,ks,zs)
    kas=csqrt(ka^2-muv);
    kss=csqrt(ks^2-muv);
    if z>=0
    Z=-(sin(kas*za)./cos(kas*za)).*cos((kas).*z)+sin((kas).*z);
    else
    Z=-sin(kas*za).*sin(kss*zs)/(cos(kas*za).*cos(kss*zs)).*(cos(kss*zs)./sin(kss*zs)
    .*cos((kss).*z)+sin((kss).*z));
    end
```

D.3 Eigmovie

D.3.1 dZn.m

```
function dZ=dZn(z,ka,muv,za,ks,zs)
    sqs = csqrt(ks^2-muv); sqa = csqrt(ka^2-muv);
    if z >= 0
    %Z = cos(sqs*zs).*sin(sqa*(za-z));
    dZ = -sqa.*cos(sqs*zs).*cos(sqa*(za-z));
    else
    %Z = sin(sqa*za).*cos(sqs*(z-zs));
    dZ = -sqs.*sin(sqa*za).*sin(sqs*(z-zs));
    end
```

D.3.2 eigmovie.m

```
clear all
    zs = -0.175;
    rhoa = 1.168;
```

```
cpa = 330;
za = 500;
cps = 160;
cs = 75;
Por = 0.25;
rhosn = 1400;
nu = 0.2;
rhop = 1.6406e+003;
sigma = 1e1;
a = 0.07;
T = 5e2; %2e6;
betam = T/1e3; %1e-2;
rfreq = 250;
rhom = T/a^2/(2*pi*rfreq)^2*(2.405)^2;
r0 = 2;%0.2;
z0 = 2; theta0 = 0;
z = 0; theta = 0;
%r = linspace(0,1,40);
r =1;% 0.0;
%pts = 21; cent = 248; freq = linspace(cent-5,cent+5,pts);
pts = 11; cent = 248; freq = linspace(cent-2,cent+2,pts);
colset = ['k','b','c','g','m','r'];
% r0 = 2; z0 = 2; theta0 = 0;
% r = 1; z = 0; theta = 0;
N = 5000; mi = 0;
for n = 1:length(freq)
omega = 2*pi*freq(n);
beta = sigma/omega/rhop;
ka = omega/cpa;
ks = omega/cps*sqrt(1+i*beta);
rhos = rhop*(1+beta*i);
[mu,kapm]=mumm(N,ka,rhoa,rhos,ks,za,zs);
plotran = 300:650;%1:1000;%600:800; %
% Figure(2)
% subplot(211); plot(real(kapm(plotran))-(2*(plotran)-1)*pi/2,colset(1+mod(n,6)));
hold on
% subplot(212); plot(imag(kapm(plotran)),colset(1+mod(n,6))); hold on
% drawnow
% Figure(3)
% subplot(211);
% plot(abs(dZnbnr(z,mu(plotran),za,zs,rhoa,rhos,ka,ks)),colset(1+mod(n,6)));
% hold on
```

```
% %plot(1,abs(Znbnr(z,mu(1),za,zs,rhoa,rhos,ka,ks)
.*Znbnr(z0,mu(1),za,zs,rhoa,rhos,ka,ks)),[colset(1+mod(n,6)),'*']); hold on
% terms =
% besselh(mi,csqrt(mu(plotran))*r0).*dZnbnr(z,mu(plotran),za,zs,rhoa,rhos,ka,ks)
.*Znbnr(z0,mu(plotran),za,zs,rhoa,rhos,ka,ks);
vterms
=i/omega/rhoa.*i/2/epsl(mi)./Phib(mu(plotran),za,zs,rhoa,rhos,ka,ks)
.*besselh(mi,csqrt(mu(plotran))*r0).*besselj(mi,csqrt(mu(plotran))*r)*...
cos(mi*theta)*rho(z,rhos,rhoa).*Zn(z0,ka,mu(plotran),za,ks,zs)
.*dZn(z,ka,mu(plotran),za,ks,zs);
subplot(211); plot(plotran,real(vterms),colset(1+mod(n,6))); hold on
%subplot(212); plot(plotran,imag(vterms),colset(1+mod(n,6))); hold on
drawnow
% Figure(4)
% plot(abs(besselh(mi,csqrt(mu)*r0).*besselj(mi,csqrt(mu)*r)),colset(1+mod(n,6)));
hold on
fprintf('f = %gHz, kappa_1 = %g + %gi\n',freq(n),real(kapm(1)),imag(kapm(1)))
%p = zeros(1,10);
% for m = 0:9
% p(m+1) = -sum(i/2/nu0(m)./Phib(mu,za,zs,rhoa,rhos,ka,ks)
.*besselh(m,csqrt(mu)*r0).*besselj(m,csqrt(mu)*r)*...
% sigma0(z0,rhoa,rhos).*Znb(z,mu,za,zs,ka,ks).*Znb(z0,mu,za,zs,ka,ks)
*cos(m*(theta-theta0)));
% %fprintf('m = %g: p1 = %g+ %gi\n',m,real(p(m+1)),imag(p(m+1)))
% end
% fprintf('|p| = %g\n',abs(sum(p)))
fprintf('real sum = %g, imag sum = %g v = %g\n',sum(real(vterms)),
sum(imag(vterms)),abs(sum(vterms)))
pause
% Figure(3)
% plot(abs(Znbnr(z,mu,za,zs,rhoa,rhos,ka,ks)
.*Znbnr(z0,mu,za,zs,rhoa,rhos,ka,ks)),colset(n)); hold on
end
```

D.3.3 epsl.m

```
function Z=epsl(m)
    if m==0
    Z=2;
    else
    Z=1;
    end
```

D.3.4 Phib.m

```
function Ph = Phib(mu,za,zs,rhoa,rhos,ka,ks)
    sqs = csqrt(ks^2-mu); sqa = csqrt(ka^2-mu);
    Ph
    =(1/2)*rhos*cos(sqs*zs).^2.*(-cos(sqa*za).*sin(sqa*za)+sqa*za)./sqa
    -(1/2)*rhoa*sin(sqa*za).^2.*(cos(sqs*zs).*sin(sqs*zs)+sqs*zs)./sqs;
```

D.3.5 secant.m

```
function [x,fval]=secant(f,x0,x1,tol)
    u=feval(f,x0);
    v=feval(f,x1);
    err=abs(x1-x0);
    while (err>tol);
    x=x1-v.*(x1-x0)./(v-u);
    x0=x1;
    u=v;
    x1=x;
    v=feval(f,x1);
    err=abs(x1-x0);
    end
    fval=abs(v);
```

D.3.6 Zn.m

```
function Z=Zn(z,ka,muv,za,ks,zs)
    sqs = csqrt(ks^2-muv); sqa = csqrt(ka^2-muv);
    if z >= 0
    Z = cos(sqs*zs).*sin(sqa*(za-z));
    else
    Z = sin(sqa*za).*cos(sqs*(z-zs));
    end
```

D.4 Membrane Problem

D.4.1 alph.m

```
function TT=alph(zs,ks,muv);
    TT=zs*csqrt(ks^2-muv);
```

D.4.2 Amn.m

```
function y=Amn(m,ka,ks,muv,zetav,za,zs,rhoa,rhos,a,z0,r0)
    Imnlv=Imnl(ka,ks,muv,zetav,za,zs,rhoa,rhos);
    kk=besselh(m,1,csqrt(muv)*a);
    ll=besselj(m+1,csqrt(muv)*a);
    kk1=besselh(m+1,1,csqrt(muv)*a);
    ll1=besselj(m,csqrt(muv)*a);
    bess1 = kk.*ll-kk1.*ll1; %bottom line
    bess2 = (-csqrt(muv).*kk1).'*besselj(m,csqrt(zetav)*a)+(kk).'*(csqrt(zetav)
    .*besselj(m+1,csqrt(zetav)*a)); %top line
    %sure want to use right divide? yes
    y=(bess2.*Imnlv)\(-i/(2*epsl(m)).*csqrt(muv).*(rho(z0,rhos,rhoa)
    *Zn(z0,ka,muv,za,ks,zs,rhoa,rhos).*besselh(m,1,csqrt(muv).*r0).*bess1)).';
```

D.4.3 char4z.m

```
function Z=char4z(ka,za,tau,ks,a,k,m,T,rhoa,omega,rhos,zs)
    %char4z(ka,za,kapr,ks,a,k,m,T,rhoa,omega,rhos,zs);
    sqg=ka^2-(tau/za).^2; % this is zeta
    llamb = csqrt(ks^2-sqg);
    sb1=besselj(m,k*a);
    sb2=besselj(m+1,csqrt(sqg)*a);
    sb3=besselj(m,csqrt(sqg)*a);
    %running into problems here. too slow. line 13, bessel function
    II1=a*(sqg-k^2).^(-1).*(csqrt(sqg).*sb1.*sb2-k.*besselj(m+1,k*a).*sb3);
    II2=a^2/2*(sb3.^2+sb2.^2)-a./csqrt(sqg).*(m.*sb2.*sb3);
    Z=-rhos*omega^2./T*1./((k^2-sqg).*sb1).*(cos(tau).*cos(llamb*zs)-rhos.*tau
    ./(za*rhoa*llamb).*sin(tau).*sin(llamb*zs)).*(besselj(m,a*csqrt(sqg)).*II1-sb1.*II2)+...
    II2.*(-llamb.*cos(tau).*sin(llamb*zs)-rhos.*tau./(rhoa*za).*sin(tau).*cos(zs*llamb));
```

D.4.4 dZn.m

```
function dZ=dZn(z,ka,muv,za,ks,zs)
    sqs = csqrt(ks^2-muv); sqa = csqrt(ka^2-muv);
    if z >= 0
    %Z = cos(sqs*zs).*sin(sqa*(za-z));
    dZ = -sqa.*cos(sqs*zs).*cos(sqa*(za-z));
    else
    %Z = sin(sqa*za).*cos(sqs*(z-zs));
    dZ = -sqs.*sin(sqa*za).*sin(sqs*(z-zs));
    end
```

D.4.5 epsl.m

```
function Z=epsl(m)
    if m==0
    Z=2;
    else
    Z=1;
    end
```

D.4.6 Imnl.m

```
function Y= Imnl(ka,ks,muv,zetav,za,zs,rhoa,rhos)
    M = length(zetav); N = length(muv);
    xiv=za*csqrt(ka^2-muv).'*ones(1,M); %l
    iotav=zs*ones(N,1)*csqrt(ks^2-zetav); %n
    alphv =zs*csqrt(ks^2-muv).'*ones(1,M);
    ttau=za*ones(N,1)*csqrt(ka^2-zetav);
    % Y1= -za*rhos*(ttau.*cos(ttau).*sin(xiv)-xiv.*cos(xiv).*sin(ttau))
    ./(cos(ttau).*cos(xiv).*(ttau.^2-xiv.^2));
    %
    % Y112 = (zs*sin(xiv)./(za*cos(ttau).*cos(xiv).*cos(alphv)
    .*(alphv.^2-iotav.^2)));
    %
    % Y121 = zs*rhos*ttau.*(cos(alphv).*cos(ttau)-cos(ttau).*cos(iotav));
    % Y122 = rhoa*za*(alphv.*sin(ttau).*sin(alphv)-iotav.*sin(iotav).*sin(ttau));
    %
    %
    zsan=1/2*(-2*sin(xiv).^2*rhoa*zs.*(alphv+cos(alphv).*sin(alphv))./(cos(xiv).^2
    .*cos(alphv).^2.*alphv)).^(1/2)+1/2*2^(1/2)*(rhos*za*(-sin(xiv).*cos(xiv)+xiv)
    ./(xiv.*cos(xiv).^2)).^(1/2);
    %
    %
    phin=1/2*2^(1/2)*(rhos*za*(-cos(ttau).*sin(ttau)+ttau)./(ttau.*cos(ttau).^2)).^(1/2)
    +1/2*(-(-2*rhos^2*ttau.^2.*cos(iotav*zs).*sin(iotav*zs)
    +2*rhos^2*ttau.^2.*iotav*zs
    +4*rhos*ttau.*tan(ttau).*cos(iotav*zs).^2*rhoa*za.*iotav
    +2*tan(ttau).^2*rhoa^2*za^2.*iotav.^2.*cos(iotav*zs).*sin(iotav*zs)
    +2*tan(ttau).^2*rhoa^2*za^2.*iotav.^3*zs-4*rhos*ttau.*tan(ttau)*rhoa*za.*iotav)
    ./(rhoa*iotav.^3)).^(1/2)/za;
    %
    % Y12 = Y121 + Y122;
    %
    % Y2=Y12.*Y112;
```

```
%
% Y=(Y1+Y2)./(zsan.*phin);
%new IMNL
Y = zs*sin(xiv).*(-zs*rhos.*ttau.*cos(iotav).*cos(ttau)-iotav.*rhoa.*sin(iotav)
.*sin(ttau)*za+zs.*rhos.*ttau.*cos(alphv).*cos(ttau)+rhoa*alphv.*sin(alphv)
.*sin(ttau)*za)./(za*(-iotav.^2+alphv.^2))+za*cos(alphv).*rhos.*(-ttau.*cos(ttau)
.*sin(xiv)+xiv.*sin(ttau).*cos(xiv))./(-ttau.^2+xiv.^2);
```

D.4.7 iota.m

```
function OO=iota(zs,ks,zeta);
    OO=zs*csqrt(ks^2-zeta);
```

D.4.8 numb.m

```
function n0=numb(za,ka,ks,zs)
    n0=round(za.*sqrt(ka.^2-ks.^2+(pi/(2*zs)).^2)/pi)+1000;
```

D.4.9 phip.m

```
function y=phip(ka,zetav,z,za,rhoa,rhos,zs,ks)
    ttaua=csqrt(ka^2-zetav);
    %phin=1/2*2^(1/2)*(rhos*za*(-cos(ttau).*sin(ttau)+ttau)./(ttau.*cos(ttau).^2)).^(1/2)
    +1/2*(-(-2*rhos^2*ttau.^2.*cos(iotav*zs).*sin(iotav*zs)+2*rhos^2*ttau.^2.*iotav*zs
    +4*rhos*ttau.*tan(ttau).*cos(iotav*zs).^2*rhoa*za.*iotav
    +2*tan(ttau).^2*rhoa^2*za^2.*iotav.^2.*cos(iotav*zs).*sin(iotav*zs)
    +2*tan(ttau).^2*rhoa^2*za^2.*iotav.^3*zs-4*rhos*ttau.*tan(ttau)*rhoa*za.*iotav)
    ./(rhoa*iotav.^3)).^(1/2)/za;
    %y=ttau/za.*(cos(ttau).*cos(ttau/za*z)+sin(ttau).*sin(ttau/za*z))/phin;
    y=-csqrt(ka^2-zetav).*sin(ttaua*(z+za));
```

D.4.10 propforz1.m

```
za=500; %rough estimate of the upper limit of the problem, units of m
    ca=330; % speed of sound, m/s
    zs=-.075; %rough estimate of lower limit of problem, units of m
    cs=170; %Compressional Wave Speed
    cp= 75; %Shear Wave Speed
    sigma = 0;
    rhoa=1.168; %Wikipedia, density of dry air at std ambient press and temp
    %Density of Air Article, units of kg/m^3
    r0=.2;
```

```
z0=2;
theta0=0;
%rrange=linspace(0.01,10,100);%
r=0.0;
theta=0;
p=[];
rtol = 5e-5;
rhop=1453;%8.1827e7/(cp^2*.27);
frange=linspace(80,300,150);
rhom=6184;%5980.04;
a=.07;
T=2e6;
betam=1000;
%zrange=linspace(-.075,.075,100); %
z=0;
NBlock=250;
N = numb(za,ka,ks,zs);
NN=1:N;
MM=0;
cnt = 1;
% omega=2*pi*f;
% ks=sqrt((omega.^2+i*omega*sigma/rhop)./cs^2);
% ka=omega/ca;
% k=csqrt((rhom*omega.^2+i*betam*omega)/T);
% rhos=rhop+i*sigma./omega;
% muv = mu(N,rhos,rhoa,ks,ka,za,zs);
%II=Imnl(ka,ks,muv,zetav,za,zs,rhoa,rhos);
YY1=[];
%for z=zrange
%for r=rrange
for f=frange
omega=2*pi*f;
ks=sqrt((omega.^2+i*omega*sigma/rhop)./cs^2);
ka=omega/ca;
k=csqrt((rhom*omega.^2+i*betam*omega)/T);
rhos=1400;
muv = mu(N,rhos,rhoa,ks,ka,za,zs);
YY=velo1(omega,rhoa,muv,r,MM,ka,ks,N,k,T,rhom,za,zs,rhos,a,z0,r0,theta,z);
disp([f,abs(YY)]);
YY1=[YY1,(YY)];
end
plot(frange,abs(YY1),'r')
```

```
%plot(rrange,abs(YY1),'b')
%plot(zrange,abs(YY1),'g')
%y=Amn(M,ka,ks,muv,zetav,za,zs,rhoa,rhos,a,z0,r0);
%zrange=linspace(0,5,200);
% for f=frange;
% %for z=zrange;
% pp(cnt)=velo1(p,rtol,N,f,sigma,rhop,cs,ca,cm,rhoa,za,zs,z,z0,r,r0,theta,theta0,a,T);
% disp([f,abs(pp(cnt))])
% %disp([z,abs(pp(cnt))])
% cnt = cnt+1;
% end
% %plot(zrange,abs(pp),'-m')
% plot(frange,abs(pp), 'r')
```

D.4.11 secant.m

```
function [x,fval]=secant(f,x0,x1,tol)
    u=feval(f,x0);
    v=feval(f,x1);
    err=abs(x1-x0);
    while (err>tol);
    x=x1-v.*(x1-x0)./(v-u);
    x0=x1;
    u=v;
    x1=x;
    v=feval(f,x1);
    err=abs(x1-x0);
    end
    fval=abs(v);
```

D.4.12 velo1.m

```
function v1=velo1(omega,rhoa,muv,r,m,ka,ks,N,k,T,rhom,za,zs,rhos,a,z0,r0,theta,z)
    v1=0;
    for ii=m
    zetav=zeta(N,ka,za,ks,a,k,m,T,rhoa,omega,rhos,zs,rhom);

    v1a=1./(i*omega*rhoa)*besselj(ii,(csqrt(zetav)*r))
    *Amn(ii,ka,ks,muv,zetav,za,zs,rhoa,rhos,a,z0,r0)*cos(ii*theta)
    *phip(ka,zetav,z,za,rhoa,rhos,zs,ks);
    v1=v1+sum(v1a);
    end
```

D.4.13 xi.m

```
function UU=xi(za,ka,muv);
    UU=za*csqrt(ka^2-muv);
```

D.4.14 zeta.m

```
function [zeta,kap]=zeta(N,ka,za,ks,a,k,m,T,rhoa,omega,rhos,zs,rhom)
    ftntol=1e0;
    sectol=5e-4;
    % width=pi/8;
    % Nlook=min(N,floor(1/2*(1+2*ka*za/pi))+100);
    lasteig=0;count=0;
    k1=zeros(1,N);k2=zeros(1,N);
    kapr=linspace(i*1e-3,500*i,2000);
    y=imag(char4z(ka,za,kapr,ks,a,k,m,T,rhoa,omega,rhos,zs));
    if y(1)>0
    I=find(y<0);
    else
    I=find(y>0);
    end
    if ~isempty(I)
    count=count+1;
    k1(count)=kapr(I(1)-1);
    k2(count)=kapr(I(1));
    end
    while count <= N
    kapr=linspace(lasteig+1e-3,lasteig+2*pi,200);
    y=real(char4z(ka,za,kapr,ks,a,k,m,T,rhoa,omega,rhos,zs));
    if y(1)>0
    I=find(y<0);
    else
    I=find(y>0);
    end
    if (m==0)|(((kapr(I(1)-1) < za*ka) & (kapr(I(1)) > ka*za)))
    count=count+1;
    k1(count)=kapr(I(1)-1);
    k2(count)=kapr(I(1));
    lasteig=k2(count);
    else
    lasteig=za*ka+1e-3;
    end
    end
```

```
% if count < N
% k1((count+1):N) = kappa((count+1):N)-width;
% k2((count+1):N) = kappa((count+1):N)+width;
% end
[kap,fv]=secant(@(kap1) char4z(ka,za,kap1,ks,a,k,m,T,rhoa,omega,rhos,zs),k1,k2,sectol);
% if N > Nlook
% NN = (Nlook+1):N;
% II = find(abs(kap-kappa(NN)) > ftntol);
% for nn = II
% ii = nn+Nlook;
% [kapc,xfv]=fmins104('prob1objf',[real(kappa(ii)),imag(kappa(ii))],[],pi/4
/real(kappa(ii)),ka,ks,k,m,za,zs,rhoa,rhop,sigma,a,T,rhom);
% kap(ii) = kapc(1)+i*kapc(2);
% fv(ii) = xfv;
% fprintf('%g ',ii)
% if mod(ii,10) == 0
% fprintf('\n')
% end
% end
% fprintf('\n')
% end
zeta=ka^2-(kap/za).^2;
```

D.4.15 Zn.m

```
function Z=Zn(z,ka,muv,za,ks,zs,rhoa,rhos)
    sqs = csqrt(ks^2-muv); sqa = csqrt(ka^2-muv);
    normz=1;%-rhos*cos(sqs.*zs).*(cos(sqa.*za)-1)./sqa-rhoa*sin(sqa.*za).*sin(sqs.*zs)./sqs;
    if z >= 0
    Z = cos(sqs*zs).*sin(sqa*(za-z))./normz;
    else
    Z = sin(sqa*za).*cos(sqs*(z-zs))./normz;
    end
```

Appendix E

Variable Definitions

This section includes only variables which are used in more than one section.

$A, B, C, ...$ - arbitrary constants (may or may not have subscripts).

a - diameter of the membrane.

c - speed of sound through a medium.

c_a - propagation speed through air.

c_s - propagation speed through porous soil.

D - region occupied by the membrane (Ch. 4 and 5).

D_m - weight function for the non-homogeneous membrane problem (Ch. 4).

F - radial function in cylindrical coordinates for separation of variables.

f - frequency.

G - angular function in cylindrical coordinates for separation of variables.

$\mathcal{G}$ - Green's function. (Ch. 4)

g - gravitational constant, $g = 9.8\,\mathrm{m/\,s^2} = 32.2\,\mathrm{ft/\,s^2}$.

H - humidity. (Ch. 2)

$H_m^{(n)}$ - Hankel Function.

$\mathcal{H}$ - porosity. (Ch.1)

i - imaginary number, $i = \sqrt{-1}$.

J - flux. (Ch. 1)

J_m - Bessel function of the first kind of order m.

k - wave number. $k = \frac{\omega}{c}$

$\mathcal{K}$ - structure constant. (Ch. 1)

k_a - wave number in air. $k_a = \frac{\omega}{c_a}$

k_s - wave number in soil. $k_s = \sqrt{\frac{\omega^2 + \frac{i\omega\sigma}{\rho_p}}{c_s^2}}$

m - index value, $m = 0, 1, 2, ...$ (unless otherwise indexed)

n - index value, $n = 0, 1, 2, ...$ (unless otherwise indexed)

P - pressure. (Ch. 1)

$\overline{P}$ - total pressure, $\overline{P} = P + p$. (Ch. 1)

p - small perturbation in the pressure, acoustic pressure. (Ch. 1).

p - pressure function. (Ch. 2).
p_a - pressure function in the air.
p_e - external pressure. (Ch. 5)
p_{inc} - incident pressure field. (Ch. 5)
p_s - pressure function in the soil.
p_{scat} - scattered pressure field. (Ch. 5)
Q - rate at which density is created per unit volume. (Ch.1)
R - small element of volume. (Ch. 1)
r - radial component in cylindrical coordinates
r_0 - radial component of the source.
S - entropy. (Ch. 1)
$\overline{S}$ - total entropy, $\overline{S} = S + s$. (Ch. 1)
s - small perturbation in entropy. (Ch. 1)
T - temperature. (Ch. 1).
$\overline{T}$ - total temperature, $\overline{T} = T + \tau$. (Ch. 1)
T - time function. (Ch. 2).
T - membrane tension (Ch. 4 and 5).
t - time.
u - fluid flow velocity. (Ch. 1)
u - vertical displacement of the membrane. (Ch. 5)
V - a small volume. (Ch. 1)
w - velocity of flow. (Ch. 1)
x - the horizontal coordinate in the standard xyz axis configuration.
Y_m - Bessel function of the second kind of order m.
y - the vertical coordinate in the standard xyz axis configuration.
Z - height function in cylindrical coordinates for separation of variables.
Z_a - height function in the atmosphere ($0 \leq z \leq z_a$).
Z_s - height function in the soil ($z_s \leq z < 0$).
z - the height coordinate in the standard xyz axis configuration.
z - the height component in cylindrical coordinates.
z_0 - the height component in cylindrical coordinates of the source
z_a - the height limit for the model of the atmosphere (maximum atmospheric altitude).
z_s - the depth (negative height) for the rigid substrate.
χ - the weight function for the depth equation, equation (4.19).
δ - small perturbation in the density. (Ch. 1).
δ - Dirac delta "function".
ε - small value added to the radial component in the Green's Function.
ε_m - values in Mathews and Walker's Green's Function. (Sec. 4.3, Ch. 5)
γ - ratio of specific heat at constant pressure to specific heat at constant volume, $\gamma = \frac{C_p}{C_v}$
κ_s - compressibility of the elastic membrane (Ch.1).
κ - substitution variable. $\kappa = z_a\sqrt{k_s - \mu}$.
λ - arbitrary constant for separation of variables, found to be $\lambda = n^2$, where $n = 0, 1, 2, ...$

μ - arbitrary constant for separation of variables, found to be $\mu = k_a^2 - \left(\frac{\kappa}{z_a}\right)^2$
Ω_a - substitution variable for $\sqrt{k_a^2 - \zeta}$. (Ch. 5)
Ω_s - substitution variable for $\sqrt{k_s^2 - \zeta}$. (Ch. 5)
Φ_n - substitution variable for $\int_{z_s}^{z_a} \chi(z) Z_n^2(z)\, dz$.
ϕ - depth condition above the membrane.
ϕ_a - depth condition above the membrane in the atmosphere.
ϕ_s - depth condition above the membrane in the soil.
ρ - density.
$\overline{\rho}$ - total density, $\overline{\rho} = \rho + \delta$. (Ch. 1)
ρ_a - air density.
ρ_p - effective density of the porous soil.
ρ_s - soil density.
π - pi, 3.14159..., the ratio of the circumference to the diameter of the circle.
ζ - substitution variable. $\zeta = \mu r^2$.
ζ - eigenvalues. (Ch. 5)
σ - flow resistivity.
θ - angular component in cylindrical coordinates.
θ_0 - angular component in cylindrical coordinates of the source.
τ - small perturbation in temperature. (Ch.1)
τ - substitution variable, $\tau = z_a\sqrt{k_a^2 - \zeta_{mn}}$. (Ch. 5)
ω - angular velocity. $\omega = 2\pi f$